Development and validation of a quick-scan algorithm for evaluation of rooftop PV potential

Tim de Vries

Technische Universiteit Delft

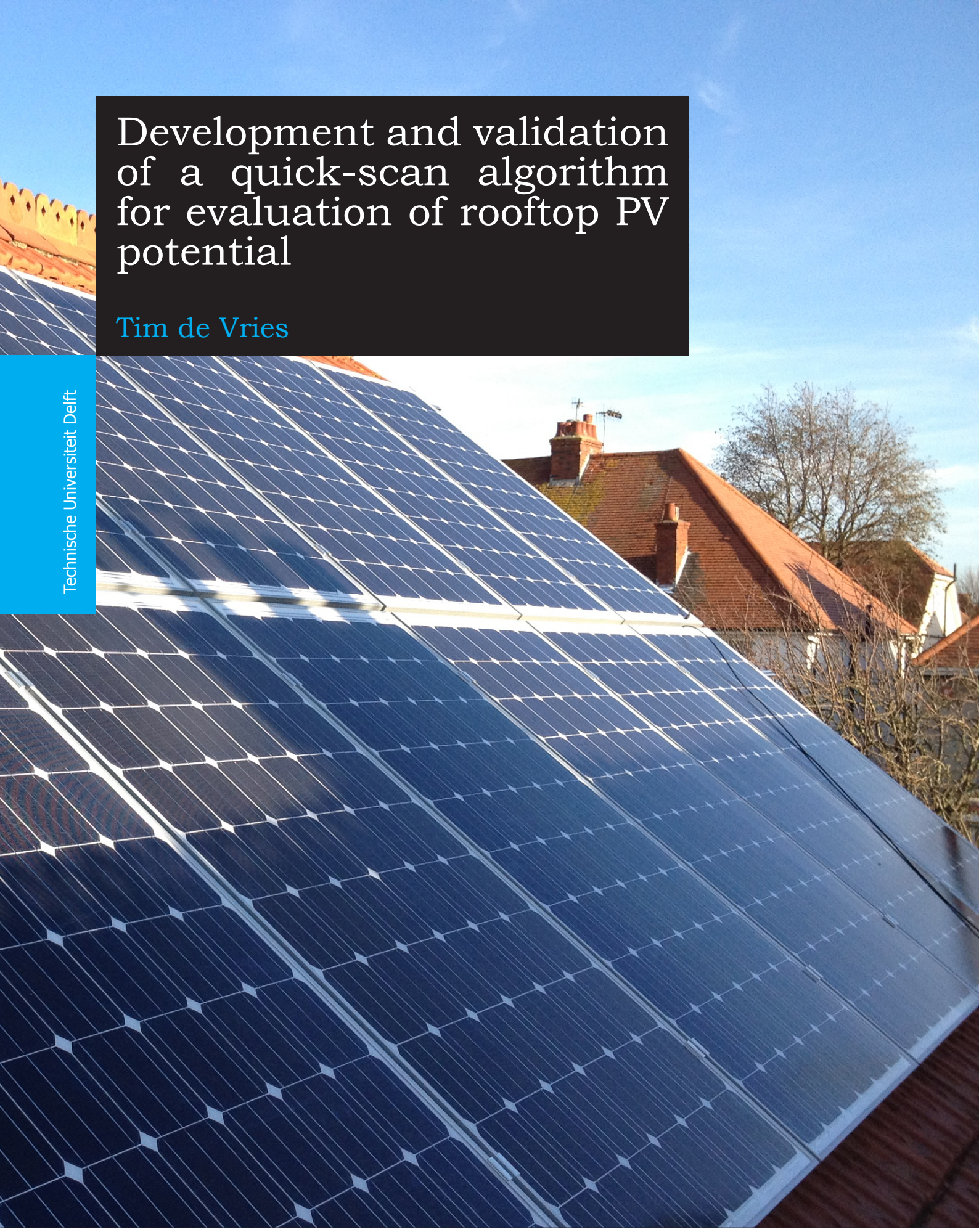

TU Delft Delft University of Technology

Challenge the future

Development and validation of a quick-scan algorithm for evaluation of rooftop PV potential

by

Tim de Vries

in partial fulfilment of the requirements for the degree of

Master of Science
in Sustainable Energy Technology

at the Delft University of Technology,
to be defended publicly on Friday October 19, 2018 at 10:00 AM.

Student number:	4153502
Project duration:	December 4, 2017 – October 19, 2018
Company daily supervisor:	Ir. J. Donker
TU Delft supervisor:	Dr. O. Isabella
TU Delft daily supervisor:	Dr. H. Ziar
Thesis committee:	Prof. Dr. M. Zeman
	Dr. O. Isabella
	Dr. M. Cvetkovic
	Dr. H. Ziar
	Ir. M. van Hoolwerff
	Ir. J. Donker

This thesis is confidential and cannot be made public until 2023-10-19.
Cover image adapted from Low Carbon Living.

TU Delft Delft University of Technology

Abstract

A quick-scan algorithm has been developed in order to evaluate rooftop PV potential in the Netherlands. Both its panel fitting and yield prediction functions have been validated with existing systems monitored by Solar Monkey. The calculation times of different parts of the algorithm were measured and decreased while keeping the accuracy of the algorithm in the desired range.

First, a new approach to determine the roof segment orientation was introduced, using both the normal vector and the longest side of the roof segment polygon. A visual inspection was carried out, in which recent aerial images were compared to 3D roof segments that were provided by Readaar. For 145 roofs, the roof segments on which PV was placed were manually selected, such that they could validate the quick-scan. From the visual inspection it was deduced that in-roof obstacles were often not detected. Sometimes the customer had no desire to use the full potential of the roof, or preferred a rectangular panel layout instead of fitting the maximum amount of panels. Another finding was that the distance kept from the roof segment edge was much smaller than initially expected. For pitched roofs, there was virtually no distance between the roof edge and installed panels, while for flat roofs around 20 cm was kept. Using zero distance from the roof edge, the panel placement algorithm still underestimates the roof potential by 17.5% on average, with a relative standard deviation of 46.3%.

Three yield calculation methods were compared: the Solar Monkey method, the SVF & SCF method, and the method without obstacles. The predicted performance or final annual AC yield was compared with the actual measured performance, both measured in kWh/kW$_p$ per year. For the three methods, relative standard deviation values of 7.2%, 7.5% and 9.1% were found respectively. The three methods could generate yield predictions for 91.0%, 92.7%, and 93.1% of the 145 roofs. For highly shaded roofs with Sun Coverage Factor values above 0.25, the method neglecting obstacles performed significantly worse. Additionally, the performance of large roofs with an average segment area above 70m^2 was generally under-predicted, while the relative standard deviation was highest. It is expected that using one obstacle view is not accurate enough for large roof segments.

The computational speed of the panel fitting algorithm for pitched roofs without internal obstacle segments was found to be 20.1 ± 5.0 m^{2}s^{-1}, whereas for flat roofs it was found to be 56.9 ± 12.0 m^{2}s^{-1}. In order to optimise the quick-scan algorithm in both speed and accuracy, two filtering steps were carried out. Segments with a pitch angle over 10° and an orientation between 0° to 60° or 300° to 360° were filtered out, since they would have an annual performance below 650 kWh/kW$_p$. Moreover, segments with an area less than 8.4 m^2 were filtered out, since they were observed to fit less than 2 panels. The quick-scan calculation times for different yield prediction methods were found to be 15.50 ± 1.01, 14.58 ± 1.13 and 2.75 ± 0.44 seconds per roof, respectively. These times were measured for data sets that had around 2 segments per roof after filtering on segment area and pitched segment orientation. It can be concluded that the method without obstacles is preferred when the calculation time is a limiting factor, whereas for accuracy the Solar Monkey method is preferred.

Acknowledgements

I would to express great appreciation to my daily supervisor, Jaap Donker, for all his help in giving my project direction. I enjoyed our weekly project updates, your sharp comments and the many things you taught me about coding.

I would like to thank my professor Olindo Isabella, who has been of great help by giving scientific guidance. Thank you for all useful input, insightful cluster meetings and critical questions that contributed to a better result.

I am particularly grateful to Hesan Ziar, who has helped me with many complications I faced throughout the project. Apart from that, his feedback on earlier versions of the report has been extremely helpful.

Throughout this project, I have had the pleasure to spend a lot of time with the Solar Monkey team. I admire Jan Pieter, Mels and Tino for their passion to grow the company, their endless interest in my project and all efforts that have already been made to commercialise my work. I had a great time with all other colleagues within Solar Monkey. I enjoyed the lunches, coffee breaks and Thirsty Thursdays.

A special thanks to Andres Calcabrini, who developed one of the three yield calculation algorithms I validated in this report. Andres has been of particular assistance in the introductory phase of my project, explaining me a lot about irradiance models and his thesis work.

Lastly, I would like to thank Sven and Martijn from Readaar, for the successful collaboration we had while validating the quick-scan algorithm. I have enjoyed our PVision meetings and I think your roof segments are very promising for further collaboration with Solar Monkey.

Tim de Vries
Delft, October 2018

Contents

List of Figures

List of Tables

1 Introduction

1.1. Solar Energy

As human kind feels daunted by the challenge to their meet their energy demand in a more sustainable and fossil-free manner, the transition to renewable energy sources such as wind and solar has begun. For the second year in a row, all newly installed renewables added more than half of the new global power generation capacities in 2016 [2]. For the first time, more solar energy was installed globally than wind energy throughout the year [2]. Moreover, the globally installed solar capacity is expected to exceed 400 GW_p in 2018 [3]. While these numbers are promising, the enormous potential of solar photovoltaic energy is only being exploited marginally. Although the European solar energy market is well-developed compared to other regions of the world, it comprises only 3% of Europe's energy demand [4]. Even though the prices of photovoltaic systems have decreased significantly over the last decades, the adoption of PV is not increasing rapidly enough [4]. Therefore, more societal push is necessary to help the solar PV industry grow.

Throughout this thesis, the terms PV module and PV panel will be used interchangeably. Whereas in scientific literature "module" is more frequently used, "panel" is preferred in the solar industry and installation practice.

1.2. Relevance of automatic PV system design

For domestic rooftop PV installations, the process from consumer interest and decision to purchase to design and installation of a system can take months. The activity of the whole solar energy market could increase from an automatic PV system design, since it would increase the productivity. Ranging from software-aided system design to PV system design with visual inspections of surroundings, the design of a rooftop PV system may take anywhere from 10 minutes to several hours [5]. Because of the fierce competition in the domestic PV system market, only a small percentage of the designs is actually built. Much time could thus be saved on the side of the PV installation companies. Moreover, an advanced design algorithm could possibly design systems with higher energy yields, better aesthetics or better cost-effectiveness than humans could do manually [5]. The optimal position for panels could be calculated, minimising the shading throughout the year. Additionally, algorithms could find alternative panel configurations that would fit more panels on the same roof. For example, it could find a balance between the yield per m^2 and total yield by comparing east-west or south-directed setups according to customer requirements.

Apart from improving the design phase of a PV system, automatic PV system design can make the sales process of PV much more efficient. It would decrease the effort and time spent by cold-calling potential customers. When designs can be made for any physical address, large batches of potential customers can be contacted with a draft design of a PV system on their roof. Additionally, they could be triggered by mentioning the amount of energy they could have generated by that PV system, and how much money they would have saved. This offers great potential to solar software companies that develop automatic design algorithms.

On the consumer side, some of the barriers that slow down the adoption of PV could be taken away by automating the yield prediction and system design. By facilitating yield prediction and system

design in a quick and user-friendly manner, consumers would have fewer concerns about the suitability of their rooftop for a PV system. Also, their perception of costs would be less discouraging if an accurate financial calculation would show the projected cash flow and payback time. A so-called ”quick-scan” algorithm could quickly provide them with a first estimate on these matters.

1.3. Solar Monkey & PVISION

This MSc thesis is part of ongoing Research & Development at Solar Monkey, a company involved in the accurate prediction of PV system yield based on geographic, meteorological and system component data. They specialise in advanced software for system design and performance prediction.

Primarily, Solar Monkey licences their system design software to PV installers. The systems designed with their software are monitored continuously and with the warnings given, problems are revealed and defects can be localised. Lastly, Solar Monkey has launched a foundation called Zonnegarant. Supported by the accurate yield predictions of the algorithms behind the software, Zonnegarant can give customers a minimum guaranteed system output.

Solar Monkey uses aereal images and LiDAR (Light Detection And Ranging) data, the latter being a height map with a resolution of 0.5 meters. The software allows solar modules to be dragged and positioned on a roof manually. Accordingly, a list of inverters that match the sizing of the designed system is given. For the designed configuration the performance can be predicted per module as a function of position, orientation, tilt angle and the shadow profile given by surrounding obstacles blocking the horizon. The horizon data is found by analysing the height of surrounding grid points in the LiDAR data.

The future goal of Solar Monkey is to develop a software that fully automates the design process and yield prediction of PV systems on rooftops. Within a consortium named PVISION, Solar Monkey is collaborating with Delft University of Technology, Utrecht University and Readaar. All partners work on certain aspects of the automatic PV system design.

Readaar is a software company that translates aerial images and LiDAR maps to usable data. This is necessary for information on the roof segments on which PV panels will be placed by Solar Monkey’s software. Delft University of Technology carries out scientific research into the effects of albedo on yield prediction and methods to detect albedo from aerial images. Both Delft University of Technology and Utrecht University are involved in scientific yield prediction and monitoring existing PV systems for performance analysis.

1.4. Market landscape

In order to determine the uniqueness and relevance of an automated panel fitting and yield prediction algorithm to be developed by Solar Monkey, it is important to evaluate the market landscape. Since the solar market is growing in the Netherlands but also globally, there are many software companies providing different tools for semi-automatic system design and yield prediction. The level of complexity and the scientific justification of these applications vary greatly. Often shading obstacles are not taken into account or the layout of panels on a roof remains undefined. These lacking aspects can greatly affect the uncertainty in yield prediction and financial prospects for customers.

In the coming sections, a market analysis will be carried out. First, the different actors within the solar software industry will be identified. After that, national and international competitors for automatic system design and yield prediction will be reviewed. Lastly, the market of free PV software tools will be investigated.

1.4.1. Design software competitors for Solar Monkey

There is a broad variety of companies and institutions involved in the design of PV systems. These parties will be assessed in different categories. First, providers of professional software will be addressed, and providers of professional online PV applications. After that, the system design services offered by component manufacturers will be analysed. Lastly, special attention will be given to direct competition in the Netherlands.

Advanced professional PV software

Swiss company PVsyst is one of the oldest PV software packages. Developed by the University of Geneva, it has a wide range of functionalities and it is possible to import meteodata and export yield

prediction data. German party PV*SOL is a professional software package that includes 3D visualisation models and detailed shading analysis. PV*SOL and PVsyst offer advanced software for system design and modelling, and are used mostly throughout the academic world and R&D departments of large energy companies. They require the shapes of surrounding obstacles to be imported manually for accurate yield prediction. An above-average level of knowledge is required in terms of electrical engineering and solar energy, making this software unsuitable for most PV installers.

Apart from these well-known parties, there are dozens of smaller parties with either full system design software or niche software applications like Solarius PV (ACCA Software), Solmetric, Archelios Pro, Solarmapper, PVComplete, PVscout, Solarpro, Plan4solar PV F-CHART, INSEL, Polysun, HOMER 2, Helios 3D, Solergo, PV-DesignPro and Skelion [6].

Online professional PV software

Large American software providers such as Aurora Solar and Helioscope have fairly strong positions in the global PV system design markets, however shading and irradiance are not taken into account automatically. Despite the fact that the design is manual and time-consuming, it must be noted that such software is often most suitable for the design of very large utility-scale systems. Generally, Solar Monkey works with better aerial images, height data and is more simple in use, which gives it preference for smaller systems.

Next to large competitors like Aurora Solar and Helioscope, there are many other parties offering their services solely online. Some examples are EasySolar, Polysun online, SOLARPlus, SolarDesignTool, Solargis-PvPlanner, SOLARMODEL and i-Pal WEB [6]. Although PV applications only accessible by smartphones or tablets do exist, they are generally too simple to compete with Solar Monkey design software.

PV system component manufacturers

Inverter manufacturers Mastervolt, ABB, SolarEdge and SMA offer their own tools to determine which inverter is preferred for specific panel layouts. They make a yield calculation according to the design that is manually made, however they do not include automatic analysis of shading obstacles. Aided PV system design and yield calculation is also offered by inverter parties Kaco, Ingeteam (Ingecon), Fronius, Samil, Omnik and Satcon [6]. The Dutch mounting system producer Van der Valk offers a planning tool that mostly focuses on ballast and the pricing of materials needed for the actual installation. Although the tools mentioned here are free of use, only systems components from these specific manufacturers can be selected. Therefore these tools are mostly designed for strengthening partnerships and creation of installer dependence on their component providers. For inverter manufacturers, also monitoring services can be upsold from the starting points of these tools.

Direct competition in the Netherlands

Although Aurora Solar, Helioscope and PV*SOL have significant market shares in the Netherlands, they have significant drawbacks for the design of small to medium-sized rooftop systems. For residential and commercial rooftop PV systems, 2solar is a relatively large party and the biggest competitor of Solar Monkey in the Netherlands. They offer an integrated package with system design, Customer Relationship Management (CRM) and quotation software. Solar Monkey consciously focuses more on the system design and yield prediction, and less on these additional services. Next to 2solar, Autarco is a significant party in the Netherlands with their software package Helios. They are collaborating with the University of Eindhoven, Utrecht University and TNO, and they sell performance guarantees just like Solar Monkey. Lastly, there are multiple smaller competitors that offer PV system design software (such as Libra Pulse developed by Ezing Solar), however they often lack accurate yield prediction or design functionality.

1.4.2. Competitors for automated design algorithms

The quick-scan to be developed encompasses automatic system design and yield prediction, using height data to determine shading losses. In this section, both national competitors Zonatlas and Novasole, and the international parties Sunmapper and Project Sunroof will be introduced.

Zonatlas

Zonatlas is probably the most direct competitor of Solar Monkey's envisioned quick-scan algorithm. Similarly to Solar Monkey, height data and land register (GIS) information of buildings are combined,

taking into account the slope of roof surface areas. Using weather data and irradiance values for specific locations, they predict the irradiance on a roof and even calculate the payback time of investments in solar panels. Using OpenStreetMap, they provide maps categorising roofs in very suitable (green), suitable (yellow) or less suitable (red), as shown in figure 1.1. The module layout is not given by Zonatlas, so this could be a selling point for the quick-scan algorithm of Solar Monkey.

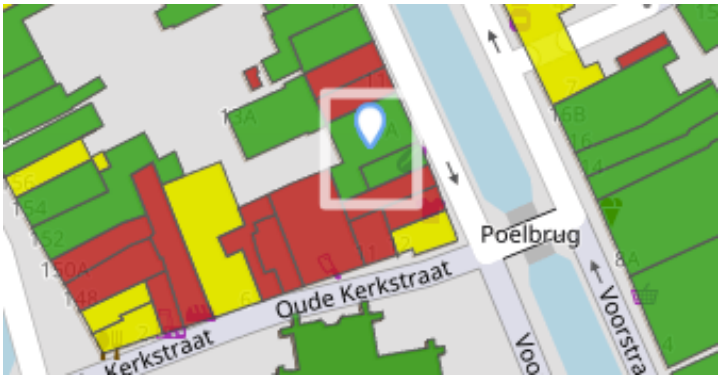

Figure 1.1: Screenshot from Zonatlas website, showing roof shapes in Delft, the Netherlands with varying suitability for PV.

Zonatlas is owned by EnShared, a company that manages and advises on complex projects in the field of energy and sustainability. Enshared offers ways to generate decentralized sustainable energy to households, businesses and municipalities. Zonatlas is an open online platform, accessible to all customers. Apart from irradiance and yield calculations, it includes government regulations such as aesthetic restrictions in historic towns. EnShared plans to help customers with the implementation of different solutions, such as PV combined with heat pumps, CHPs and storage systems [7]. If more than 5 building requests are done from on IP address, a pop-up appears, stating that the application is only meant for consumers. For PV installers, Zonatlas claims to help with accurate data to send high-quality quotations. Since Solar Monkey also wants to sell the quick-scan for large-batched quotations, the added value should be in the accuracy and system design above what Zonatlas offers.

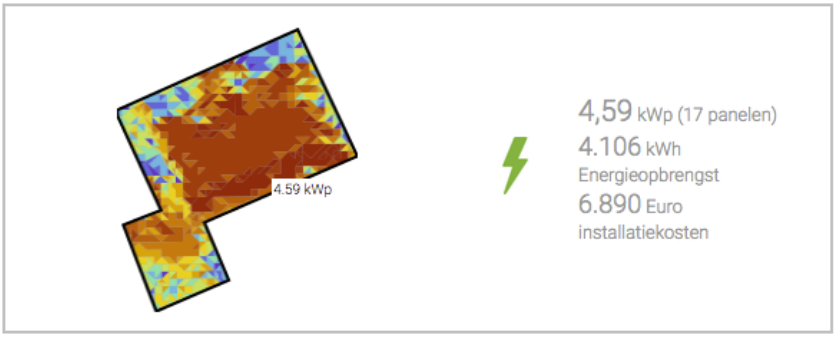

Figure 1.2: Screenshot from Zonatlas website, showing an AC yield prediction of 4.1 kWh/year for a system with 17 panels.

According to conversations with installers and utility companies, several customers of Zonatlas are not satisfied with the application. The results are often found to be incorrect and sufficient scientific explanation is missing for losses within the PV system. As shown in figure 1.2, the more detailed irradiance map of a roof does not give any information about surrounding obstacles or the orientation and tilt of a roof. Additionally, many assumptions made for the yield estimation are not specified towards costumers [8]. This leads to the impression that the scientific foundation of their algorithm is inadequate. One of the main goals for Solar Monkey should thus be to clearly define the uncertainty in the outcome of the quick-scan, along with the assumptions made to come to this result.

Novasole

The Dutch Novasole platform named Solar Assets Management (SAM) offers various services, of which their ”roofscan” (Dutch: dakscan) is the most well-known. They introduced a Betaversion in 2010 and

updated their product various times since then. It is meant to give a first indication of the savings that PV panels could offer for a specific roof. With this roofscan, PV installers can send quotations in a pre-made format or in their own corporate layout.

In 2015, the software of Novasole was audited by specialists of ISSO according to the EDR (Energy Diagnosis Reference) requirements and the handbook for Solar Energy [9]. Ever since, they are selling their roofscan with the ISSO quality certificate (kwalitetiscertificaat+) for PV design and calculation software. Over 10,000 private and business customers have already used the roofscan application [10]. Novasole offers the roofscan via an accessible API in exchange for a monthly fee.

As visible in figure 1.3, roofs are divided in roof segments with different orientations, and every roof segment is evaluated with a mark between 5 and 10, ranging from unsuitable to excellent. Judging from the roof segmentation, Novasole definitely uses height data, either gotten from LiDAR or stereo imaging. It must be noted that segmentation is far from perfect and neglects substantial parts of the roof surface. However, as Novasole also collaborates with Readaar for their roof segments, this problem is expected to be resolved in the near future, since Solar Monkey has no exclusivity for obtaining the roof segments by stereo-matching. Although no information could be obtained about the yield prediction algorithm and shading analysis, the scientific justification is expected to be at least reasonable, judging from the ISSO certificate.

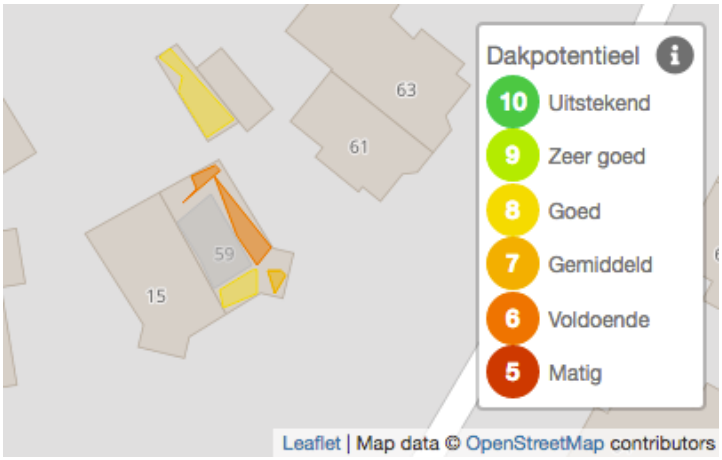

Figure 1.3: Screenshot from Novasole roofscan, showing the segmentation of a roof in Heerlen, the Netherlands.

The quick-scan to be developed still has potential to offer added value in calculating the actual layout of panels on roof segments. Also, more openness regarding the assumptions done in calculations would give the quick-scan added value over the Novasole roofscan.

Sunmapper

Sunmapper is an interactive platform for potential rooftop PV customers in Denmark. At an early stage, potential customers get access to knowledge like the irradiance, pitch angle, orientation and area for the address of their roof. Within 30 seconds, they thereby give a quick indication of the system size, costs, financial and CO2 savings per year. The tools is currently only available for addresses in Denmark. Furthermore, this tool does not take into account the module layout on a roof.

Sunmapper states to estimate irradiance on a basis of 3D data and shadow analysis. It seems to take shading obstacles on the roof into account. In figure 1.4, it can be seen that the on-roof obstacle causes shading. However, by examining their results for various addresses it is doubtful whether height data of the surroundings are included for this shadow analysis, or only the obstacles on the roof. It is clearly visible that the amount of irradiance on the plane of the roof changes with it's pitch and orientation. However, there is no difference in irradiance intensity for planes on the same roof with the same orientation and pitch angle..

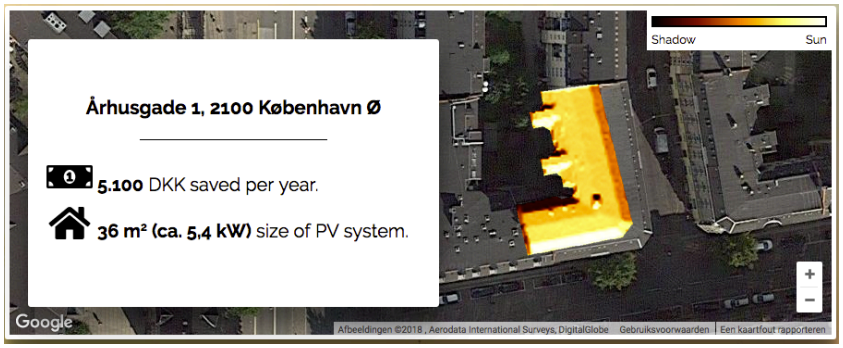

Figure 1.4: Screenshot from Sunmapper website, showing irradiance on a roof in Kopenhagen.

In figure 1.4, a shift in the position of the building and the coloured irradiance map can be noticed. Also, for 7 of 10 the tested addresses in Denmark, an error message appears, where the tool states it cannot be used for this address yet. All in all, Sunmapper is not yet seen as a threat to the quick-scan of Solar Monkey.

Google Project Sunroof

Since 2015, Project Sunroof calculates the energy yield and financial prospects of a PV system for any rooftop in the United States of America. Project Sunroof does not ask any money for their service, however their financial model is based on redirecting customers to PV installers (lead generation). The enormous amount of visitors on their website has a great value for marketing and interested customers lead to high conversions once redirected to PV installers.

The aerial imagery of Google is used for rooftop and existing installation detection. A 3D model is generated by combining multiple views of each area, such that the shapes of all the buildings, trees, and other shading objects are captured. This process is identical to the one that builds the 3D shapes in Google Maps or Google Earth. Sunroof performs raycasting for every hour of the year to determine a shade map for that hour, and combines that with hour-by-hour typical weather data to build up the solar potential of each point.

All nearby shapes are taken into account for the raycasting: A grid of tiles is used to choose which 3D objects are taken into account, but the maximum distance taken into account is always at least 100m and can be as much as 500m [11]. The 3D model is generally good enough to capture nearby shadow-casters and the local surface tilt. Reflected irradiance is not modelled. As shown in figure 1.5, the surfaces of different roof segments show lower irradiance values near shading obstacles such as trees. Moreover, the website shows the predicted financial savings, the roof surface area available for PV modules, the environmental impact of installing a system of recommended size and it gives three ways to finance the installation of such PV system (buy, lease or loan).

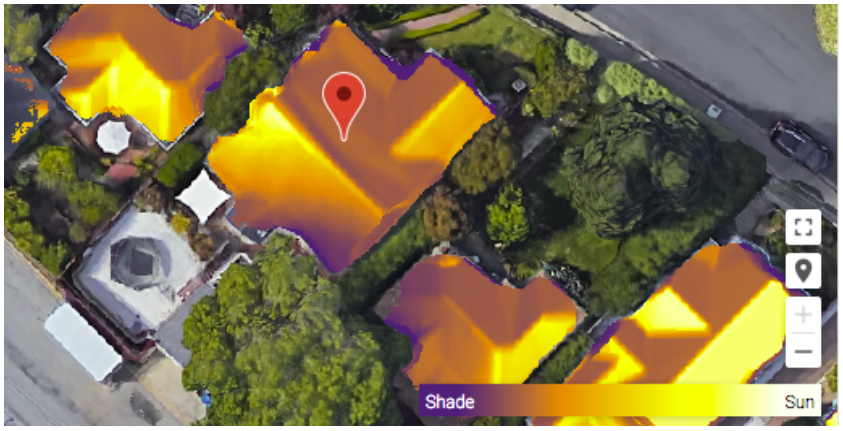

Figure 1.5: Screenshot from Project Sunroof website, showing irradiance on a roof in Redwood City, California.

Most system components and their efficiencies are implemented at a late stage of the calculation

and could just be scaled linearly for different inverters or modules. However, the several non-linearities would occur, for example for module temperature. The temperature-induced degradation of modules and the effect of wind speed, ambient temperature and solar irradiance on that temperature is modelled according to the "Mattei 1" model [12].

Although Project Sunroof is currently only active in the U.S., they will expand to other countries in the future. Project Sunroof has a partnership with E.ON in Germany, and has plans to enter the British and Italian market by the end of 2018 [13]. They are not yet a direct competitor to Solar Monkey, but they pose a large threat to the quick-scan of Solar Monkey. Nonetheless, Solar Monkey's quick-scan does already take into account the module layout of the PV system on a roof. In order to differentiate from competition, this is an essential component to be implemented in the quick-scan.

1.4.3. Free PV design tools

Apart from paid PV system design tools, there are hundreds of global, national and regional parties providing irradiance maps and additional PV data for free. The most important ones are discussed.

PVGIS

PVGIS offers a free online solar PV calculator for different types of stand-alone and grid-connected systems. It was developed by the Joint Research Center (JRC), supported by the European Commission. The software of PVGIS estimates the power output of PV systems within Europe, Asia and Africa. It is integrated with Google Maps and therefore easy to operate.

Since the outcomes of PVGIS are openly accessible, their irradiance data and yield calculations are used by many solar developers. For example, Solar Monkey uses their API to get irradiance data and the solar position throughout the year for specific locations [14]. In terms of the calculation results, PVGIS functions as a first estimation, unless many variables are filled in manually. System losses like inverter losses, various mismatches, cable losses, and module degradation with ageing are loosely modelled by a combined loss of 14%. Apart from that, the error caused by diffuse irradiance is unknown and reflected irradiance is fully neglected [15].

Since PVGIS is oriented globally, they are struggling with the size of their horizon data. For the calculation of PV performance the surroundings like mountains and hills are taken into account for defining the horizon of a system [16]. However, the resolution of the height-grid is around 90 meters, such that houses and tress are not included. Although there it is possible to upload the horizon information for a specific location, this should be uploaded manually. Their next step would be to use digital elevation model (DEM) data at 1 arc-second resolution per evaluated location in Europe [17]. This would bring the horizon accuracy towards a resolution of 30 meters, however still houses and trees will not be included as shading objects. This is why PVGIS is not seen as a direct competitor of Solar Monkey's quick-scan.

System Advisory Model

The freely accessible System Advisory Model (SAM) is developed by the United States National Renewable Energy Laboratory (NREL). Thanks to its many applications and detailed options for configuration, it can be considered in the league of aforementioned professional software packages PVsyst and PV*SOL. It however does require above-average technical knowledge for successful use.

Suncalc

Suncalc is a free online application to ascertain the sun movement with interactive map. Information such as the sunrise, sunset, shadow length, solar eclipse, sun position, sun phase and sun height during the day is easily accessible for the whole world and visualised in a user-friendly way. Although the information of Suncalc can be useful for PV system design, it requires additional sources for irradiance and height data. It is not regarded as a competing tool for the success of the quick-scan. Additionally, parts of this tool are offered on many more websites such as PVGIS, Sun Position (Sustainable By Design), `timeanddate.com` and `sunearthtools.com`.

Dutch PV Portal 2.0

This Dutch PV website was developed by Veikko Schepel within the PVMD group of Delft University of Technology. It is an improved version of Dutch PV Portal 1.0, developed by Arianna Tozzi. The portal was designated to make information on solar energy in the Netherlands publically accessible. The

historical and real-time measurements of the Royal Netherlands Meteorological Institute (KNMI) were combined with the scientific research and modelling expertise of the Photovoltaic Material and Devices (PVMD) group. Although the portal offers a PV system design function, the module layout and shading are not taken into account for yield prediction. The PV Portal 2.0 is not considered a competitor for Solar Monkey's quick-scan.

Other free PV software

Apart from PVGIS, SAM, Suncalc and the Dutch PV Portal there are many other free tools that can help with system design. Several examples are SISIFO, PVWATTS, RETScreen (CAN), HOMER Legacy, Hybrid2, calculationsolar.com, DIAFEM and Easy-PV [6]. Also, several professional PV software providers offer a free lite version of their software, like PV*SOL online and Skelion.

1.4.4. Comparable scientific projects

Throughout the last years, much research has been done into the potential of rooftop PV for urban areas [18, 19]. Most of these projects take into account the pitch angle and azimuth of roofs to determine the POA irradiance. Some investigations also include skyline profiles per roof, however the actual placement of panels is seldom taken into account. An exception to that is a research carried out by Mainzer et Al. in Germany last year [20]. They have used geodata and image recognition techniques to virtually place panels on roofs. However, the panel fitting methodology is still quite inaccurate and the algorithm is not a commercially available product. The research projects that were encountered thus do not form a threat to the quick-scan algorithm to be developed for Solar Monkey. Since there are thousands of scientific projects that are somehow related to determining PV rooftop potential for urban areas, further exploration and categorisation of this was determined to be outside of the project scope.

1.4.5. Conclusions regarding market landscape

As discussed in the previous section, the multitude of parties involved in irradiance mapping and PV system design does not make the market landscape very transparent. According to the research carried out, the software of Solar Monkey has added value in its user-friendliness, especially combined with its many functionalities and accurate yield prediction. Regarding the envisioned quick-scan algorithm, there are four main competitors: Zonatlas, Novasole, Sunmapper and Google Project Sunroof. In order to have added value over Zonatlas and Novasole, the assumptions for calculation of any given results and the uncertainty in yield prediction should be known to the user. Moreover, the module lay-out and thus panel fitting on roof segments is an essential component of the quick-scan. This would give it added value over its four competitors and make its outcomes more visually appealing to customers. The free software and tools available on the market cannot be seen as direct competition for the software of Solar Monkey or the quick-scan algorithm. They rather enhance general knowledge than posing a threat in the current market. In the case of PVGIS, their open source data is even used for Solar Monkey's daily operation.

1.5. Thesis objectives

The main goal of this thesis project is to contribute to the development on models and algorithms dedicated to automating the generation of PV system designs. Essentially this comprises of taking an address or geographical location as input, and providing feasible designs for PV systems at that location as a result. Such designs should take into account constraints such as the actual fitting of panels on a roof, but also financial constraints from the customer. Lastly, feasible designs should give an indication of the expected energy yield, taking into account shading losses due to surroundings.

To this purpose, a quick-scan that evaluates rooftop potential will be developed, in order to judge the potential of a PV system on a rooftop prior to the actual design phase. The error of the quick-scan algorithm should be acceptable to the business value of Solar Monkey, i.e. support their public image of generating high accuracy predictions. Validation of this quick-scan algorithm will be done with respect to more extensive yield prediction methods. Using data provided by Readaar and Solar Monkey, the algorithm will also be compared to the actual yield of monitored systems.

1.5.1. Steps in the quick-scan development

The development of the quick-scan algorithm can roughly be divided into the following phases:

1. Given the address or coordinates of a house, the algorithm should be able to access the shape, orientation and pitch angle of its different roof segments.
2. For different roof segments, it should be analysed how many PV modules would fit in the most ideal module layout. This layout should be aesthetically acceptable.
3. Using a fast calculation method, the surroundings of the roof should be taken into account for yield prediction of the PV system. Different models will be analysed to account for shading. Firstly, the method using horizon data and solar paths that is already used by Solar Monkey, and secondly a method that only requires the Sky View Factor and Sun Coverage Factor for yield prediction.
4. The suitability of the roof for a PV system and its generation potential should be evaluated, so it can be displayed in a simple way according to customer needs.

1.5.2. Research questions

For the proper development of a quick-scan algorithm, several scientific research questions are of importance. Three main research questions will be introduced for each question a possible approach will be described.

Question 1: How realistic is the amount of modules fitted on a roof by the panel fitting algorithm?
Approach: A validation of the algorithm should be carried out, which compares the panel fitting on Readaar's roof segments with the PV systems that were actually built.

Question 2: How accurate is yield prediction carried out by the quick-scan?
Approach: Comparison of predicted values to the real-time generation of monitored PV systems for three different yield prediction methods.

Question 3: How fast are different parts of the quick-scan and how can this be optimised?
Approach: Measurement of the calculation speed for different parts of the quick-scan algorithm and an inventory of methods to increase the calculation speed while keeping the preferred accuracy.

1.6. Thesis Outline

This thesis will shed light on the development of a quick-scan algorithm for the evaluation of rooftop PV potential. The research will follow up on the work of Bronkhorst and Calcabrini [5, 21].
In the following chapter, a theoretical introduction will be given for the topics that will be discussed in later chapters. It will cover the conventions used to define the position of the sun and the orientation of a PV module. Moreover, different models will be introduced to determine the irradiance on a module and predict yield and performance.
Chapter 3 will present the roof segment data set used to test and validate the quick-scan. Also the limitations of the data will be mentioned, and how some of these problems have been resolved.
In chapter 4, the algorithm of the quick-scan will be explained in more detail, comprising both the panel fitting and yield prediction components. The chapter elaborates on the assumptions done for the quick-scan, and the challenges that were faced while developing the algorithm.
Chapter 5 will consist of the results found for the panel fitting on roof segments, and the validation with respect to real systems. Additionally, the deviations between fitted and actually placed panels will be discussed.
The results of yield and performance prediction will be discussed in chapter 6. The performances of different methods will be compared. Finally, the chapter will investigate the effect of different settings on the results of the quick-scan.
Conclusions will be drawn in chapter 7. Furthermore, recommendations will be given for further research and improving the accuracy of the algorithm.

2

Location issues and irradiance models

This chapter will give a theoretical introduction for the topics that are discussed in later chapters. It will cover the conventions used to define the solar position and module orientation. Then, different models will be introduced to determine the irradiance on a PV module and to predict yield and performance.

2.1. Solar position and module orientation

In order to define the solar position and module orientation, a polar coordinate convention is adopted such as shown in figures 2.1 and 2.2. Here the azimuth angle A_s is defined clockwise starting at 0° in the Northern direction and the altitude a_s is defined 0° when the sun is positioned at the horizon for the observer. Similarly, the module azimuth A_M is measured with respect to the North and the module altitude a_M is 90° when the panel is placed flat on the flat roof, whereas the module tilt θ_M is then defined 0° .

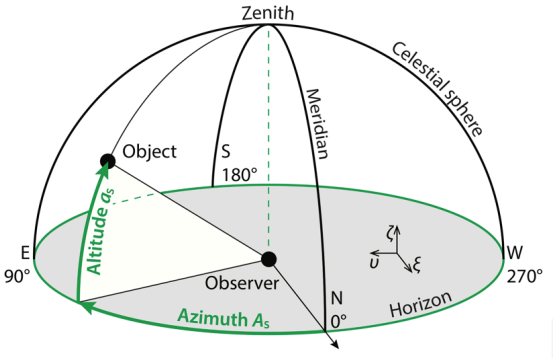

Figure 2.1: Horizontal coordinate system to define the altitude and the azimuth of the sun, where the North is at the bottom of the figure. Adapted from [22].

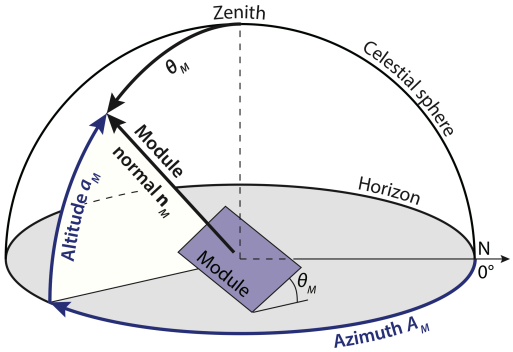

Figure 2.2: Horizontal coordinate system to define the angles used to describe the orientation of a PV module installed on a horizontal plane, adapted from [22].

2.2. Irradiance components and models

In the following part, the irradiance on a PV module will be described. Different components of irradiance will be mentioned to arrive at a formula for the total irradiance on a PV module.

2.2.1. Global irradiance on a module

For the prediction of generated energy by a PV system, the incoming irradiance must be estimated for the surface of each photovoltaic module. Meteorological data stations such as KNMI in the Netherlands

can provide irradiance values of the last years, and weighted averages can be used to predict the conditions for coming years.

The global irradiance on a module can be divided in multiple components. As visible in figure 2.3, G_M^{dir} stands for the direct irradiance that comes from the sun. The centre of the sun is often assumed to be a point source of direct irradiance. Diffuse irradiance (G_M^{dif}) is caused by photon scattering throughout the atmosphere. This can be seen as direct irradiance undergoing multiple reflections while bouncing against air and water particles in the air, thereby changing direction. Lastly, there is also ground-reflected irradiance (denoted by G_M^{albedo}), which is irradiance that was originally direct or diffuse, and then reached the module via the ground or other surfaces. The albedo value or reflectivity of the ground or surface is essential for this component of irradiance.

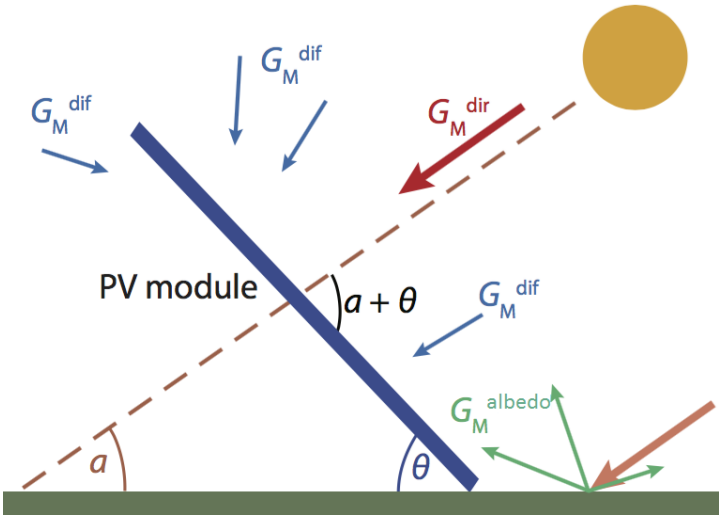

Figure 2.3: The three contributions to the irradiance on a PV module, adapted from [22].

On a flat plane, the three components of irradiance can thus be summed in the following way:

$$G_M^{tot} = G_M^{dir} + G_M^{dif} + G_M^{albedo} \tag{2.1}$$

2.2.2. Direct irradiance

During days with a clear and cloudless sky, the contribution of direct irradiance can be up to four times larger than diffuse irradiance in the Netherlands [23]. Direct irradiance is the only component of irradiance that is taken into account in clear sky models. If the full sun is blocked due to obstacles or a thick layer of clouds, direct irradiance is absent.

Direct normal irradiance (DNI) refers to the direct light that is incident on the plane that is perpendicular to the sun. The direct irradiance on a flat PV module can be obtained by $G_M^{dir} = DNI \cdot cos(AOI)$, where the angle of incidence (AOI) is the angle between the normal vector of the PV module surface and direction of the sun rays. The angle of incidence can be calculated as follows:

$$cos(AOI) = sin(\theta_M) \cdot cos(a_s) \cdot cos(A_M - A_s) + cos(\theta_M) \cdot sin(a_s) \tag{2.2}$$

It must be noted that only positive values must be considered for $\cos(AOI)$ if modules are not bi-facial. Negative values refer to situations where the angle of incidence is larger than 90°, so the sun is located behind the module.

2.2.3. Diffuse irradiance

The irradiance that is scattered by the atmosphere and reaches the horizontal plane at the ground surface is named diffuse horizontal irradiance (DHI). Although direct irradiance is often the the largest component of irradiance, diffuse irradiance can comprise a significant part of the global irradiance on a PV module. As mentioned earlier, if you only consider the direct irradiation on clear days, you would lose at least one fifth of irradiation [23]. On cloudy days, diffuse irradiance is much more important.

In simple irradiance models such as the diffuse irradiance model of Liu and Jordan, the diffuse light is assumed to be isotropic [24]. This means that the intensity of diffuse irradiance is constant in each direction in the celestial sphere. The Liu and Jordan model allows for quick derivation of the diffuse irradiance from the global irradiance, however in some geographical locations it might not be very accurate [25].

More advanced diffuse sky models identify multiple components of diffuse irradiance. The Hay and Davies diffuse model identifies two components: isotropic and circumsolar diffuse irradiance [26]. Circumsolar diffuse irradiance is caused by forward scattering of direct irradiance, and is concentrated on a disk around the sun.

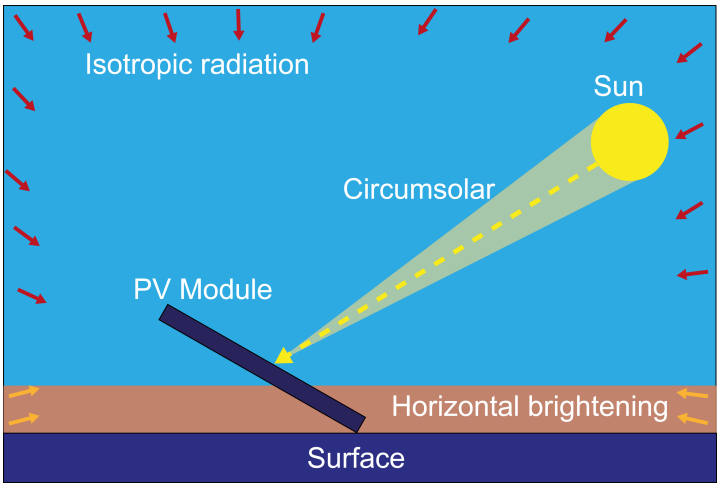

Figure 2.4: The three components of diffuse irradiance on a PV module as mentioned by the Reindl and Perez diffuse sky models, adapted from [27].

As shown in figure 2.4, both the Reindl and Perez models divide diffuse irradiance in three components [28, 29]. Apart from isotropic and circumsolar irradiance, a horizon brightening component is added. This is an increased amount of irradiance right above the horizon. By the introduction of the Reindl diffuse sky model, it was the most accurate model available [30]. Perez however used empirical factors to make results even more accurate [29].

His model describes the total diffuse irradiance by the following equation:

$$G_M^{dif} = DHI \cdot \left[(1 - F_1)r_D + F_1 \frac{a}{b} + F_2 \sin(\theta_M)\right] \tag{2.3}$$

where r_D is the isotropic diffuse view factor, a is the maximum between 0 and $\cos(AOI)$, b is the maximum between $\cos(85°)$ and $\sin(a_s)$ and F_1 and F_2 are empirical coefficients. The full derivation of these empirical coefficients can be found in [29].

Next to this empirical approach, some diffuse irradiance models have been based on the solar altitude and clearness index of the sky [31]. Several models have been developed using multiple predictors. The Boland–Ridley–Lauret (BRL) model uses 5 predictors: hourly clearness index, daily clearness index, solar altitude, apparent solar time and a measure of persistence of global radiation level [32].

In the software of Solar Monkey, the Liu and Jordan model is used for extraction of the diffuse irradiance. For the validation of the yield prediction method described in section 2.4.2, the Perez diffuse sky model was implemented.

2.2.4. Ground-reflected irradiance

The ground-reflected irradiance is mostly related to the isotropic diffuse view factor. This factor is determined by the tilt angle of a module and represents the fraction of the celestial sphere that is visible under a free horizon. The isotropic diffuse view factor is defined as:

$$r_D = \frac{1 + cos(\theta_M)}{2} \tag{2.4}$$

From this, the ground-reflected irradiance can be approximated as follows:

$$G_M^{albedo} = GHI \cdot \alpha_{ground} \cdot (1 - r_D) \tag{2.5}$$

In this equation GHI stands for global horizontal irradiance and α_{ground} stands for the albedo of the ground. The albedo stands for the fraction of the incident sunlight that a surface reflects [33]. Therefore, the albedo is calculated by the following equation:

$$\alpha = \frac{\phi_{reflected}}{\phi_{incident}} \tag{2.6}$$

In general albedo values are estimated between 0.14 and 0.22 for urban environments [27]. However, in cases of snow or buildings and roads painted in white, albedo values can be significantly higher. For very accurate irradiance prediction, albedo values should thus be measured. Since the exact albedo at a given location is unknown throughout this thesis, the albedo was set to 0.2 for yield prediction. A list of assumptions and standard settings for the quick-scan can be found in appendix A.

2.2.5. The effect of obstacles on irradiance components

The afore-mentioned equations are valid for a free horizon profile, however for situations where the skyline (obstacle view) is above the horizon, the Sky View Factor (SVF) has to be used instead of r_D. The SVF will be explained in more detail in section 2.3.2.

The Global Horizontal Irradiance in equation 2.5 should be modified accordingly, as shown in [21].

- If the sun is above the skyline and $cos(AOI) > 0$:

$$GHI = DNI \cdot sin(a_s) + DHI\left[(1 - F_1) \cdot SVF + F_1 \frac{a}{b}\right] \tag{2.7}$$

- If the sun is below the skyline:

$$GHI = DHI \cdot [(1 - F_1) \cdot SVF] \tag{2.8}$$

2.2.6. Final expression for total irradiance

Composing all expressions for irradiance components mentioned above, the total irradiance on the surface of a PV module would be given by:

$$G_M^{tot} = G_M^{dir} + G_M^{diff-iso} + G_M^{diff-cric} + G_M^{diff-hb} + G_M^{albedo} \tag{2.9}$$

$$\begin{aligned} G_M^{tot} = {} & DNI \cdot \cos(AOI) + DHI \cdot (1 - F_1) \cdot SVF + DHI \cdot F_1 \cdot \frac{a}{b} \\ & + DHI \cdot F_2 \cdot \sin(\theta_M) + GHI \cdot \alpha_{ground} \cdot (1 - SVF) \end{aligned} \tag{2.10}$$

This expression was used for the validation of the yield prediction method presented in section 2.4.2.

2.3. Obstacles and shading analysis

The irradiance is now known for a free horizon profile, however most PV installations are not located near an obstacle-free horizon. In the next sections, the approach to include obstacle shading will be explained.

2.3.1. LiDAR data height mapping

For PV applications it is desired to know the exact location and dimensions of obstacles. Therefore, a source of height data is useful for accurate yield prediction. Laser altimetry is a technique that uses a pulsed laser and measures the reflected pulses to determine the distance between the laser source and an object. It is a cost-effective manner to determine the height of large regions and have accurate measures in all three directions. The light detection and ranging (or LiDAR) method has been used to develop a height map of the Netherlands. This Open Data source is made available by the Dutch

government at a resolution of 0.5 meters. As such, every square meter contains 4 height points that result from multiple LiDAR measurements. The Dutch height data is called AHN (Actueel Hoogtebestand Nederland). AHN2 is the newest version that covers the whole Netherlands, captured from 2008 to 2013. Out of all grid points, 99.7% is within 20 cm of the actual height [34]. Currently, the newest version is AHN3 data, which has already been published for about 75% of the Netherlands [35].

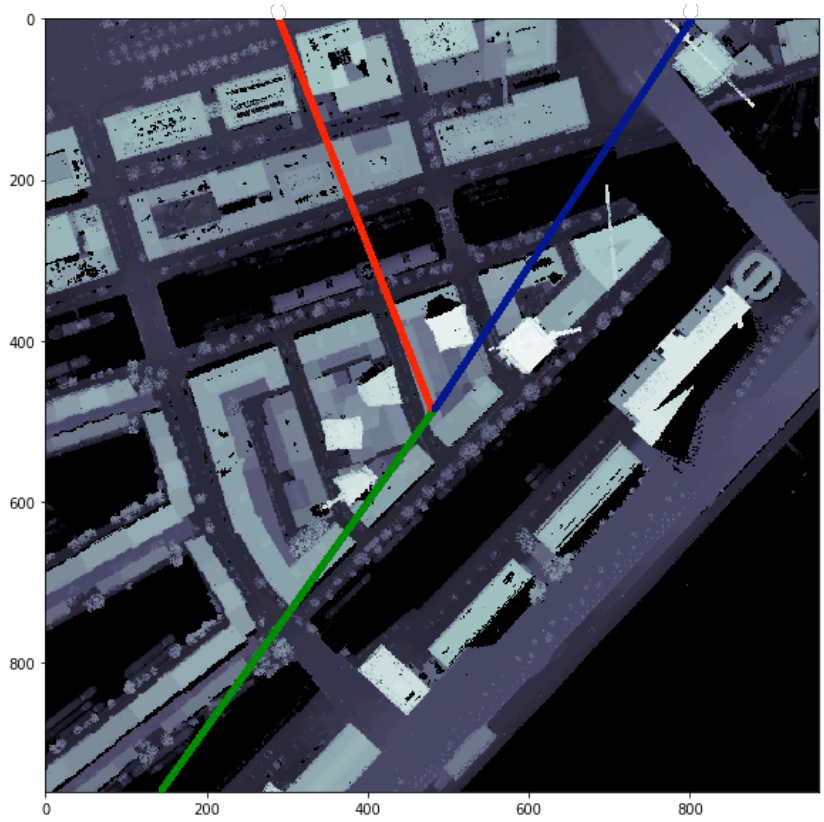

Figure 2.5: AHN height data for Bierstraat 18, Rotterdam, the Netherlands. Coloured lines are viewing directions in figure 2.6.

Figure 2.5 shows the AHN data for a central location in Rotterdam, showing a clear height difference between skyscrapers and lower residential buildings. Moreover, one can see how rows of trees are aligned with streets and the canals. Since the water generates the lowest height data in the image, the canals and the Maas river are visible in black.

2.3.2. Sky view factor calculation

The Sky View Factor (SVF) is a parameter that is used intensively in different urban and climate-related disciplines. Within the field of irradiance studies, it is defined as the ratio of visible sky with respect to the whole sky dome, containing both the visible part and the obstructed parts of this half sphere surface [36]. By definition, the SVF is limited to be between 0 for a fully obstructed sky, and 1 if the entire sky is freely visible.

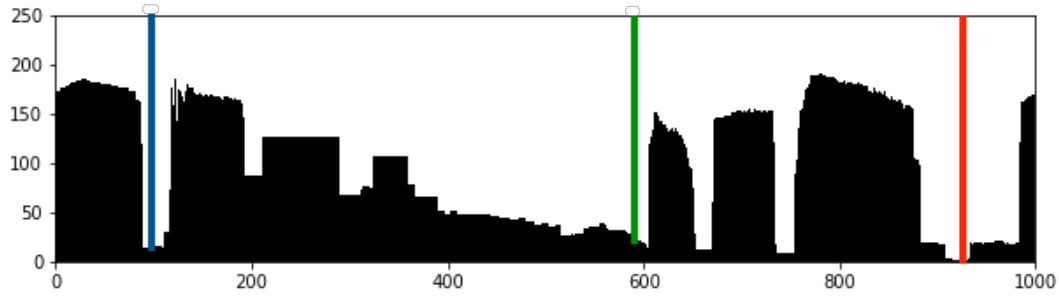

Figure 2.6: Obstacle view from the roof of Bierstraat 18, Rotterdam, the Netherlands. Coloured lines are viewing directions in figure 2.5.

In Solar Monkey, obstacle views are calculated from the AHN data and defined in rectangular matrices of blocked or unblocked view points in the hemisphere. In order to do this, the azimuths are defined clockwise from North in 1000 steps of 0.36°, summing to 360°. Similarly, the vertical axis is divided in 250 steps of 0.36°, summing to 90° perpendicular to the ground plane. This results in an image 250,000 pixels. In figure 2.6, such obstacle view can be seen for a roof in the centre of Rotterdam, the Netherlands. Comparing the coloured viewing lines with the ones in figure 2.5, the different skyscrapers can be recognised.

Throughout literature, the SVF is often determined by the use of a circular mesh grid with weighted sectors [21, 37]. The skyline profile is projected on this grid and then all sectors on the grid are either blocked by obstacles or free of obstacles. By dividing the sum of all weights of the free sectors by the sum of all weights in the mesh grid, the SVF can be obtained.

The rectangular obstacle views however pose a problem for the regular calculation of the SVF, since it cannot easily be converted to such a circular mesh grid. Throughout this research, a rectangular sensitivity map has been used to determine the Sky View Factor. A sensitivity map depicts a surface's sensitivity to incident light as a function of the hemispherical angle of incidence [38]. For a certain module azimuth and tilt, a sensitivity map therefore gives the significance of light coming from all possible directions.

The sensitivity (S) of each pixel in a sensitivity map can be calculated as follows:

$$S = \frac{I_{abs}}{I_{dn}} \tag{2.11}$$

In this equation, I_{abs} is the absorbed irradiance and I_{dn} is the direct normal irradiance. If reflected light by nearby surfaces is neglected, the maximum sensitivity of a surface is 1. For a panel placed on a flat roof with zero module tilt, S would be exactly 1 in the middle of both axes of the sensitivity map, being at location (500,125) of figure 2.6.

The SVF is calculated by summing the sensitivity values for all pixels where the obstacle view was unobstructed, and dividing this by the sum of all sensitivity values within the sensitivity map. In an equation, this would be:

$$SVF = \sum_{n_x=1}^{1000} \sum_{n_y=1}^{250} \frac{f_v(n_x, n_y) \cdot S(n_x, n_y)}{S(n_x, n_y)} \tag{2.12}$$

where f_v is a visibility function that is 1 for a freely visible sky and 0 when obstructed, and n_x and n_y would be steps in both dimensions of the obstacle view. Referring back to figure 2.6, a fully obstructed (black) figure would result in an SVF of 0 and a fully white (unobstructed) figure would yield a SVF of 1.

2.3.3. Sun coverage factor calculation

For the method of irradiance prediction that was developed by Andres Calcabrini, two factors should be known: the SVF and the SCF [21]. The Sun Coverage Factor stands for the number of hours that the sun is blocked, divided by the number of sun hours per year. Naturally, this variable is closely-related

to the amount of obstacles that are positioned in the direction of the sun throughout the year. SCF is zero at a location with a free horizon, and 1 if the sun is behind obstacles throughout the whole year.

For a specific location, the altitude of the skyline profile a_{sp} can be expressed as a function of the azimuth, where $A \in [0°, 360°$ [21]. When the horizon is free, a_{sp} is zero for all values of A.

In a more scientific notation, the SCF can then be formulated as:

$$SCF = \frac{\sum^{year} f_{sp}\left(A_s(t), a_s(t)\right)}{\sum^{year} f_{fh}\left(a_s(t)\right)} \tag{2.13}$$

where f_{sp} is a function that is equal to unity when then the sun is blocked by the skyline profile, and f_{fh} is a function that is equal to unity when the Sun is above the horizon line at a free horizon location:

$$\text{where} \quad f_{sp}\left(A_s(t), a_s(t)\right) = \begin{cases} 1 & 0 < a_s < a_{sp}(A_s) \\ 0 & \text{else} \end{cases} \tag{2.14}$$

$$\text{and} \quad f_{fh}\left(a_s(t)\right) = \begin{cases} 1 & a_s > 0 \\ 0 & \text{else} \end{cases} \tag{2.15}$$

where A_s is the sun azimuth, a_s is the sun elevation or altitude, and $a_s p(A_s)$ is the skyline profile elevation for a given solar azimuth.

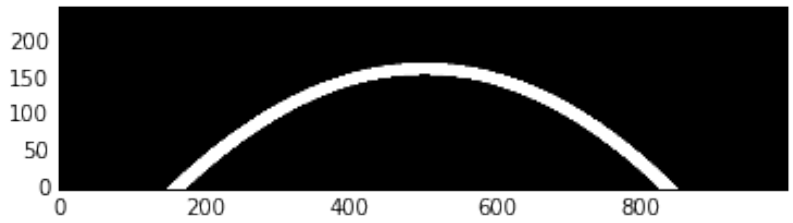

Figure 2.7: Solar position during the month of July for The Hague, The Netherlands, shown in obstacle view dimensions of Solar Monkey.

In this research, the SCF was calculated by finding the ratio between blocked points and all points on a sun path as shown in figure 2.7 for each month. This was done by combining an obstacle view such as shown in figure 2.6 with the sun path during each month, and then taking an average of the monthly values to obtain the annual SCF for that specific location.

2.3.4. Effect of panel tilt on SVF and SCF

Apart from the skyline profile, the pitch angle of a roof segment and module tilt also have an effect on the SVF and SCF. As visible in figure 2.8, the visible part of the hemisphere decreases as the plane of array is tilted. This directly affects the SVF and it can affect the SCF if the invisible part of the hemisphere crosses with the sun path throughout the year.

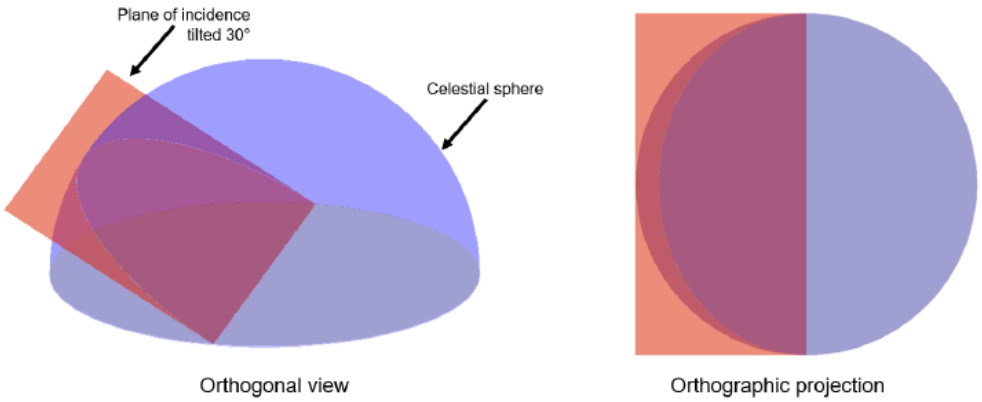

Figure 2.8: Representation of the intersection between a tilted plane and the celestial sphere, showing the effect on the visible part of the hemisphere, adapted from [21].

In this research, the effect of panel or roof tilt on the SVF and SCF has been taken into account by using a relative irradiance map or sensitivity map as shown in figure 2.9. A sensitivity map is composed for a specific combination of panel orientation and tilt. The grey parts in the image show the parts of the hemisphere that are behind the panel, in which the sensitivity is 0. In these cases, the angle between the normal vector of the panel and the direction of the grid point is more than 90°. These parts are thus considered to be blocked during the SVF and SCF analysis. This obstruction of parts of the sun path by a non-zero segment slope or module tilt was the only addition made to the SCF calculation.

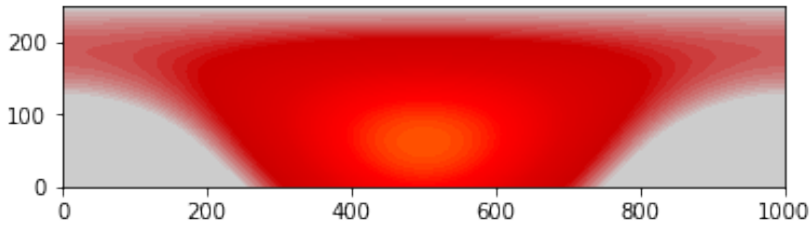

Figure 2.9: Relative irradiance map for a panel tilted by 45° and directed precisely towards the South, shown in obstacle view dimensions of Solar Monkey.

The SVF calculation method was also altered to deal with this effect. The numerator of the SVF was still calculated as discussed in section 2.3.2; all sensitivity values for unobstructed pixels were added up, and grey areas in the sensitivity map do not contribute as their sensitivity is zero. However, this sum was divided by the sum of all sensitivity values of the sensitivity map of a panel with 0° module tilt or roof segment tilt as follows:

$$SVF = \sum_{n_x=1}^{1000} \sum_{n_y=1}^{250} \frac{f_v(n_x, n_y) \cdot S(n_x, n_y)}{S_{z-t}(n_x, n_y)} \tag{2.16}$$

where S_{z-t} is the zero-tilt sensitivity value for a panel placed horizontally on a flat roof. In this way, the SVF would decrease according to the invisible part of the hemisphere. To ensure that the sensitivity map would take this effect into account correctly for the SVF, the SVF was calculated for an unobstructed sky, for different values of module tilt. The results are shown in figure 2.10, and are according to the validation of two SVF calculation methods that were presented in [21].

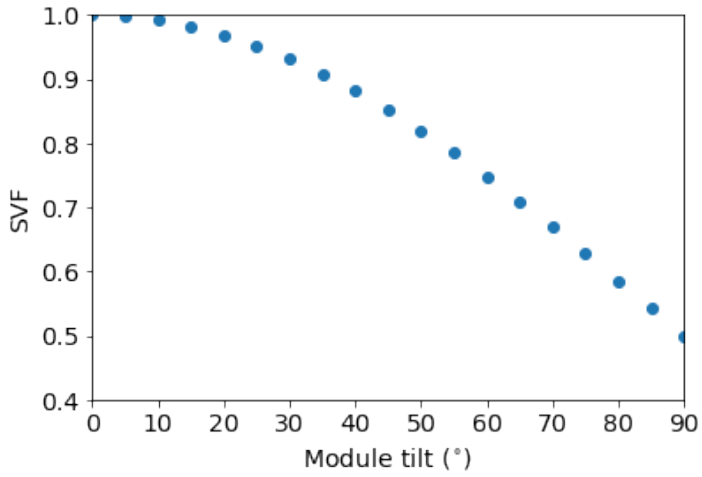

Figure 2.10: The effect of module tilt on the SVF.

2.4. Irradiance and yield modeling

In this section, two methods of irradiance prediction will be explained. The first method is currently used by Solar Monkey and the other one was developed at Delft University of Technology [21]. After that, the method of conversion from irradiance to AC yield will be described. Lastly, a yield prediction method will be introduced that does not take into account skyline profiles.

2.4.1. Irradiance prediction of Solar Monkey

Solar Monkey has the following approach for calculating the performance of a solar panel:

1. First, 200x200 meters of the elevation data of the Netherlands around the panel is retreived [39].
2. Knowing the height of the panel itself, Solar Monkey has developed their own algorithm to efficiently store the obstacles in a matrix similar to figure 2.6.
3. The optimal irradiance (average daily sum of global irradiance received by the a system with the optimal tilt angle) is obtained from the PVGIS API for the specific location and orientation of the roof in Wh/m^2.
4. Knowing the azimuth of the panels, the tilt angle of the panels, and the pitch angle of the roof, the global irradiance on the module surface is determined per month, under a free horizon.
5. The relative intensity is constructed for the orientation and tilt angle of the module or pitch angle of the roof segment (figure 2.8).
6. The monthly sun paths are calculated for a set of geo-coordinates (figure 2.7).
7. The average global irradiance on a PV module is calculated for every month, taking into account the obstacles, relative intensity and the solar position throughout that month.
8. Knowing the rated power of the panel, the global irradiance is used to compute DC power. This will be explained further in section 2.4.3.

Due to the Intellectual Property of the Solar Monkey algorithm the steps are only described globally. The sensitivity of this information that forms the basis of their software does not allow for these steps to be described into further detail.

2.4.2. Irradiance prediction by SVF and SCF

In his research, Calcabrini used five irradiance components: direct irradiance, reflected irradiance, and the three diffuse components as recognised by Reindl and Perez: circumsolar, isotropic and horizontal brightening [21]. These components are schematically shown in figure 2.11.

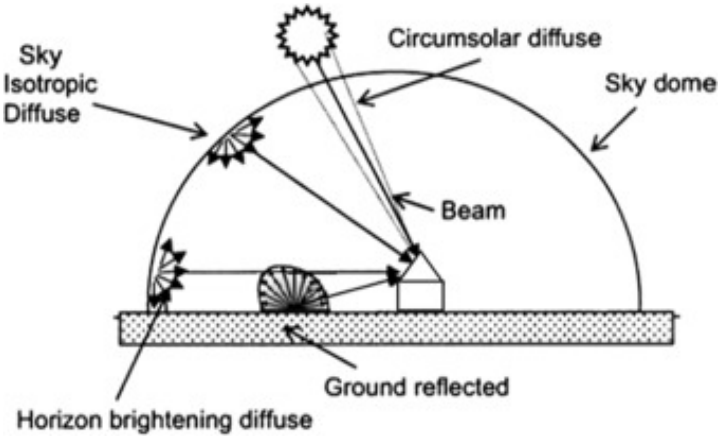

Figure 2.11: Schematic view of the distribution of solar radiation on a tilted surface according to anisotropic diffuse sky model, adapted from [40].

Since rooftop PV often concerns urban environment, the horizontal brightening effect is minimal [21]. Therefore, this component was neglected and only four irradiance components from equation 2.9 were taken into account.

Calcabrini divided the total POA irradiance in two parts, one related to the SVF and one related to the SCF, shown in equation 2.4.2.

$$I_y = I_y^{SCF} + I_y^{SVF} \tag{2.17}$$

In this equation I_y^{SCF} is related to the direct irradiance component and the circumsolar diffuse irradiance, since they are both directly related to the sun being behind an obstacle. The I_y^{SVF} is related to the isotropic diffuse irradiance and the reflected irradiance, as can be expected from equation 2.2.6.

Calcabrini carried out a validation study with 80 synthetic skyline profiles and 12 real skyline profiles. For these locations he calculated the expected irradiance with equation 2.4.2. After that, a quadratic fit was done for I_y^{SCF} and I_y^{SVF}. It was found that I_y^{SVF} could be estimated with a linear function. The following two fitting functions were developed, predicting annual irradiance with $\pm$10% accuracy [21]:

$$I_y^{SCF} = \sum_{k=1}^{3} c_k \cdot \left(SCF^k - 1\right) \tag{2.18}$$

$$I_y^{SVF} = \left(c_4 + c_5 \cdot \alpha_{ground}\right) \cdot SVF \tag{2.19}$$

The fitting coefficients are dependent on the orientation and tilt angle of a module and lastly the location of the roof. The ground albedo α_{ground} is usually assumed to be around 0.2. Once the 5 fitting coefficients and albedo are known, the total irradiance on a PV module can be calculated solely by knowing the SCF and SVF. As will be discussed in section 3.3, the roofs investigated in this report are located in the region of Eindhoven, the Netherlands. Therefore, the WGS coordinates of Eindhoven [51.44, 5.470] have been used to calculate the coefficients according to Calcabrini's approach, presented in [21].

For the validation study done in this research, the 5 fitting coefficients were calculated for 35 orientations and 10 tilt angles and the 350 possible configurations were saved in 5 matrices. The orientation was varied clockwise from North by steps of 10 degrees, whereas the tilt angle was incremented from zero degrees by steps of 10°. Once the five coefficient matrices were known, the irradiance could be calculated for every roof segment with a known orientation and tilt angle, after calculating the SCF and SVF. Since the coefficients were only known for steps of 10°, 2D linear interpolation was done for the coefficients by their orientation and tilt angles.

2.4.3. Irradiance conversion to AC yield

The irradiance can now be predicted via two methods. The next step is to convert the influx of irradiance into electricity within the PV module. While the solar irradiance reaches the surface of the

solar panel, the incoming photons will create pairs of charge carriers, inducing direct current. The process of DC electricity generation is affected by the temperature of the module, as well as by the intensity of irradiance. Figure 2.12 shows the I-V and P-V curves for a crystalline Silicon PV panel with a nominal power of 200 W at different temperatures. For higher temperatures, the voltage decreases drastically while the current only increases marginally. This results in lower module efficiency at higher temperatures.

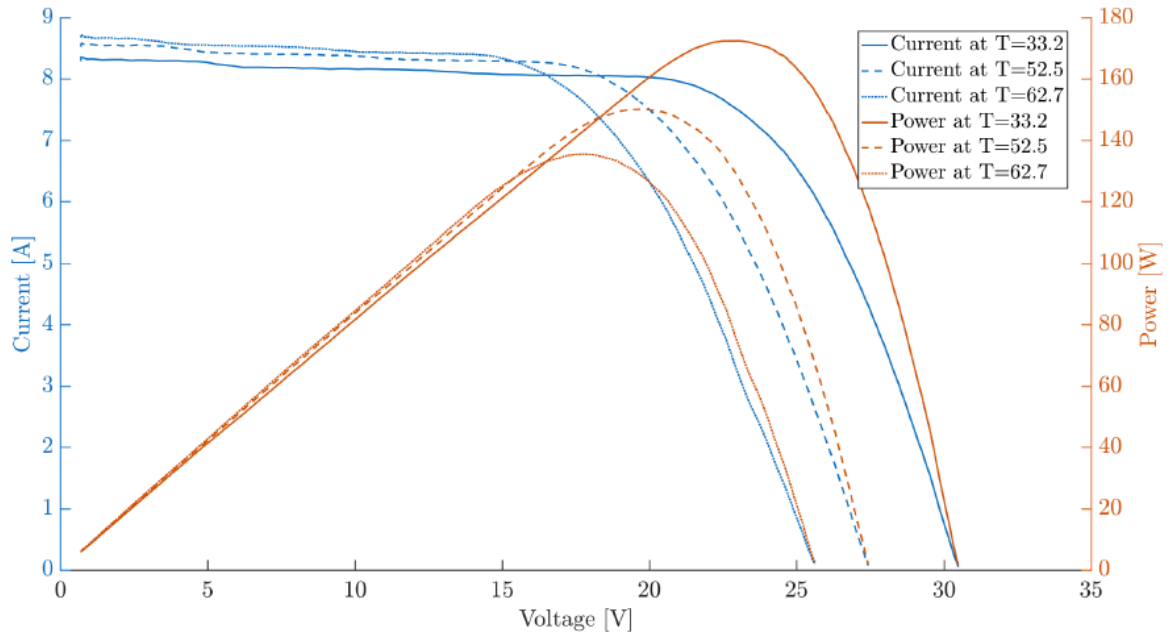

Figure 2.12: I-V and P-V curves at varying temperature for Multisol P6-54 Series 200W c-Si panel by Scheuten Solar, gotten from [41].

Besides temperature, the power curve of PV modules is also affected by the intensity of irradiance itself. To take these temperature and irradiance effects into account, different thermal models can be used to estimate the cell temperature and an electrical model can be implemented to quantify the generation and transport of charge carriers under the given meteorological conditions.

The generated DC electricity needs to be converted to AC for most domestic appliances. This conversion takes place in an inverter. The average operational efficiency of this conversion is between 95 and 99% for most modern inverters [42]. Their efficiency depends on the topology of hardware and also changes with a varying DC power and input voltage [43]. Since the operational efficiency of an inverter depends on its load profile, it depends on the generated power by the PV system. The efficiency can be estimated by the European inverter efficiency, an averaged operating efficiency encompassing a yearly power distribution for a central-European climate.

Throughout the whole process of electricity transport, part of the electricity is lost due to the resistance of the conducting cables, often referred to as Ohmic losses. Ohmic losses are usually found acceptable below 2% for large plants and below 4% for residential and commercial plants, according to [44].

The quick-scan developed in this thesis is meant to serve for many different purposes. It is to work for a wide range of panels, system designs and electrical components. The quick-scan is developed for a first indication of yield prediction, and not designed for academic accuracy. Therefore, it was chosen not to focus on the various categories of losses from irradiance to AC electricity.

Solar Monkey currently takes into account the factory STC efficiency for PV modules to convert irradiance to DC electricity. After this, an additional loss of 7% is attributed to cable losses, inverter losses, soiling losses, and the effects that temperature and irradiance have on module efficiency. In this research, validation will be done in terms of the measured AC yield of existing installations. Therefore, the average percentage of losses will be tuned after yield prediction in order to achieve the best

prediction.

In many parts of this research, instead of the AC system yield, the system performance will be studied. The system performance is expressed in kWh/kW$_p$ per year, and is a measure for the performance of the system, independent of the amount of PV panels or their rated Wattpeak. This allows for comparison of systems with different sizes and panels with different amounts of nominal power.

2.4.4. Yield prediction without obstacle view

The third yield prediction method that was used in this research did not take into account the obstacle view from a roof. It uses the API of PVGIS, introduced in section 1.4.3, to calculate the anual AC yield [45]. The API is used with the following settings:

- The latitude and longitude of the central point on the roof are used for the for the average irradiance.
- The landscape horizon height is taken into account, although this effect is minimal in the flat landscape of the Netherlands.
- The peak power is defined as the amount panels times their rated power.
- Crystalline silicon is chosen as PV technology.
- The segment pitch angle, tilt and the azimuth of the fitted panels are send to the API. They are chosen to be fixed, so without solar position trackers.

PVGIS already takes into account the spectral losses/gains, temperature-dependent module losses and low irradiance losses. These losses are expected to contribute for around 4%. For other system losses, such as cable losses and the inverter efficiency, an additional 3% is expected to be lost. In this way, for the method without obstacles also a combined 7% is taken into account beforehand. As mentioned earlier, the actual percentage of losses will be determined by setting the yield prediction to a zero-mean average deviation.

2.5. Statistical parameters for validation of quick-scan

In this section, different parameters are introduced that will validate the results of the quick-scan. First, a method will be explained with which predictions can be made unbiased. After this, the concepts of mean absolute deviation and relative standard deviation will be discussed.

2.5.1. Optimisation of the prediction

In this research, the yield prediction will be optimised for large sets of roof segments. All yield prediction values can be factorised to obtain a prediction method that has the same mean value as the measured yield values. By doing this, different yield prediction methods can be compared in terms of their statistical spread in accuracy.

2.5.2. Mean absolute deviation

When evaluating the accuracy of a yield prediction, it seems intuitive to consider at the mean absolute deviation from the measured yield. The mean absolute deviation (MAD) then gives a measure for the accuracy of the prediction and the statistical dispersion. Expressed in percentage of the actual measured value, this variable is called mean absolute percentage error (MAPE) or mean absolute percentage deviation (MAPD). However, several issues arise with using this metric [46]. Whereas MAD is a robust statistic, MAPE is not. For forecasts which are too low the percentage error cannot exceed 100%, but for forecasts which are too high there is no upper limit to the percentage error [47]. This results in a bias towards lower forecasts when MAPE is used to compare the accuracy of prediction methods [47, 48]. Therefore the MAPE will not be used as a measure of the spread in the yield prediction results.

The same bias occurs for mean percentage over-prediction of the amount of fitted panels with respect to the actually placed panels. The fitted panels can be a maximum of 100% lower than the panels that were actually installed, but the percentage of panel fitted more than actually installed is not limited. Therefore the mean percentage over-prediction is biased. However, since only one panel fitting method is used it is considered acceptable to still used this metric.

2.5.3. Relative standard deviation

Standard deviation is a widely-used metric for the spread of outcomes in statistical models. The standard deviation has the same unit as the predicted variable, however when expressed as a percentage of the mean prediction, it is referred to as the relative standard deviation (RSD) or coefficient of variation (CV). Compared to the MAPE, the RSD is always at least as high as MAPE. The quadratic nature of calculating standard deviation results in outliers having a larger effect than in the MAPE. Since distances from the mean are squared, this makes the deviations of a small number of outliers more dominant. The RSD will be used to compare different yield prediction methods in terms of their spread in prediction accuracy.

Chapter summary

This chapter introduced the conventions to define the solar position and module orientation. Different irradiance components and ways to model them were described. Then, obstacle views were presented, and how they relate to the sky view factor and sun coverage factor. Lastly, two prediction methods for the irradiance on a module were introduced and the losses that occur in a PV system were mentioned. Additionally, a yield prediction method was introduced that neglects the skyline profile. The three methods will be used in the quick-scan algorithm for yield and performance prediction.

3

Roof shape information

In order to design a quick-scan that works for any address it is necessary to have information about its roof. For the fitting of panels, it is vital to know the roof area available for PV. For yield prediction, it should also be known what is the slope and orientation of the roof. Land register data is freely accessible data of buildings contours in the Netherlands. However, most roofs do not consist of one flat plane without any obstacles. Readaar is involved in the PVISION project, to divide roofs in segments with different slope and orientation. The roof segments will enable the quick-scan algorithm to be more accurate than with solely the perimeters of buildings.

This chapter will introduce the building contours and roof segment data set used to test and validate the quick-scan. After explaining the principles to prepare these roof segments for panel fitting and yield prediction, the limitations of the data will be mentioned, and how some of these problems have been resolved. Then, this chapter will present the approach to determine an optimal panel orientation aligned with the roof segment edge. Lastly, a final selection of roofs is made for validation of panel fitting and yield prediction.

3.1. Land register data

The Dutch Cadastre, Land Registry and Mapping Agency, named Kadaster, collects spatial and administrative data on Dutch properties and spatial regulations. This information is uploaded to an independent national mapping system an accessible as open data via the API of PDOK (Publieke Dienstverlening Op de Kaart).

In this research the land register data is essential for enclosing the roof segments that were constructed by Readaar. The land register data contains the building contours of virtually every building in the Netherlands, which quite precisely corresponds to the roof edge. For flat one-segment roofs, these contours could even be enough for accurate yield prediction. This will be validated in section 6.4. In that section, also a boundary scenario will be investigated, where only the building contours are used, and no roof segments.

3.2. Aerial mapping and roof segment recognition

PVISION partner Readaar creates roof segments, making use of stereo photos and LiDAR height data of the Netherlands. A roof is selected by using the building contours from land register data for the roof of interest. A disparity map can be made by comparing and matching the roof points of a pair of aerial images taken from a different angle. This technique is often referred to as stereo-matching in the geographic information system (GIS) industry. High objects which are closer to the camera will displace more than the ones that are lower and thus further away. Since the difference in angle between the two images is known, the displacement of a point between the two images is solely dependent on the height [49]. Therefore, the disparity map shows a 3D point cloud for the all roof points that were compared, as shown in figure 3.1.

Figure 3.1: Stereo aerial images and a disparity map of a roof, gotten from Readaar [49].

Since different segments have different orientations and pitch angles, their colours are slightly different on a picture. In order to split the roof into different segments, a first segmentation is done on the basis of colour. This colour filtering creates a large amount of different segments, as visible on the left of image 3.2. After this, the height data is used to unify segments with similar orientations and pitch angles. These orientations and pitch angles are found by calculating the normal vectors on the planes that form the segments. After this, the remaining segments form a 3D representation of the roof segments and potential obstacle segments like chimneys or roof windows. This process is described in further detail in research of Vermeer, carried out at Readaar [50]. The whole process can be seen in figure 3.2.

Figure 3.2: Colour filtered roof segments unified by height Data and shown in 3D, gotten from Readaar [49].

On average, it takes Readaar one forth of a second to construct the roof segments of a building, where 93% of the roofs larger than 1 m^2 are detected [49]. Small roof segments and segments that are on the shadow side of an aerial image are more difficult to detect. This is respectively caused by a lack of height data points for small segments and little contrast to find a stereo-pair of pixels in the shade. Also, the difference in colour at the borders of segments is harder to detect for shaded roof segments [49].

3.3. Roof segment data of Readaar

For this research, roof segment data was created by Readaar. The buildings that were chosen to be analysed, currently have PV systems installed on their roof, which are monitored by Solar Monkey. The roofs that were studied are located mostly in the region of Eindhoven, since Solar Monkey has most customers with monitored systems in this region.

The roof segments are provided as shapefiles (or polygons), containing the 3D coordinates of the contours for each roof segment. Each segment is marked with a bag id (which is linked to a Kadaster data file for every unique building) and a Readaar id, which is unique for each roof segment they identified. The shapefile also contains the segment slope (pitch angle) and direction (orientation in horizontal plane).

Throughout this research two sets of roof segment data have been used:

1. The first set of roof segments, referred to as ”set 1” comprises a set of 952 roofs, divided into 4316 roof segments, so on average 4.5 segments were identified per roof.

2. The second set of roof segments, referred to as ”set 2” comprises a set of 345 roofs, divided into 1292 roof segments, so on average 3.7 segments were identified per roof.

Set 1 was obtained exactly according to the method described in section 3.2. Set 2 was created as a prospected improvement to set 1. To make the segments cover a larger part of areas within building contours, three methods were used [51]:

1. For neighbouring roof segments which intersect in 3D, such as for hipped roofs and gable roofs, the line of intersection between the planes was determined. The roof segments are filled from both sides up to this line.

2. For neighbouring roof segments that do not intersect, but have a height difference, a line of intersection is drawn in the middle when looking at them in the z-direction. The roof segments are filled from both sides up to this line.

3. For the parts of roof segments that stretch to the edges of the building contour, the segment will be filled up to the edge of this cadastre shape.

In figure 3.3, a group of roof segments is shown, generated with the methods used in set 1 and set 2. It can be seen that the edges of roof shapes are much more straight.

Figure 3.3: Aerial image and roof segments of Readaar, created by method for set 1 (left) and set 2 (right), gotten from [51].

Since the segmentation of roofs is dependent on the building contours and both the contrast and colours in the aerial image, the segments in both sets still contain several flaws. These will be addressed in the following section.

3.3.1. Limitations of roof segments

There are multiple limitations to the roof segments in data set 1. Firstly, the edges of roof segment shapes in set 1 are often not straight. This is because the segmentation is done based on points, and not lines. Segments are cut off by land register data, so the outer edges of the roofs are usually sharply defined, however the line between two roof segments is often not very straight.

Some shaded roof segments are only detected partially or not at all. This is often a problem for low flat roofs next to higher houses. For shaded roofs fewer points can be matched.

Sometimes existing roof segments are not detected because they were outside of the land register shape. This could be because of a house renovation or because land register data was not correct. Garden sheds, garages and building extensions can be overseen for this reason.

3.3.2. Dealing with in-roof obstacles

Many obstacles are detected or left out of roof segments by the stereo-matching. They are either excluded from all segments, or they form separate roof segments. If obstacles are excluded from any

roof segment, this actually means the height points found by stereo-matching could not be added to the plane of the neighbouring roof segment. In data set 1, these areas remained unconsidered if they are small. If the area of an obstacle was sufficiently large, the algorithm of Readaar converted it to a separate roof segment. Since a minimum segment area was used to filter for panel fitting, most obstacles could be filtered out for panel fitting.

Sometimes obstacles are detected, however they form a segment within another roof segment. An example is shown in figure 3.4. Both the chimney and the dormer were detected. The chimney was excluded from the roof segmentation, however the dormer is positioned within the another segment on the roof. The current format of obtaining segments poses a problem. The dormer segment is not defined as a gap ("hole") in the larger roof segment, but as another segment on which panels could be fitted. This results in the detected obstacle segment being counted twice by the panel fitting algorithm, instead of neglected.

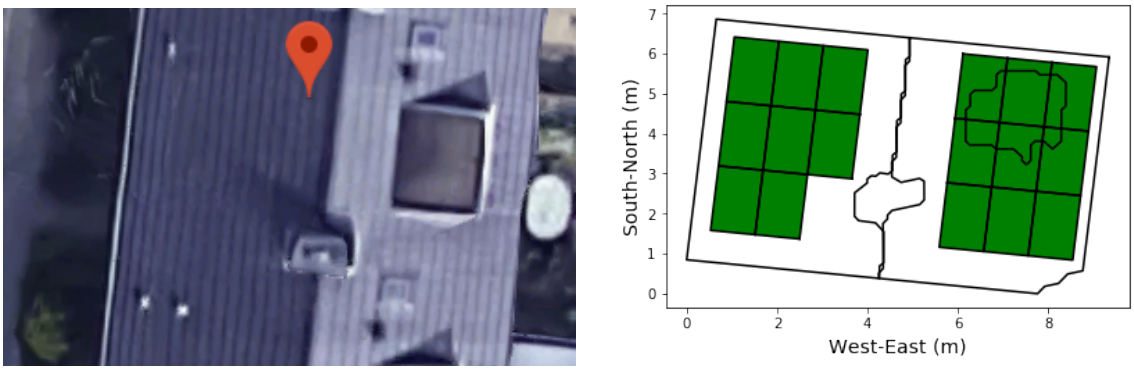

Figure 3.4: Aerial image and visual schematic of fitted panels on roof with bag id 772100000318351 in set 1.

Although many obstacles on roofs are detected, there are still multiple examples of unidentified dormers, roof windows, air-conditioning units and chimneys. Although obstacle detection is not the focus of this study, this does limit the accuracy of the quick-scan algorithm. More limitations and complications related to roof segment data will be discussed in section 6.6.4.

3.4. Determining roof segment orientation

In order to fit the maximum amount of panels on a roof segment and generate the largest amount of energy, it is necessary to know the orientation of a roof. For highly pitched roof segments, the orientation of the roof segment is chosen for the panels. However, for flat roof segments, panels are preferred to be directed towards the South, often aligned with the shape of the roof. Throughout this research, roof segments with a slope of less than 10 degrees were categorised as flat, and segments with a higher slope were considered pitched. Throughout the roofing industry, this boundary is chosen between 5 and 15 degrees, with the Eurocode 1991-1-4 mentioning 5 degrees and multiple roofing websites reporting values in between 9.5 and 15 degrees [52–55]. No scientific studies were found to set this variable according to PV standards, such that it was decided to keep the boundary at 10 degrees.

In the data set of Readaar, both an angle of inclination (pitch) and orientation are given. For each roof segment, a plane was fitted through all the points in the 3D point cloud of the disparity map as mentioned in section 3.2. The normal vector to this plane was decomposed in the roof segment pitch angle and an orientation in the horizontal plane. The orientation of a roof segment was determined by taking the horizontal projection of the normal vector to the segment plane.

This method seems to be a logical approach for pitched segments, however for nearly flat segments the marginal pitch of a segment towards a certain orientation is of minimal importance. If, according to the height data, a segment is pitched by 0.5 degrees in a certain direction, this direction is not related to the preferred panel orientation.

Even for highly pitched roof segments the orientation found for the horizontal projection of the normal vector was often found to be misaligned with respect to the roof shape by several degrees. There are various phenomena that cause the the orientation found to deviate from the exact orientation

of the roof. Firstly, some roof segments found by Readaar contain obstacles or are in fact containing multiple roof segments. These mistakes in segmentation will lead to outliers in the point cloud and they will change the fitted plane. Therefore this will lead to errors in the direction of the normal vector and orientation. Secondly, small roof segments will have larger errors in the orientation found, since there are fewer height data points. Lastly, shaded segments have fewer data points that can be matched on the basis of colour recognition, such that the inaccuracy in segment orientation becomes larger.

3.4.1. Alternative method for orientation calculation

Knowing that the given orientation was useless for flat segments and inaccurate for pitched segments, another method for determining the panel orientation for maximum panel placement was developed. The roof segments in the dataset are polygons, that exist of a list of (x,y,z) coordinates, which are connected by lines. The length of each line segment was determined for the x and y coordinates, and then the longest line segment within the roof segment shape, the longest polygon side, was chosen. For the longest polygon side, the orientation could be determined by the following equation:

$$A_{ls} = tan^{-1}\left(\frac{x_2 - x_1}{y_2 - y_1}\right) + 180° \tag{3.1}$$

In this equation A_{ls} stands for the azimuth of the longest side, x_i and y_i refer to the x and y coordinates of a point in the roof shape and 180° is added to make the angle positive, defined clockwise starting from the North.

In the Northern hemisphere, panels should be directed to the South as much as possible for a high performance. To place a maximum amount of panels it is often preferable to align them with the roof edge. The alignment with the edge of the roof is preferred since it will usually fit the largest amount of panels. Moreover, it is often regarded to be more aesthetic. In figure 3.5 an example is shown, in which 33% more panels can be fitted for an aligned setup, whereas the output per panel would only drop marginally.

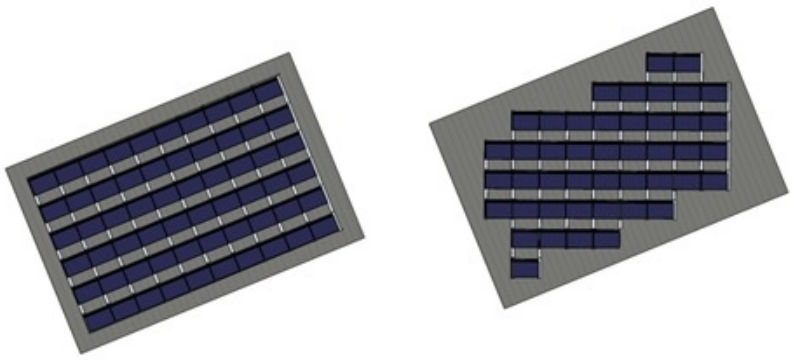

Figure 3.5: Aligned with roof vs due south panel layouts for flat roof, adapted from [56].

Most roof segments have rectangular shapes or perpendicular angles. Considering this, for flat roofs the following angles were calculated:

$$B_i = A_{ls} + \sum_{i=1}^{3} 90 \cdot i \tag{3.2}$$

$$\begin{cases} A_i = B_i & B_i < 360° \\ A_i = B_i - 360° & B_i \geq 360° \end{cases} \tag{3.3}$$

Where i= 1,2,3 so A_i are the three orthogonal components to A_{ls}, which are always between 0° and 360°, ensured by equation 3.3. From here, the direction closest to the South (180°) will be chosen as the panel orientation for all flat roof segments. An example is shown in figure 3.6.

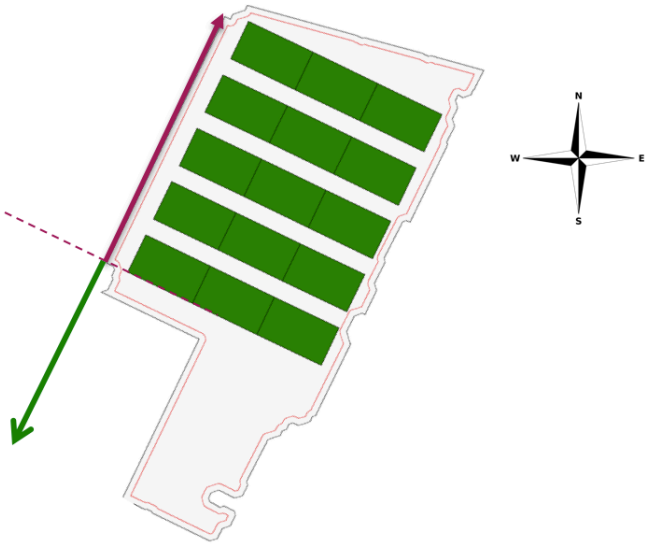

Figure 3.6: Determining of the panel orientation for maximum panel placement on flat roofs. The purple arrow represents the direction of the longest polygon side, whereas the green arrow represents the orthogonal component closest to the South.

For pitched roof segments, the orientation given in the data set is used as a reference. However, the closest orthogonal component of the longest polygon side turned out to be more accurate. An example of a highly pitched roof (24° pitched towards the West) is shown in figure 3.7. The orthogonal components are calculated by use of equations 3.2 and 3.3 and the direction closest to the normal vector orientation (the blue arrow) is chosen.

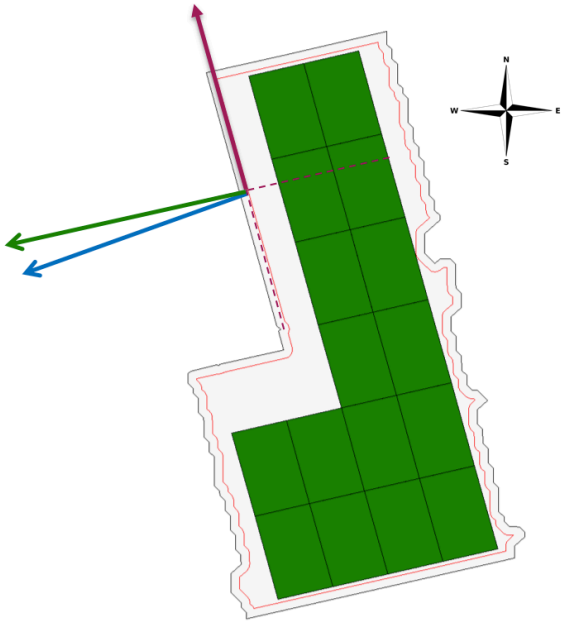

Figure 3.7: Determining of the panel orientation for maximum panel placement on pitched roofs. The blue arrow represents the horizontal projection of the normal vector, given in the data set. The purple arrow represents the direction of the longest polygon side, whereas the green arrow represents the orthogonal component closest to the orientation that was originally given.

Beware that the longest polygon side is not always the longest side of the roof segment. Since some side of the roof segments are very uneven or wobbly, the side containing the longest straight line might be a different one. However, since most segments are rectangular or contain only perpendicular

angles, this doesn't pose a large threat for the method. Additionally, this problem occurs far less in data set 2, where the edges of roof segments are much straighter.

3.4.2. Panel orientation approach for different roof segment types

The approach described for finding the segment orientation was validated for a set of 520 roof segments. The difference was calculated (in °) between the given segment orientation and the calculated nearest orthogonal component of the longest side direction. This error was visualised for different roof pitch angles in figure 3.8.

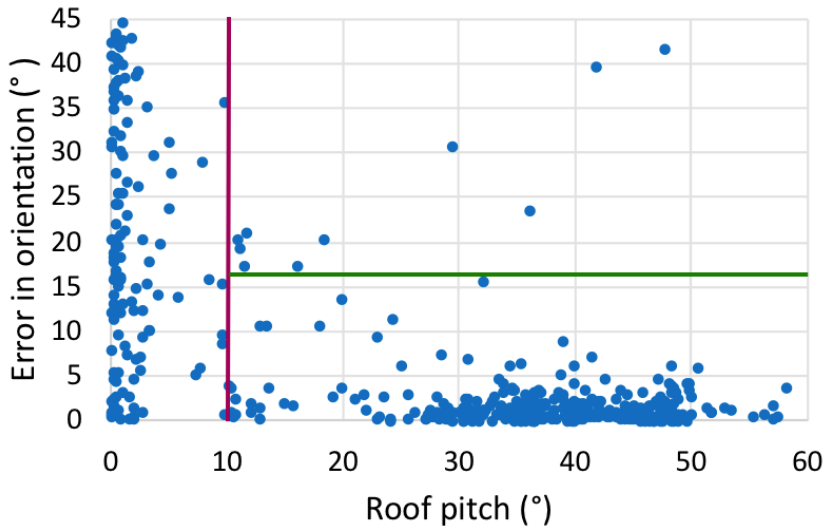

Figure 3.8: Degrees of error between closest orthogonal component of longest polygon side and horizontal projection of normal vector for a set of 520 roof segments. The purple line splits up pitched and flat roof segments. The green line shows an error boundary of 16°, above which issues were identified with the current approach for pitched segments.

It can be seen that for flat roofs, with a roof pitch less than 10°, the orientation given in the dataset is useless. The error between this orientation and the orientation found by the longest polygon side method is evenly distributed between 0 and 45 °. For pitched roofs, with a roof pitch higher than 10°, the deviations between the two sources are generally much lower. The absolute error was found to be within 6.3° for 95% of the pitched segments.

The green line in figure 3.8 shows another empirical boundary that was set. Manual inspection was carried for all pitched segments with an orientation error larger than 5°. For this set of 28 roof segments aerial images were used to determine which of the two orientations was right. It was found that for errors below 16°, the closest components of the longest polygon side was always the correct orientation.

Table 3.1: Issues for pitched roofs with deviations of over 16° between two sources of segment orientation.

Amount of segments	Issue
4	Large error in orientation of normal vector
3	Closest longest polygon side is correct
2	Over-segmentation, no correct orientation found
1	Normal vector orientation true (segment triangular)

For errors larger than 16° between the two orientations, different issues were identified, as shown in table 3.1. This group of 10 roof segments comprises 1.9% of the original set of 520 roof segments. The contents of the table will be explained:

- For 4 out of the 10 segments, the orientation deducted from the normal vector contained a large error. Therefore, the closest component of the longest polygon side was not the right one, but

another component of the longest polygon side was the actual orientation. There is currently no method to resolve this issue.

- For 3 out of 10 roof segments, the original approach for pitched segments worked well. The closest component of the longest polygon side was the right one.
- For 2 segments, the segmentation of the roof had gone wrong. Actual roof segments had been divided in a multitude of segments, thereby making both methods unable to find the actual orientation. There is currently no method to resolve this issue.
- One segment turned out to be triangular, and therefore the orientation of the normal vector was right, but the one found by the longest polygon side was off by 30°.

As can be seen, the original approach for pitched segments was found to be only 30% accurate for these cases. The problems finally occurred with 7 segments, being 1.3% of the initial amount of roof segments. Still, since no better alternative method was available, this method was used for pitched segments with large orientation errors. However, in the outcomes of the quick-scan, it will be indicated if the panels are fitted on a roof segment with such large orientation errors. Therefore, errors can be expected in this subset of the results.

3.5. Final selection of roofs

Although the whole Readaar data set 1 contains almost a thousand roofs, only 237 roofs were used for the validation study in this thesis. This was decided upon four reasons:

- The roofs used for validation needed at least one year of yield data measurements.
  - Many roofs had less measurement data than this, thereby making validation of annual yield prediction impossible.
- The module layout of the actually placed systems needed to be known and saved in the correct format within the database of Solar Monkey.
  - Throughout the last years, the amount of modules and their configuration for systems in the Solar Monkey database had been saved in different ways. Therefore, some of the total amounts of panels were incorrect or inaccessible.
- Even if the module layout was present in the Solar Monkey database, this could contain errors. Manually encountered errors were filtered out.
  - Two systems with bag id 150100000032246 and 772100000327176 were found to have an incorrect amount of panels in the database of Solar Monkey. These cases were identified since they had a very high annual performance of above 1300 kWh/kW$_p$, which is unrealistic for PV in the Netherlands. The reason is that the PV installer placed a different amount of panels on the roof, than he had placed in the software design.
- Each system needed to be connected to one single land register number, such that the same roof surfaces that were considered for PV in reality could be accessed by the quick-scan.
  - Incidentally, data such as the land register number (bag id) was missing, making automatic validation impossible without manual check of the true building used for PV installation.

In set 1 there are 237 roofs, divided in 1311 roof segments that meet these requirements. Set 2 contains 210 roofs and 807 roof segments that meet the same requirements.

Chapter summary

In this chapter the concept of building contours and roof segments were introduced. First, the techniques to compose roof segments set were described. After this, the data features and their limitations were explained. A novel approach was introduced to find the desired orientation of panels for different types of roof segments. Finally, two sets of roof segments were narrowed down based on three criteria.

4

Quick-scan algorithm

The quick-scan can be divided in several steps. Figure 4.1 shows the three stages identified: segment selection, maximum panel fitting and yield calculation. A more detailed depiction of the algorithm structure can be found in appendix B.

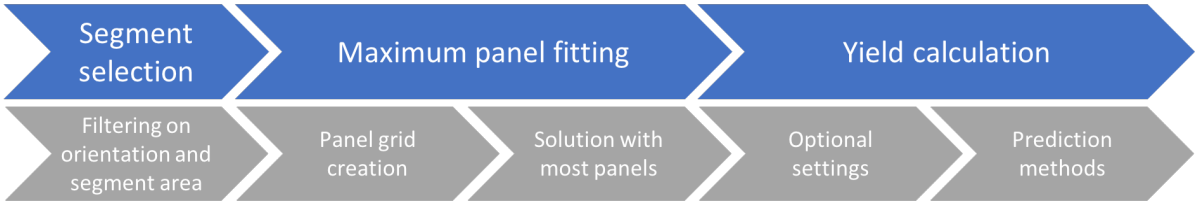

Figure 4.1: Global structure of the quick-scan algorithm.

During the selection of segments, roof segments with a low potential for PV are filtered out. These segments are either filtered out because they are too small to fit an interesting amount of panels, or because they are pitched towards the North, and therefore will have a low energy yield.

During the maximum panel fitting step, different assumptions will be done to create a panel grid. This grid will be shifted over the roof, counting the solution fitting the most panels.

Then yield calculation is carried out. Several options are incorporated in the algorithm to make it serve different purposes. The user can choose whether to align panels with the roof edge or not. Additionally, the user can choose whether to use east-west setups for panels. Regarding prediction methods, three prediction methods can be selected as explained earlier: the Solar Monkey method, a method using only the SVF and SCF, and a direct call to PVGIS, neglecting the skyline profile. For the first two methods, one central point on each roof segment is chosen to retrieve the skyline profile.

This chapter will describe the various steps in the quick-scan algorithm that was developed. It will introduce the assumptions made, how parameter values were set and how the quick-scan can be configured.

4.1. Segment selection and filtering

As mentioned earlier, the roof segments are provided as 3D-polygons. These files contain the 3D coordinates of the contours for each roof segment, a bag id per roof, Readaar id per roof segment, and the average orientation and pitch angle for the plane of the segment. Both id's, the orientation and pitch angle within the shapefile are imported in a dataframe of the Python package called Pandas. This is done for the ease of further operations during the quick-scan.

Naturally, the algorithm could be used for any segment, however, in order to speed up the calculation of rooftop potential it was useful to filter out segments with little potential at an early stage. Therefore, two optional filtering steps are implemented, on the basis of orientation and segment area. These filtering steps and the extraction of segment coordinates are described in the following sections, along with the distance to be kept from the roof segment edge.

4.1.1. Filtering on orientation of pitched segments

As mentioned before, the roof segments are divided in flat and pitched segments. At this stage, flat roof segments do not pose constraints for the orientation of panels. However, for aesthetic and ballast reasons, pitched roof segments do require panels to be mounted in a flat manner. Therefore the direction towards which a segment is pitched determines the azimuth of the panels.

For the northern hemisphere the POA irradiance is much lower for panels tilted towards the North. This results in a lower performance. However, the minimal acceptable performance is not a number that customers have set clearly in their mind. From conversations with solar installers, it was found that a payback time is a more tangible measure to consumers [57]. The payback time is the amount of years in which the initial investment for a solar system has been earned back by costs savings thanks to the electricity generation of the solar system. Neglecting interest and non-linearity in the investment costs for residential solar systems, the payback time can be calculated as follows [22]:

$$\text{payback time} = \frac{\text{initial investment}}{\text{annual return}} \tag{4.1}$$

Filling in this equation for PV systems, this would result in payback time t_{pb} of:

$$t_{pb} = \frac{N_p \cdot P_r \cdot C}{p_e \cdot E_{y,AC}} \tag{4.2}$$

In which N_p stands for number of installed panels, P_r stands for rated power per solar panel (in kW_p), C is system costs (in €/W_p), p_e is the electricity price (in $€/kwH$) and $E_{y,AC}$ is the annual AC energy yield of the system (in kWh/y). Equation 4.2 can be made independent of the amount of fitted panels by inserting the system performance, expressed in kWh/kW_p per year. This results in:

$$t_{pb} = \frac{C}{p_e \cdot Y_f} \tag{4.3}$$

In this equation, Y_f stands for system performance, also mentioned as final annual yield in other literature [58, 59]. The value of C has been set to 1300 €/W_p and the electricity price has been estimated at 0.2 $€/kWh$, according to common values for solar installers that are using the Solar Monkey software [57]. The value for C seems reasonable when compared with the combined system costs, installation costs and balance of system costs in the Dutch solar trend report of 2018 [60]. According to these installers, customers want their system to pay itself back within a maximum of 10 years [57]. Therefore, roof segments with Y_f below 650 kWh/kW_p per year can be neglected by the quick-scan algorithm.

The performance without taking into account shading profiles was calculated by using the yield calculation method explained in section 2.4.4. Obstacle losses are neglected in this yield prediction method. Taking this into account, it is estimated that systems with a calculated performance of 700 kWh/kW_p will not have a higher actual performance than 650 kWh/kW_p. This 7% is assumed the minimum loss for shading by the skyline profile and panel mismatch due to (partially) shaded panels in series. This seems acceptable because shading is reported to be as high as 17 to 27% for urban environments [61].

In table 4.1, segment orientation features are shown for pitched segments with less than 700 kWh/kW_p per year. As can be seen, these low-performance segments are all located in the range of 0.3 to 60.3° and 299.6 to 359.2°.

Table 4.1: Orientation features for pitched segments in data set 1 with Y_f less than 700 kWh/kW_p per year, predicted by the method neglecting skyline profiles.

Orientation condition	**Minimum A_M**	**Mean A_M**	**Maximum A_M**
A_M<180°	0.34°	16.46°	60.30°
A_M>180°	299.61°	335.43°	359.18°

Since the daily position of the sun is symmetric around the South (180°), the borders of our orientation filtering will be set at 60° and 300°. In other words, all segments with both: (1) a segment pitch angle of above 10°; and (2) a segment orientation below 60° or above 300°, will be filtered out

beforehand, since they result in undesirably low performance values. Moreover, it will save the quick-scan algorithm time, since it can neglect all roof segments with this set of properties. Out of a subset of 1909 roof segments in data set 1, 450 were found to have orientation below 60° or above 300°, comprising 23.6% of the roof segments.

4.1.2. Extraction of segment coordinate lists

After this first filtering step, the coordinates of the remaining segments are extracted from the dataframe. The amount of coordinates per segment is counted and the average height is determined per segment. This average height will be used later in the yield calculation, when determining the obstacle view in section 4.3.2.

4.1.3. Distance from the roof segment edge

For reasons concerning aesthetics, ballast, safety and ease of installation there is a minimum distance PV modules should be away from the edge of a roof. For pitched roofs this is about 30 centimetres, mostly determined by the regulations for the installation of mounting systems [62].

For flat roofs, common distances from the edge are 50 to 100 centimetres [56]. Mounting systems generally require a minimum of about 60 centimetres from the roof edge of flat roofs for product warranty [63]. Sometimes fences are placed for the safety of system installation, which require about 1.4 meter from the roof edge [62]. For installation without fences on high roofs, the distance should be increased to around 3 meters of buffer zone [62]. Nevertheless, there are also options for installation via scaffolds or rope-secured access, which do not require the minimal distances of 1.4 and 3 meters.

In this research, the distance from the roof edge has been set to 60 centimetres for flat roofs and 30 centimetres for pitched roofs. However, when carrying out manual checks, it was found that the actual distance from the roof edge greatly varied between different PV systems. Even the minimum requirements of 0.3 meter and 0.6 meter were not always kept for the systems installed on pitched and flat roofs respectively. In many cases installed solar panels were virtually touching the edges of a roof. Therefore, the distance from the roof segment edge is a large factor in the inaccuracy of maximum panel placement.

4.1.4. Filtering on segment area

If a segment is smaller than the area of a PV panel, it does not make sense to take it into account for panel placement. Moreover, as described in the previous section, the usable area of a roof segment significantly decreases by the distance to be taken from the edge. Even if one single panel could be fitted on the usable area of a roof segment, this is often not desirable. Since the POA irradiance and shading pattern can be very different from those of other roof segments used for a PV installation, this one panel should be optimised separately. Because of panel mismatch, it is often not desirable to connect this panel in series to panels with a different orientation, tilt angle or shading profile. Apart from that, it is aesthetically very unappealing to place one panel on a roof segment. Therefore placing one panel on a different roof segment is not preferable.

Table 4.2: Area features of roof segments in data set 1 per amount of panels fitted on them.

Fitted panels	Minimum segment area [m^2]	Mean segment area [m^2]
1	4.33	12.48
2	8.46	16.82
3	12.53	19.80

In order to make the quick-scan time-efficient, it was therefore decided to require a minimum segment area for panel fitting. Table 4.2 shows the minimum segment area and mean segment area for roof segments on which a certain amount of panels was fitted by the quick-scan algorithm. From this, it can be deducted that roof segments smaller than 8.4 m^2 would not fit more than 1 panel. Therefore, all roof segments with an area less than 8.4 square meters are filtered out in this step of the quick-scan algorithm. Out of a subset of 1909 roof segments from data set 1, 971 were found to be smaller than 8.4 square meters, comprising 50.9% of the roof segments. Combining this filtering

step with the earlier filtering on pitched segment orientation, 1197 of the 1909 segments were filtered out, being 62.7% of the original roof segments.

4.2. Panel fitting algorithm

In the following part the panel fitting algorithm will be described. The different assumptions that were done will be explained, and the method for panel fitting will be presented.

4.2.1. Standard panel features

For the quick-scan algorithm, the following settings were chosen to be standard:

- Standard panel dimensions of 165 by 99 centimetres. The thickness of the panels is not used for the quick-scan.
- The generation capacity of a panel was set to 300 W_p. This was decided since the quick-scan should show the full potential of a roof and therefore high-efficiency panels were chosen for the indication of system size. Naturally, a customer could also set this to 275 W_p if that is preferred.

All other standard settings for the quick-scan can be found in appendix A.

4.2.2. Segment orientation

For determining the segment orientation and the orientation of aligned panels, an approach was used as described in section 3.4.2. For flat roofs, the longest edge was found like in section 3.4.1, and after that the orthogonal component closest to the South was chosen for panel orientation. For pitched roofs, the given segment orientation was taken as a reference instead of the South.

4.2.3. Panel alignment with roof shape

As mentioned in the previous section and shown in figure 3.5, for flat roofs often it is preferable to align panels with the edges of a roof. However, in some circumstances it can be feasible to not follow the shape of the roof directly, but direct the panels precisely towards the South. This is an option that is built-in for the quick-scan. The user of the quick-scan can choose whether to align panels with the shape of the flat roof segments, or to choose for 180 degrees precisely. For east-west configurations, the panels would then be directly pointed towards the East and West, instead of aligned with the roof edges.

4.2.4. Panel fitting on flat roofs

For flat roof segments, the following settings were defined as standard. All modules were expected to be installed in a landscape manner, since this is by far the most dominant configuration on flat roofs [57]. A tilt of 13° was chosen for panels, since this is a common setting for panels in the Netherlands and mounting systems are often available for this angle [57]. Apart from that, low module tilt minimises ballast requirements and maximises the roof area utilisation.

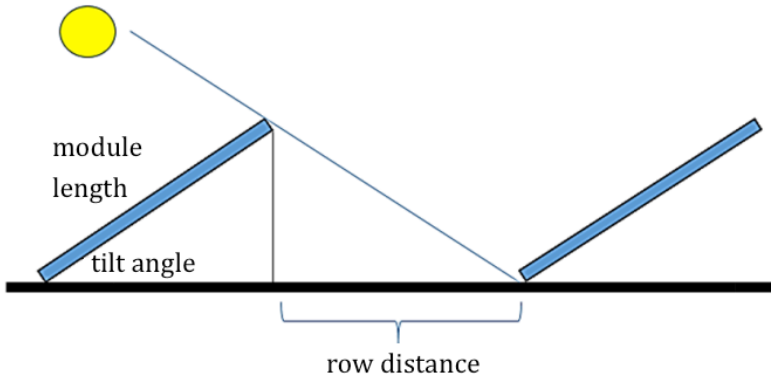

Figure 4.2: Schematic view of row distance between panels.

In this research, the row distance was defined as in figure 4.2. A distance of 70 cm was maintained as the horizontal distance between the projected end of a tilted panel and the ground side of a consecutive row. This setting was chosen based on preferences of PV installers working with Solar Monkey software [57].

East-west layouts

East-west layouts can be beneficial for multiple reasons. First of all, this type of layout generally allows for more panels to be placed on top of a roof than in the traditional south-directed setup. This increases the roof area utilisation, and often also the total system yield (in kWh/year). On the other hand, the investment costs of a system with more panels are higher and the performance per panel (in kWh/kW$_p$) would be lower than in a South-directed panel layout. For off-grid purposes, east-west setups have a flatter yield generation pattern, with more generation at the start and end of a day, and a lower peak during mid-day. This generally requires less storage capacity, since supply and demand are matched better throughout time. For grid-connected systems, east-west setups can also be beneficial. In the Netherlands for example, industrial and commercial rooftop PV do not benefit from the same financial structure as residential rooftop PV. Since there is no net-metering regulation in place for these large systems, it is more beneficial to use as much generated energy as possible for self-consumption. The flatter generation peak of east-west setups is then preferable.

As mentioned in section 4.2.3, east-west setups can be roof aligned or not. For example, if a flat roof is rectangular but not directed precisely towards east and west, a setup with panel orientations 75° and 255° could be chosen as ideal east-west setup. Alternatively, the panels can be directed precisely towards the East and West. For the quick-scan, the standard row distances and tilt angles for flat roofs were also chosen for east-west setups.

4.2.5. Panel fitting on pitched roofs

For pitched roof segments, the panel is placed directly onto the segment. This means that the segment azimuth and pitch angle determine the panel orientation, and no additional module tilt is added. There is no row distance between panels, so panels are placed directly next to each other. For all pitched roof segments, the fitting algorithm is carried out twice. Namely, the module layout can be in portrait or landscape, and both options have to be investigated to find the maximum panel configuration.

4.2.6. Panel grid creation and maximum panel fitting on roof segment

A panel grid is created according to the settings specified for flat and pitched roofs. For an easy example of panels with zero tilt, a visual impression is given in figure 4.3. The panel grid, in this case with zero row distance, is shifted with small steps in the x and y direction. For the quick-scan, the step size was set to 10 cm in both directions. For every new position of the grid, the amount of panels within the roof shape minus a set distance from the edge are counted. The distance from the edge is chosen 30 cm or 60 cm, as explained in section 4.1.3. The position in which most panels are fitted gives the maximum panel fitting solution.

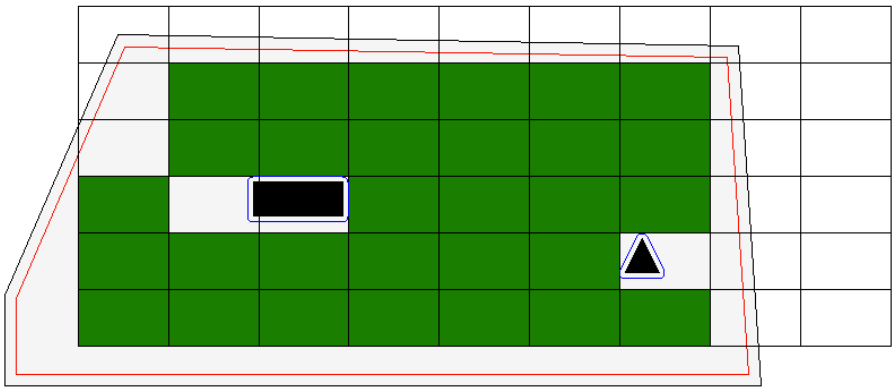

Figure 4.3: A panel grid is translated over a roof shape in the x and y direction, while counting the panels that fit within the roof edge minus a buffer distance without intersecting with obstacles, gotten from Bronkhorst [5].

In his thesis, Bronkhorst also provides a method to take into account obstacles within a roof segment. The algorithm then always checks if panels are intersecting obstacle segments. In some cases obstacles within roof segments are identified by Readaar. An example was previously shown in figure 3.4. Currently these obstacle segments are not taken into account by the fitting algorithm, however this could be a nice improvement to implement for Readaar in the future.

Naturally, realistic roof segment shapes are not automatically aligned with the x and y axis of a panel grid. Therefore, a roof segment is always rotated around its centre by desired azimuth of the panels. Then the panel grid is created. After this step, the roof shape and panel grid are rotated back and the grid is translated in steps parallel and perpendicular to the panel azimuth. All in all, the technique of panel fitting is the same as described in figure 4.3, but the process is slightly complicated by rotation of the roof segment shape.

4.3. Yield prediction

In this part different yield prediction algorithms will be explained. The quick-scan was designed in a modular way, so different yield prediction methods can be applied and their results can be tested independently.

4.3.1. Current prediction method Solar Monkey

In section 2.4.1 the various steps were described for yield prediction carried out in the Solar Monkey design software. In their software, Solar Monkey calculates an obstacle view for the centre of each panel that is placed on a roof. In order to take into account generation losses due to the panel mismatch, all obstacle views of panels in the same string are summed. This way the direct irradiance is expected to be zero for the whole string if one of the panels in a series string is shaded. The yield calculations in the Solar Monkey app take about 1 second per panel, so this only takes long for roofs with large amounts of panels.

4.3.2. Quick-scan for central point on segment

For the quick-scan, the same approach is used as for yield prediction in Solar Monkey. However, instead of calculating the obstacle view for every panel, it is only calculated for one point in the centre of a roof segment. The expected irradiance is converted to AC energy by taking into account the STC output of the panel and applying a combined system loss of 7%, as explained in section 2.4.3.

At first, only AHN height data was used to determine the height of the central point, from which the obstacle view could be determined. However, this resulted in many roof segments with very high obstacle losses from 60% to 100% for about 7% of all roof segments. The problem was caused by the view point being virtually under the roof, therefore seeing the roof itself as an obstacle. Small errors in the AHN height data or small obstacles right next to the central point on the roof segment could cause this.

Another method of determining the height of the central point on the roof was taking the average between the highest and the lowest z-coordinate in the roof segment polygon that was provided by Readaar. However, using this method only, there was a similar amount of roof segments were roof segments with high obstacle losses occurred. This could be due to an inaccuracy in the roof plane fitted through the point cloud as described in section 3.2. Nonetheless, since the polygons were not derived from the AHN data, the problems occurred at another subset of roof segments.

The problem was eventually resolved by using both height sources. In order to always calculate obstacle losses for a point that is located above the roof level, the maximum of two height data points was taken. One height measurement for the central point was taken from the AHN grid, whereas the other was the average of the highest and lowest z-coordinates that were provided in the Readaar roof segment shapefiles. By basing this reference height on two data sources (LiDAR and stereo-matching) problems with the shading analysis were overcome. There were no roof segments left with over 60% obstacle losses.

The new method did result in slightly higher yield predictions, since the obstacle view could be taken for a point that was in reality positioned 10 to 30 cm above the roof. Resolving the initial problem was however seen as more important than the increase in yield prediction of 0.1 to 0.3% that was observed for roofs that had not had obstacle with the old method.

Yield prediction for east-west layouts

For east-west setups, yield prediction is done for both panel orientations. Unfortunately, the current algorithm cannot yet count the amount of panels directed to the east and west respectively. Therefore, in east-west setups it is expected that half of the panels are east-oriented and half towards the west. This is still a flaw in the current algorithm, however as the quick-scan is meant as a first indication for the expected yield, it was outside of the current project scope to resolve this problem.

4.3.3. Quick-scan via SVF and SCF

This yield prediction method is coded according to the steps mentioned in section 2.4.2. There are five matrices with fitting coefficients for every 10° azimuth and tilt angle. Linear interpolation is carried out between the coefficient values, knowing the actual orientation and tilt of the panels on a roof segment. After that, the SVF and SCF are calculated. Equations 2.18 and 2.19 lead to the total irradiance expected on the panel. The expected irradiance is converted to AC energy by taking into account the STC output of the panel and applying a combined system loss of 7%, as explained in section 2.4.3.

4.3.4. Quick-scan without obstacles

In this yield calculation method, the skyline profile is not taken into account. A direct call is done to PVGIS, so only the panel orientation and tilt are affecting the performance, as explained in section 2.4.4.

Chapter summary

In this chapter the quick-scan algorithm was explained in detail. The first part introduced the different functions for the selection of the segments and filtering them by orientation and size. By applying these two filtering steps, 62.7% of all roof segments in data set 1 were determined to be irrelevant for the quick-scan algorithm. The second part explains how panels were fitted within the roof segment shapes. Lastly, the different methods of yield prediction were described.

5

Maximum panel fitting

In this chapter the results of the panel fitting stage of the quick-scan will be presented. Apart from assessing the performance of maximum panel fitting method, this chapter is meant to discuss the problems and complications that were faced and how they were dealt with.

First, several problems that were encountered will be discussed. Then, the results will be shown for different types of roofs. Finally, the results will be validated with respect to real systems and reasons for deviations will be explained.

5.1. Problems that were faced

Different complications were encountered:

- The first challenge that was encountered for panel fitting, was finding the desired panel orientation. The approach to this was described in section 3.4.
- As mentioned earlier in section 3.5, it was important to have information about the actual PV systems placed on the roofs that were studied. To validate the results of this research, the amount of fitted panels and their module layout had to be extracted from the Solar Monkey database. During the last years, the method of saving panel layouts in the Solar Monkey software had changed. Therefore it was not possible to access all systems. The final selection of roofs was therefore made according to 3.5, for which the amount of installed panels was known and easily accessible.
- After subtracting a distance from the edge of a roof segment, sometimes small roof segment turned out to not exist anymore. Therefore, a check was added to see if a roof segment polygon was empty after this subtraction.

5.2. Individual results for different roof types

The panel fitting algorithm was carried out for different types of roofs. The results will be shown for flat and pitched roofs will be shown throughout the next sections. The goal is to give an qualitative impression of the maximum panel fitting results.

It can be noticed that the roof segments in set 1 have more uneven edges and more undetected roof surface than the roof segments in set 2. However, in set 1, more obstacle segments were either excluded from segmentation or detected as separate roof segments.

5.2.1. Individual results for flat roofs

In this section several examples will be shown for roofs with at least one flat segment. The panel fitting algorithm generally works well for rectangular roofs with few obstacles. As visible in figure 5.1, a setup was designed which closely related to the actual system. The row distance in the real system was chosen to be larger, however the distance from the edge seems fully neglected. The lower roof is not fully identified since it is in the shade, however this turned out positively for the panel fitting

performance: only one panel was placed on the lower roof. Naturally, the panel could still be deleted by filtering the results on a minimum of for example 2 panels per roof segment. The small obstacle on the east side of the roof was not identified during the segmentation.

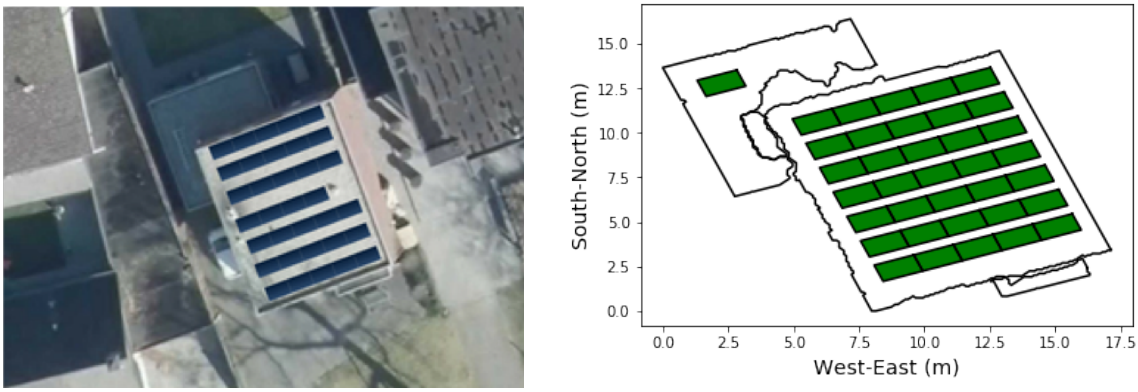

Figure 5.1: Aerial image and visual schematic of fitted panels on a set 1 roof with bag id 794100000400819.

Figure 5.2 shows a combination of a flat and a pitched roof segment. In the real system, panels were only installed on the pitched segment, however as an indication of potential the quick-scan performed well. Apart from that, it can be seen that the obstacle problem occurs as mentioned in section 3.3.2. Although the obstacle segment was identified, the segment is not defined as a gap within the larger roof segment.

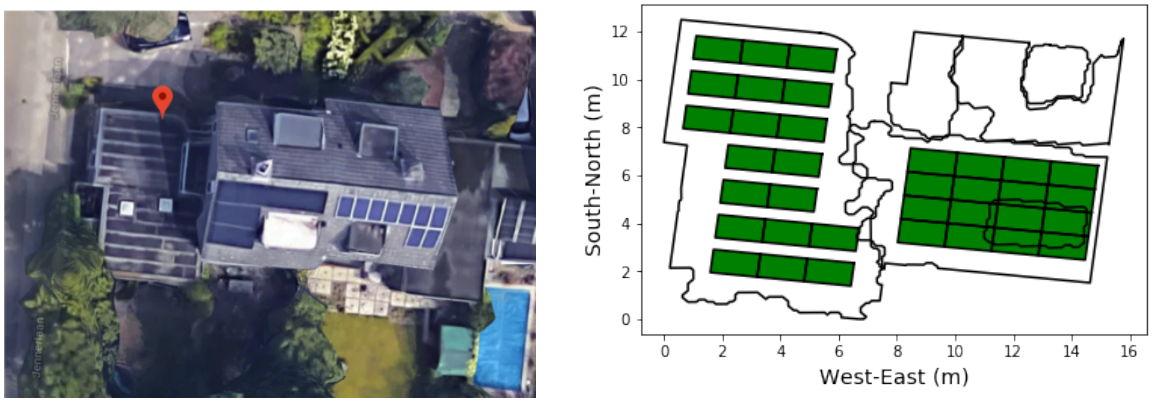

Figure 5.2: Aerial image and visual schematic of fitted panels on a set 1 roof with bag id 772100000256155.

5.2.2. Individual results for pitched roofs

In this section, two examples will be shown for panel fitting on pitched segments. In figure 5.3 an ideal panel fitting situation is shown for a pitched roof in a terraced house. The chimney is excluded from both roof segments. Apart from that no complications occur for this roof type.

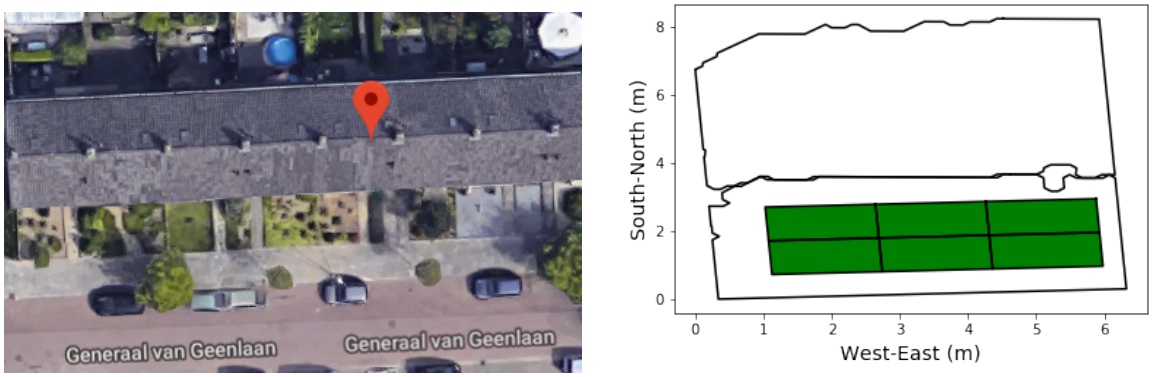

Figure 5.3: Aerial image and visual schematic of fitted panels on a set 1 roof with bag id 772100000314974.

Figure 5.4 shows panel fitting on two sides of a pitched roof. It can be noted that one roof window is detected on the west side, while another dormer on the east side is not found. Therefore the final amount of fitted panels is not realistic.

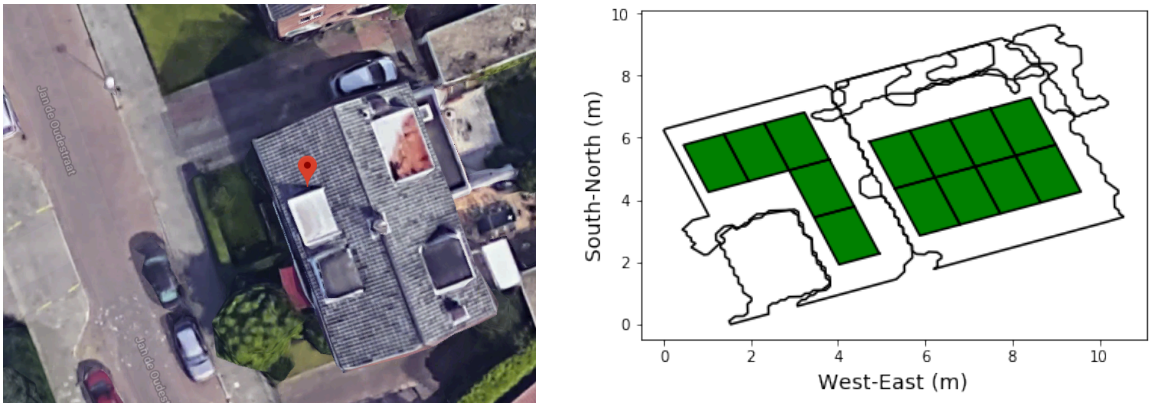

Figure 5.4: Aerial image and visual schematic of fitted panels on a set 1 roof with bag id 772100000281885.

5.2.3. The effect of distance from the roof edge on panel fitting

This section will focus on the effect that the distance to be kept from the roof edge has on the panel fitting results. Zooming in on the West segment of figure 5.4, it is interesting to see how a slight change in the minimum distance from the roof edge can drastically change the panel layout. Figure 5.5 shows how the panel layout changes when the distance from the roof edge is incremented from 15 to 20 centimetres.

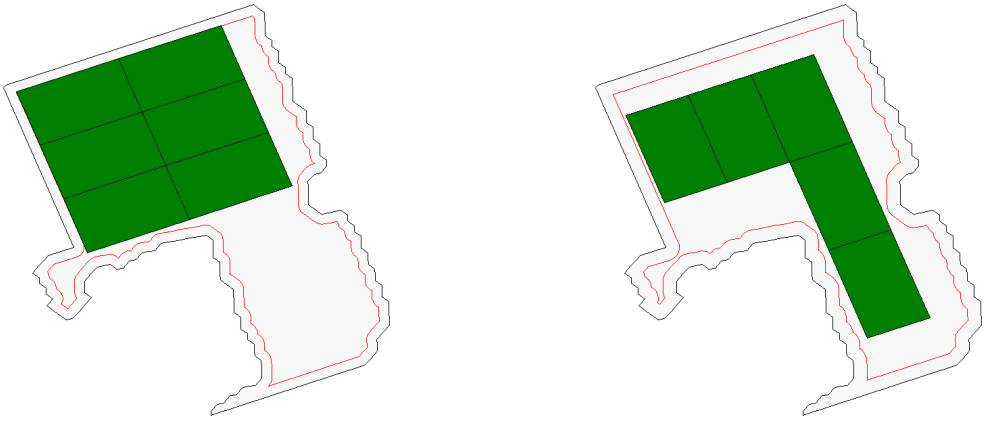

Figure 5.5: Visual schematic of fitted panels on a West-oriented roof segment in set 1 with bag id 772100000281885, carried out for 15 and 20 cm from the roof segment edge.

A more extreme case was found in data set 2 when investigating why a roof that was expected to be high-performance by the quick-scan, actually had a much lower annual yield. In figure 5.6, it can be seen that panels were drawn on a flat roof with zero tilt and virtually no distance from the edge. Moreover, no panels were placed on the pitched roof, that has a near-ideal orientation for PV.

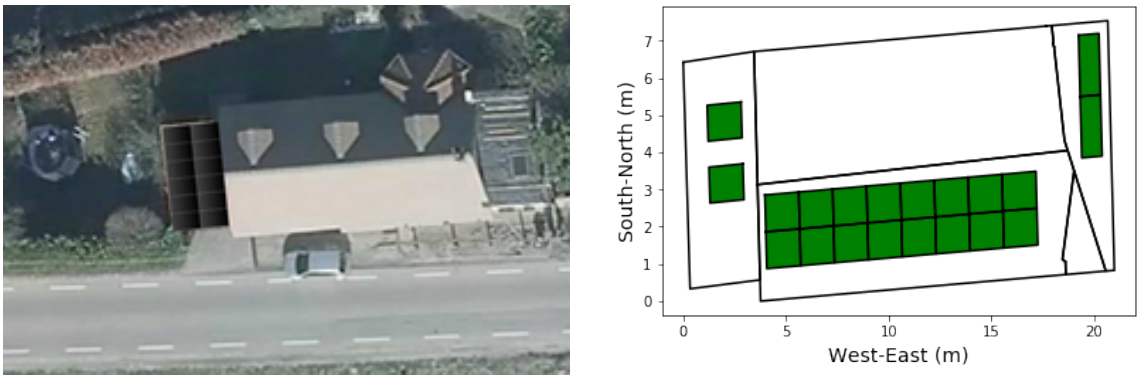

Figure 5.6: Aerial image and visual schematic of fitted panels on a set 2 roof with bag id 677100000598161.

The great variation observed in the chosen distance from the roof edge makes it very difficult to verify the panel fitting approach. However, for the first testing of maximum panel fitting, standard settings for the distance from the roof segment edge will be used as mentioned in appendix A.

5.3. Validation with existing systems

In this part, a statistical validation will be carried out for the panel fitting algorithm on the roof segments of set 1 and 2. The amount of panels fitted on all selected roof segments of a roof is compared to the amount of panels that was actually installed.

5.3.1. Set 1

Panel fitting was first carried out with standard settings as described in appendix A. As such, the minimum area was set to 8.4 square meters and all pitched roof segments with an orientation between 0° and 60° or between 300° and 360° were filtered out. Also, the distance from the roof edge was 30

cm for pitched roofs and 60 cm for flat roofs. The results of the maximum panel fitting algorithm are shown in figures 5.7 and 5.8.

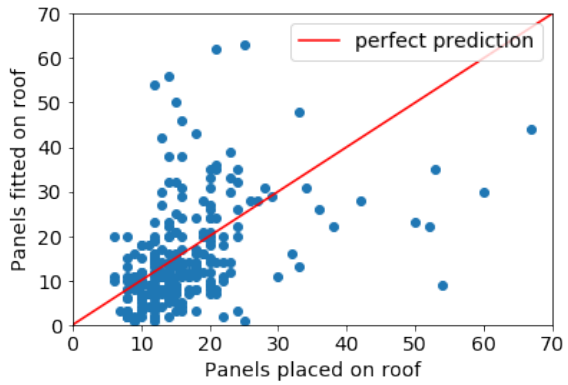

Figure 5.7: Scatter plot for panel fitting on 235 roofs divided into 446 roof segments in set 1 according to standard settings.

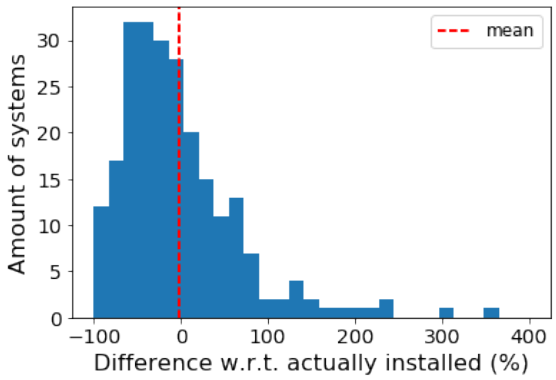

Figure 5.8: Histogram for panel fitting on 235 roofs divided into 446 roof segments in set 1 according to standard settings.

It can be seen that there is an average under-prediction of 1.8%, whereas the relative standard deviation in between the fitted and actually placed amount of panels was 72.7%. It was at this time unknown what was the reason for these large deviations. For example, it could be caused by filtering out the wrong roof segments, or too large distances taken from the roof segment edges. That's why a boundary condition test was carried out, as explained in the following section.

Boundary condition test

A boundary condition test was carried out for the maximum panel fitting, with conditions that would allow for the absolute maximum amount of panels to be placed on all roof segments. The goal of this test was to see if there would still be roofs where the algorithm would fit less panels than the amount that was actually placed.
The following settings were used:

- No azimuth filtering for pitched segments
- No minimum segment area
- Distance from roof edge is always 0 cm

In figures 5.9 and 5.10 the results of the boundary condition test can be seen. Naturally, the algorithm overestimates the amount of panels on the roof, on average by 122%. A more unexpected result is that still for 13.8% of the roofs, less panels are fitted than actually placed on the roof.

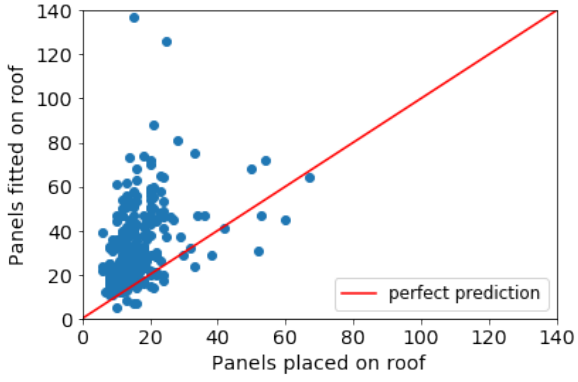

Figure 5.9: Scatter plot for panel fitting on 237 roofs divided into 1311 roof segments in set 1 according to described settings.

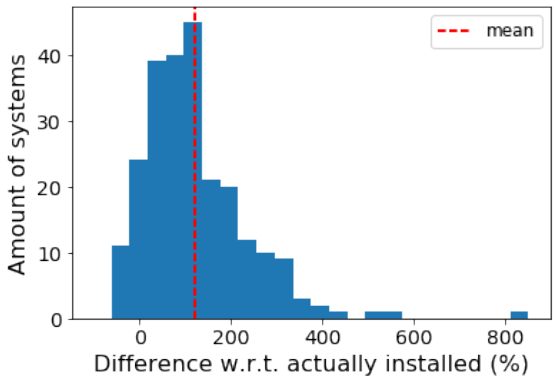

Figure 5.10: Histogram for panel fitting on 237 roofs divided into 1311 roof segments in set 1 according to described settings.

The fact that less panels are fitted for this collection of roofs is a clear indication that panel fitting is not going well for those roofs. It is highly unlikely that all roof segments, so very small or North-directed ones, would be used. Even if this was the case, the distance kept from the roof edge was expected to be larger then 0 cm. The under-prediction of panels is expected to be caused by unnecessary over-segmentation or non-detection of parts of the roof.

5.3.2. Set 2

Roof segment set 2 was created to straighten the edges of roof segments and detect larger parts of the full buildings contours. The maximum panel fitting was carried out again, using the same set of standard settings. Figures 5.11 and 5.12 show the results.

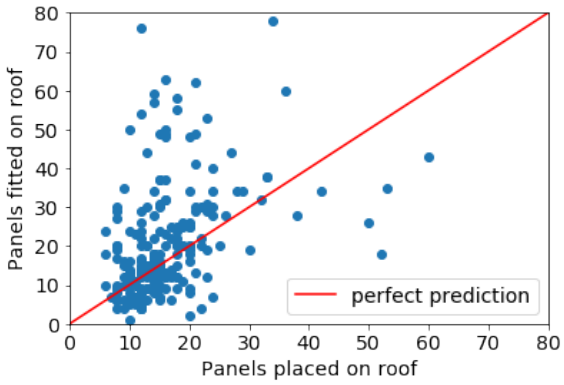

Figure 5.11: Scatter plot for panel fitting on 208 roofs divided into 452 roof segments in set 2 according to standard settings.

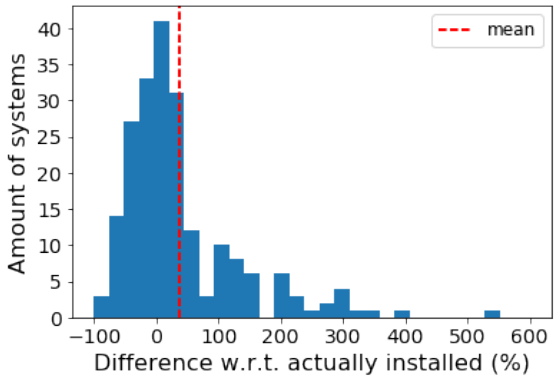

Figure 5.12: Histogram for panel fitting on 208 roofs divided into 453 roof segments in set 2 according to standard settings.

The mean over-prediction of panel placement was 38.4%, while the RSD was reduced to 65.1% with respect to set 1, where it was found to be 72.7%.

Boundary condition test

The same boundary condition test was carried out for set 2. In this way it could be checked if there would still be cases where less panels were fitted than actually installed. Results are shown in figures 5.13 and 5.14.

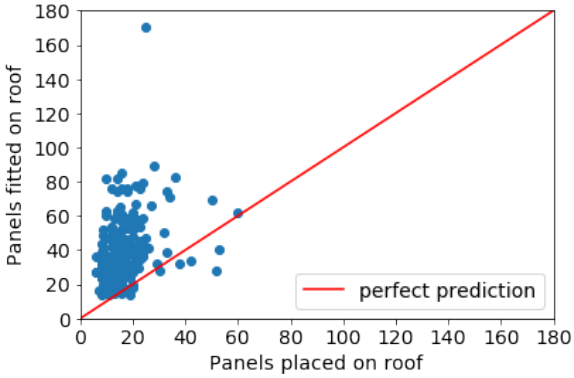

Figure 5.13: Scatter plot for panel fitting on 210 roofs divided into 807 roof segments in set 2 according to described settings.

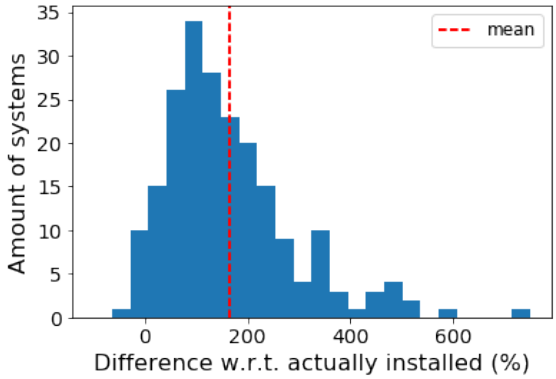

Figure 5.14: Histogram for panel fitting on 210 roofs divided into 807 roof segments in set 2 according to described settings.

The average over-prediction for panel placement had increased from 122% to 164% for this second boundary condition test. Under-prediction with respect to actually installed panels only occurred for 4.3% of the roofs, while this was 13.8% for the first data set.

5.3.3. Reasons for deviations from installed amount of panels

For the roofs where underestimation took place, various areal images and system layouts were checked manually. The most severe reasons will be discussed.

- Most problems were caused by shape flaws in the roof segments, as can be seen in figure 5.15. For example, over-segmentation was found to be a frequent cause of fewer panels to be fitted. Moreover, parts of segments in shade were occasionally not detected by the stereo-matching, decreasing the usable area for panels to be placed.
- In a single case, it was found that panels were placed on a garden house or garage instead of the building for which the land register data was available. This is problematic, however this issue was only encountered once, as visible in figure 5.16.

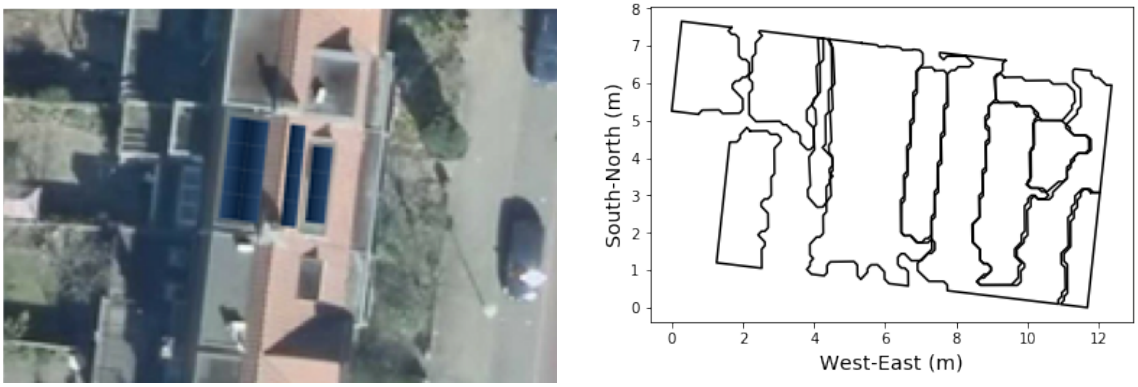

Figure 5.15: Aerial image and visual schematic of fitted panels on roof with bag id 772100000262124.

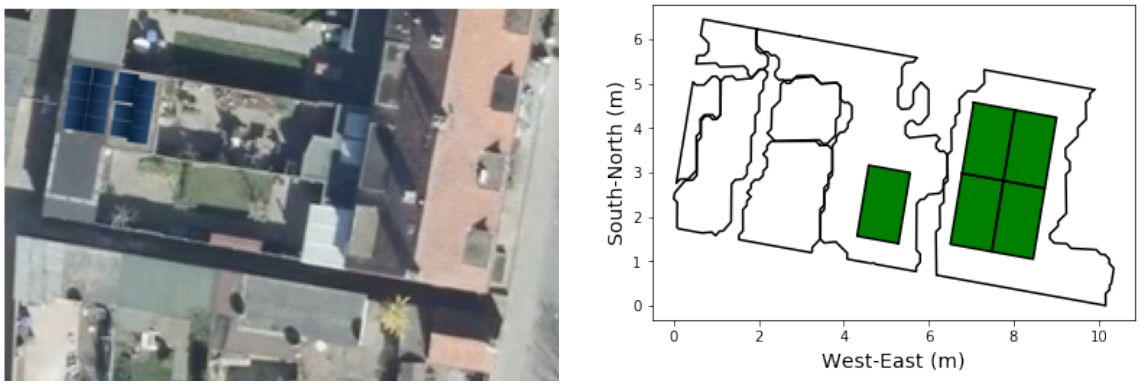

Figure 5.16: Aerial image and visual schematic of fitted panels on roof with bag id 772100000260479. Note that the quick-scan is performed at the right roof while the actual panels were placed on the garden shed or garage on the left.

The maximum panel fitting algorithm is generally hard to validate in any automatic manner. The desired amount of panels to be placed does not have to be the maximum amount that fit on a roof. For example, consumers might not have sufficient energy demand to install the full potential of PV. Moreover, consumers could choose low-performing segments, if they are preferred for aesthetic preferences. Apart from that, east-west layouts can be placed on flat roofs, instead of panels directed to the South. A better way to validate panel fitting, would be by manually selecting the right segments.

5.4. Manual selection of roof segments

A visual inspection was carried out for 208 roofs. For this set of roofs, recent aerial images were compared with the roof segments from set 2 that were provided by Readaar. For the ones where it was

clearly visible, the segments on which PV panels were actually placed were added to a list of manually selected roof segments. In this way, panel fitting and yield validation could be done more precisely.

The following results were found:

- 104 segments were fully used for PV. The maximum amount of panels seemed to be placed on these segments. Sometimes one actual roof segment filled with PV was divided into smaller segments. In this case all smaller segments were selected to approach the amount of fitted panels.

- 66 segments were used for about two-thirds of their surface. The most common reason was that obstacles within the segment were not detected. Sometimes, the customer had no desire to use the full potential of the roof, or choose for a rectangular (aesthetic) panel layout instead of fitting the maximum amount of panels.

- 45 segments were only used for about one-third of their surface. The most common reason was that the customer had no desire to use his entire roof for PV. However, in twenty cases very large obstacles or a multitude of them were not detected.

During the visual inspection, the following observations were noted down:

- The distance kept from the roof segment edge was much less than expected. For pitched roofs, there was virtually no distance between the roof edge and installed panels, or at most 10 centimetres. For flat roofs a range of 0 to 30 centimetres was encountered for these domestic rooftop systems.

- No roof segments had been found on which less than 3 panels were placed. Panels were placed in strings of at least 3 in the set of aerial images that had been assessed.

- East-west setups were only encountered twice in this subset of roofs.

- Out of all of the flat segments found, there were only two systems where panels were not aligned with the roof edge.

Divided over the 3 categories, 161 buildings and 215 segments were left from the eventual data set 2. According to the visual inspection, 104 segments were fully used for panel fitting, whereas the amount of panels fitted on 66 roof segments was multiplied by 2/3 and the panels fitted on 45 roofs was multiplied by 1/3 to compensate for not all the roof surface being used.

5.4.1. Over-segmentation due to PV in aerial image

Throughout the visual inspection of aerial images and roof segments of set 2, many roofs were found the segmentation has severely gone wrong. Upon further inspection one of the reasons for this was found: the aerial images used for creating the segments of set 2 had been too recent, therefore incidentally recognising PV strings as separate segments. Figure 5.17 shows an example of such over-segmented roof. The segment 99605 was created around the 4 installed panels, whereas the three segments of 99603, 99605 and 99601 should have been 1 roof segment.

Figure 5.17: Example of over-segmentation by panel detection, bag id 766100000003079.

Unfortunately, the Readaar only had a licence for recent aerial images and therefore the segmenting could not be repeated while preventing this problem. All 16 roofs with over-segmentation that could be the result of underlying panels were filtered out of the manually selected data set. This left 145 roofs for the final validation of the quick-scan.

5.4.2. Panel fitting on manual selection of roofs from set 2

In order to better validate the maximum panel fitting algorithm, it was also used on the manually selected subset of roofs, without over-segmentation errors. Since it had been seen that distances from the edge were close to zero, this feature had been set to 0 cm. As explained in section 5.4, the areas of identified section were either fully used, used for two-thirds or one third. The results are shown in figures 5.18 and 5.19.

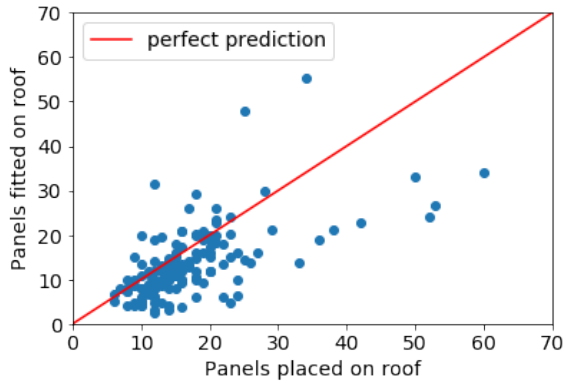

Figure 5.18: Scatter plot for panel fitting on 145 roofs in manual selection of set 2 without distance from the roof edge.

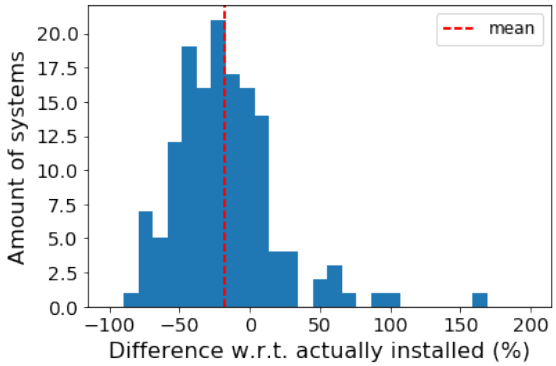

Figure 5.19: Histogram for panel fitting on 145 roofs in manual selection of set 2 without distance from the roof edge.

The panel placement was underestimated by 17.5% on average, however the RSD decreased to 46.3%, compared to 65.1% when using the entire data set 2. For 70.3% of the roofs the amount of fitted panels was too low, however mostly by a small fraction. Only 13.1% of the roofs had more than double the amount of installed panels with respect to what was fitted by maximum panel fitting.

There could be many reasons for the under-estimation of panels on the segments were panels were placed.

- The categories of panel placement ratios were only set manually by looking at low-resolution

images. More panels could have been added if roof segments were divided over more panel placement categories, and if the inspection was carried out in a more precise manner.

- The wrong segment could have been written down in the first place. Since roof segments were often not perfectly aligned with the roof edges in the aerial image, this made it harder to choose the right segments.

- The settings for module layouts could be different. Smaller panels could be used, and on flat roofs less module tilt and therefore smaller row distances could be chosen. These options were not investigated in further detail.

- It was found that sometimes, systems were spread over multiple buildings, which made it impossible to achieve the same amount of panels by the current quick-scan. Most other reasons were already already mentioned in section 5.3.3.

5.5. Panel fitting time per segment

The panel fitting time was measured for 240 roofs containing 817 roof segments from data set 1. It took 61.7 minutes, resulting in an average panel fitting time of 1.01 $\pm$ 1.08 seconds per segment. Since the time per roof is completely dependent on the segments within a roof, the panel fitting time per roof (in this case 3.43 s/roof) is not analysed further in this section. The large standard deviation in panel fitting time per segment comes from the wide variety in segment area within the data set. Figure 5.20 shows the panel fitting time per segment area.

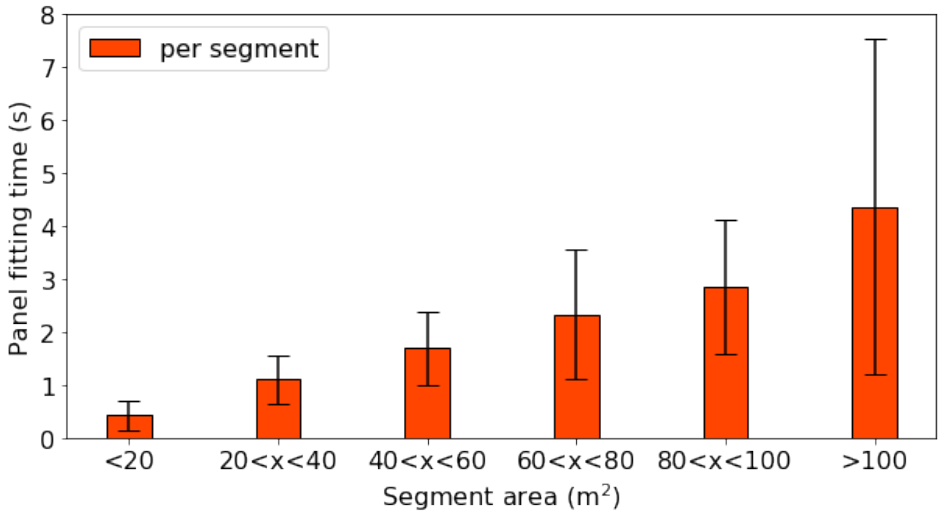

Figure 5.20: Panel fitting time per segment.

It can be noted that even per segment area category, the standard deviation values are still large. This is caused by the difference in panel fitting time between flat and pitched segments. For flat segments, only landscape setups are chosen by the quick-scan algorithm, while for pitched segments both landscape and portrait setups are possible. This results in more than twice the calculation time for pitched segments, since twice as many calculations need to be carried out, and the best of both maximum panel placement solutions has to be selected. The panel fitting time per segment was divided in flat and pitched segments in figure 5.21.

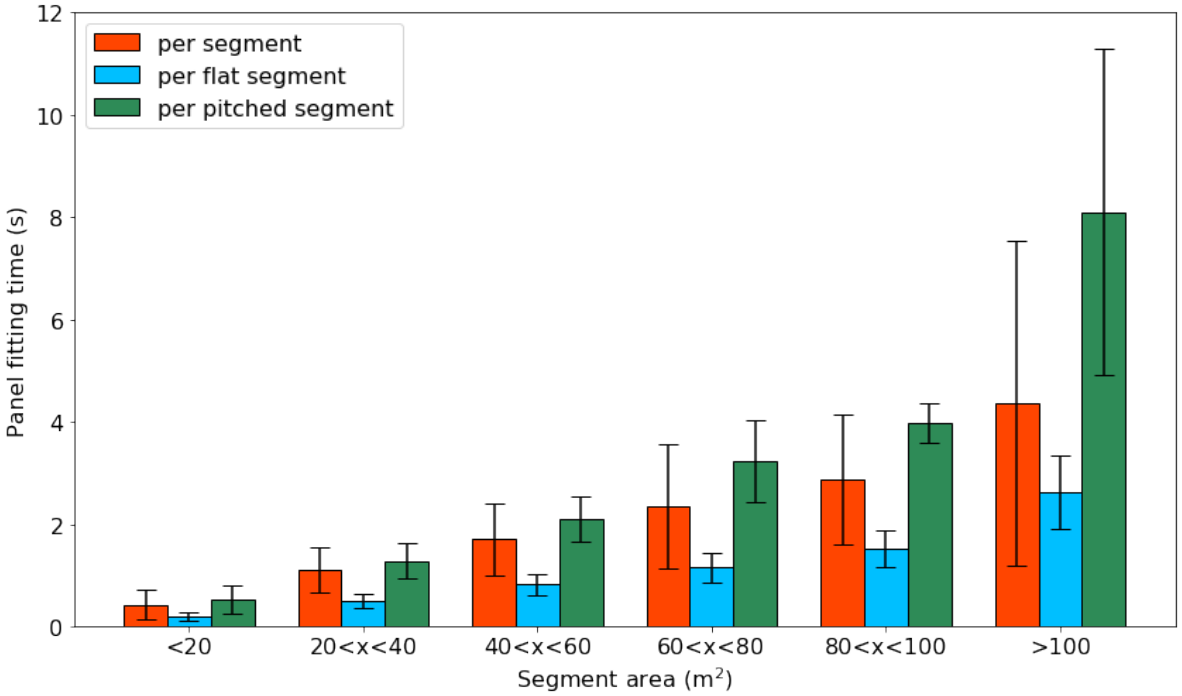

Figure 5.21: Panel fitting time per segment type.

The panel fitting speed was found to be 30.4 $\pm$ 18.2 m^2s^{-1}. The panel fitting speed for pitched roofs without internal obstacle segments was found to be 20.1 $\pm$ 5.0 m^2s^{-1}, whereas the panel fitting speed for flat roofs was found to be 56.9 $\pm$ 12.0 m^2s^{-1}.

The latter is about half as fast as the value reported for flat roofs without internal obstacle segments by Bronkhorst, being 120.7 $\pm$ 16.4 m^2s^{-1}, [5]. This is however not a surprise, since many elements have been added to the initial algorithm, such as: loading the segment polygon from a large shapefile, determining its area, accessing the given pitch angle and orientation of the segment from a large dataframe, determining the segment orientation according to the approach of 3.4.2 and many "if"-statements regarding panel alignment with the roof, east-west configurations, flat or pitched roofs. Apart from that, many variables needed to be saved, since the purpose of the quick-scan is not only to visualise the module layout on a segment, but also to carry out a yield prediction and make the results insightful. Lastly, due to the growth of Solar Monkey, the calculation capacity of the server was often divided between multiple users, whereas this was not the case during the work of Bronkhorst.

As explained previously by Bronkhorst, the maximum panel fitting algorithm could also be made faster by increasing the step size when sliding the panel grid over the roof [5]. The step size was set at 10 cm during this research, and was not increased in order to avoid additional inaccuracy.

Chapter summary

In this chapter the results of the panel fitting algorithm were presented and discussed. It can be concluded that the panel fitting algorithm works reasonably well for roof segments with few obstacles, both flat and pitched. Still, improved roof segment data with defined obstacle segments could improve the panel fitting substantially. The panel fitting algorithm still underestimates the amount of panels that can be placed on a roof, on average by 17.5%. Better validation could be carried out by manually setting the same panel configuration as used for individual PV systems.

6

Yield and Performance Prediction

In this chapter, the expected AC yield of each virtual PV system is compared with the measured yield of the real system. In order to make this comparison independent of the earlier shown panel fitting algorithm, the roof performance was calculated. This performance is expressed in kWh/kW$_p$ per year. Normal performance values in the Netherlands are between 700 and 1100 kWh/kW$_p$ per year [64].

For each roof segment on which panels were fitted, a segment performance was calculated by dividing the predicted annual AC yield by the amount of panels and the rated power per panel in W$_p$. After that, a roof performance was calculated as an average of all segment performances, weighted by the amount of panels that were fitted on them. In this way, larger roof segments have a larger contribution to the roof performance.

This chapter will introduce the results on yield and performance prediction by the quick-scan algorithm. First, it will mention the different problems that were faced for making a proper comparison. After that, the quick-scan will be compared with the method that is currently used by Solar Monkey and prediction without 3D roof segments. Then, different performance calculations methods will be compared to each other, under different conditions. Lastly, the chapter will propose two methods for categorising the roof potential, and mention the calculation time per yield prediction method.

6.1. Problems that were faced

Several complications were encountered while carrying out the performance calculation. First of all, only systems of older than one year could be selected for analysis. Also, the number of panels and annual yield measurements needed to be well-registered in the Solar Monkey database. As mentioned earlier in section 3.5, only subsets of the entire sets of roofs were used for performance validation.

The following complications and the ways in which they were overcome will be elaborated on in the following sections:

- Some systems turned out to have period of lacking yield measurement data, contributing to much lower annual yield values. This was probably caused by loss of wireless data connection with the inverter.

- Several roof segments were found to have incredibly high obstacle losses. As discusses earlier in section 4.3.2, this was generally caused by errors in the LiDAR height data, making the reference point of a roof lay physically lower than the roof segment plane and therefore causing high obstacle losses.

6.2. Filtering of results

For the exploration of our performance results, the Solar Monkey algorithm was used for one central point on each selected roof segment of set 1, and other settings of the quick-scan were as per table A.1. Because of the filtering on minimum segment area and pitched segment orientation, only 235 roofs were left in the data set. This effect will be discussed further in section 6.5.1. The first results of

the performance validation are shown in figure 6.1. As can be seen, there is a wide spread in predicted and measured performances.

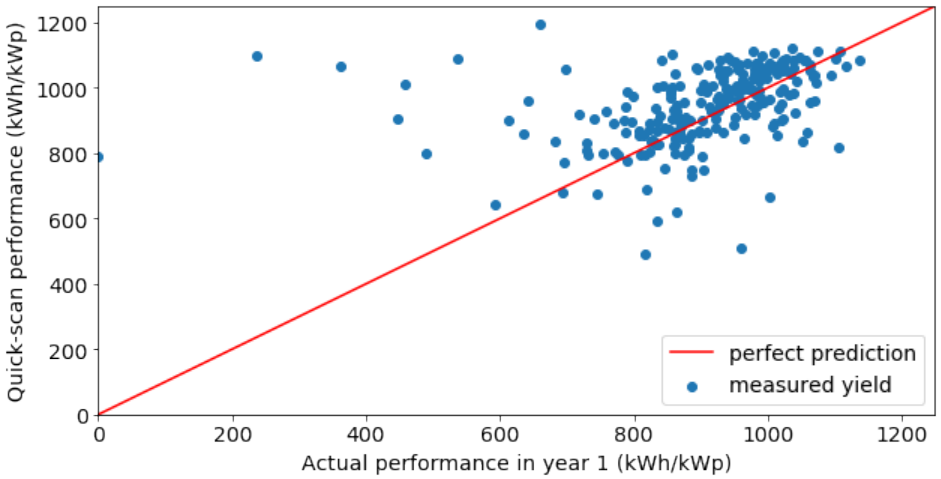

Figure 6.1: Performance prediction versus measured yield data for 235 roofs and 446 roof segments of set 1.

The first problem that was tackled was the existence of under-performing systems. The points with an actual performance less than 600 kWh/kW$_p$ were examined and it was found that they were the result of missing yield measurement data. This is expected to be caused by disconnected inverters due to Wifi network problems. Out of the 235 systems left in, there were only 45 systems that did not have any missing yield measurement data.

In order to resolve this problem yield estimates were carried out by Solar Monkey for the time of lacking measurement data of actual systems, using the actual module setup and one obstacle view per panel. For 203 of the 235 systems, the sum of the estimated yield contributed to less than 2% of the total annual energy yield, so it must be stressed that in most cases the loss of measurement data was incidental. Once these estimates were carried out, the actual performance of under-performing systems increased. The light blue points in the performance plot shifted towards the dark blue points that can be seen in figure 6.2.

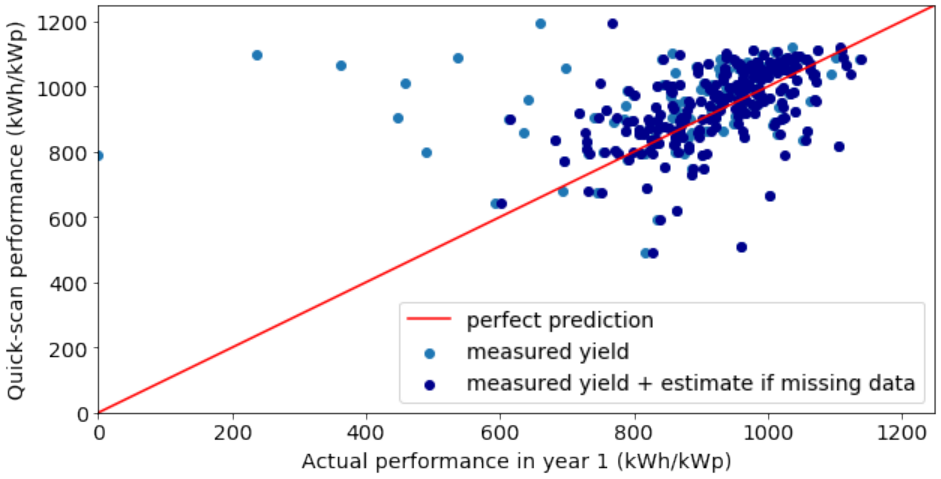

Figure 6.2: Performance prediction versus measured yield data with and without yield estimates for periods of missing yield measurement data, for 235 roofs and 446 roof segments of set 1.

Still, the quick-scan calculated low performances for certain roofs. This was because it still took all selected roof segments into account, whereas some of them would be extremely shaded. As discussed in section 4.1.1, a payback time of 10 years is considered maximum for most customers, which results

in a minimum annual performance of about 650 kWh/kW$_p$. The last filtering step was thus to discard all roof segments that had a performance below 650 kWh/kW$_p$. After this step still 232 roofs and 426 roof segments were left. The results are shown in figure 6.3.

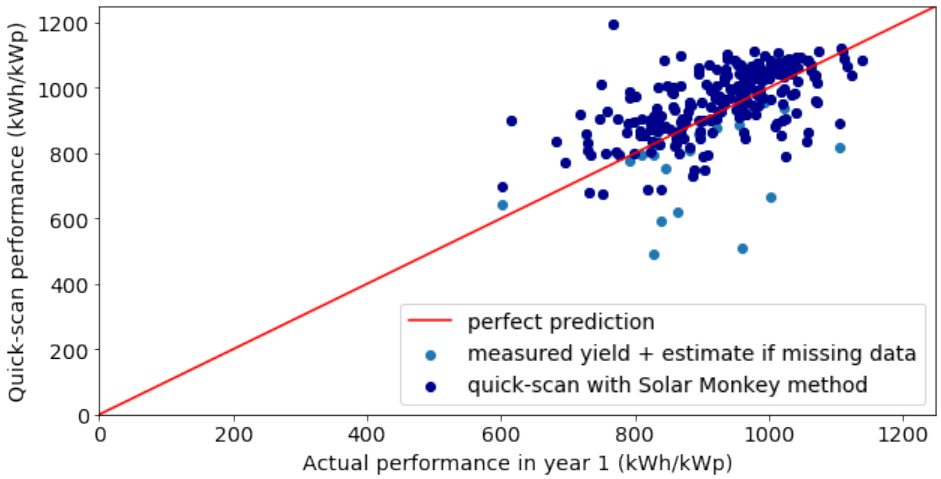

Figure 6.3: Quick-scan performance prediction Solar Monkey method for 232 roofs with 426 roof segments of set 1, after segment performances below 650 kWh/kW$_p$ were filtered out.

The current average over-prediction of performance by the quick-scan is 4.12%, whereas the relative standard deviation is 9.24%. A last step that can be performed to optimise the quick-scan is to make the average prediction as close as possible. As mentioned in section 2.4.3, the AC energy yield is simply calculated by the STC efficiency of the panel and a factorisation of 0.93 to take into account cable losses, inverter losses, and the effects that temperature and irradiance have on module efficiency. Naturally, this approach is not very accurate. The actual loss can be found more easily by determining the mismatch between the mean prediction of the quick-scan and the mean of the measured performances.

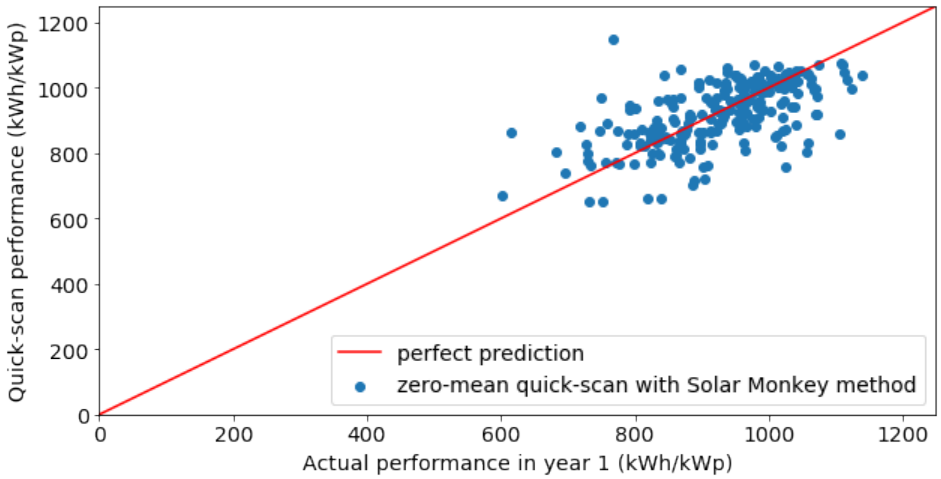

Figure 6.4: Quick-scan performance prediction for 232 roofs with 426 roof segments of set 1, made unbiased by division by its over-prediction.

The over-prediction of the quick-scan results is made zero-mean by dividing each performance by the mean over-prediction (or under-prediction), in this case by 1.0412. This results in an optimised prediction shown in figure 6.4. Zero-bias estimates will also make it easier to compare different prediction methods later in this report.

6.3. Comparison with actual Solar Monkey estimate

In figure 6.5, the zero-bias quick-scan performance estimate is compared to the performance estimate that was made by Solar Monkey for the actual systems. The prediction of Solar Monkey was carried out with an obstacle view for every panel on the roof, on the exact location they are placed.

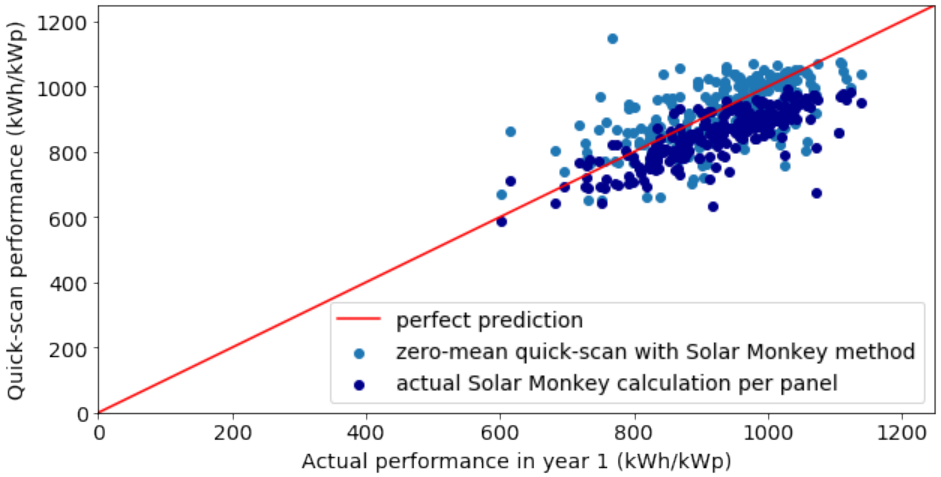

Figure 6.5: Zero-bias quick-scan performance compared to Solar Monkey yield calculation with one obstacle view per panel.

It can be seen that the performance predictions done by Solar Monkey are lower but also more coherent, showing a relative standard deviation of 6.95%. The average estimation was 7.78% lower than the actual performance. This can be explained by the contribution of temperature, dirt and cable losses. Apart from the 7% combined system losses, Solar Monkey had newly introduced additional methods to take these into account. Unfortunately, these methods were not yet known at the time this research was carried out.

Although the underestimation is evident, the performance estimations carried out by Solar Monkey have significantly fewer outliers. It must be noted that the performance validation of Solar Monkey is slightly biased by adding the Solar Monkey estimated yield in periods with missing yield measurement data. However, since the estimates comprise only a small part of the total yield for most systems, the validation is still relatively accurate.

6.4. Land register data vs. roof segments

In this section, yield prediction was carried out with only land register data. In this way, the added value of yield prediction with roof segments could be proven. For yield prediction with only building contours, all roofs were expected to be one-segment and flat. With this assumption, the same panel settings were used as for flat roof segments.

In figure 6.6 the performance prediction can be seen for 237 roofs, neglecting nearby obstacles. It can be noted that the quick-scan predicts an almost constant performance, since all roofs are supposedly flat, all panels have the same tilt, and no obstacles are taken into account. The lowest value found is 1030 kWh/kW$_p$ and the highest is 1114 kWh/kW$_p$. The only deviations in performance are caused by the slight difference in panel orientation due to alignment with the roof edges and the difference in horizon height as given by PVGIS. However, it can be concluded that this performance prediction does not have any added value for the customer.

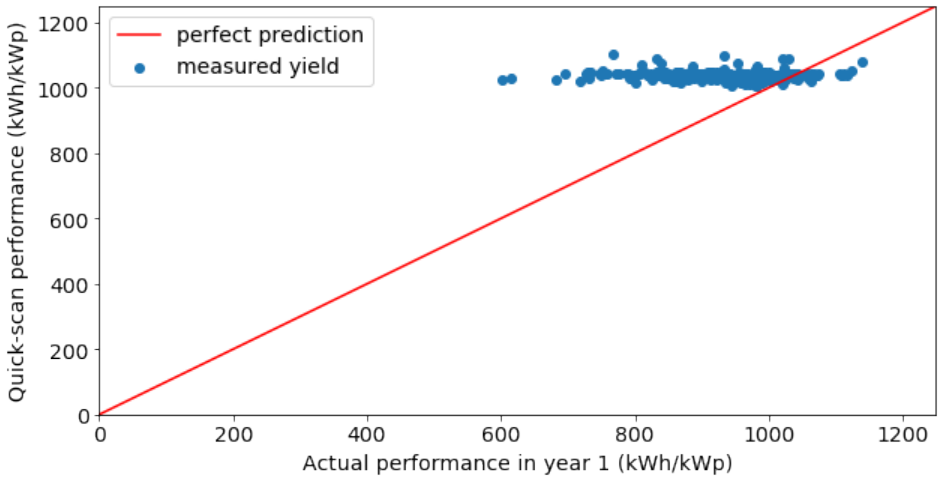

Figure 6.6: Performance prediction using only land register data and no obstacle view for data set 1.

In figure 6.7 the same performance prediction is carried out for 237 roofs, however including the obstacle view obtained from the surrounding LiDAR data. The predicted performance shows a wide spread of results, both in under and over-prediction. With 20.37% relative standard deviation this form of performance estimation is not useful. Taking the obstacle view from one central point on a roof with multiple segments is not a reliable method for determining the losses due to shading. The filtering step of deleting roofs with less than 650 kWh/kW$_p$ performance could not be done, since it implied deleting 16 entire roofs instead of deleting the worst segments from roofs.

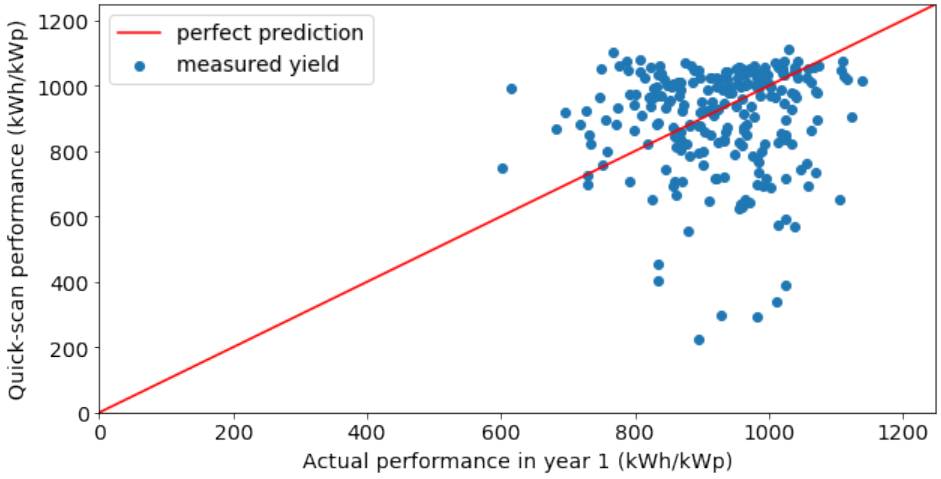

Figure 6.7: Performance prediction using land register data and the obstacle view for the most central point on the roof for data set 1.

6.5. Results for different yield calculation methods

In this section, different yield prediction methods will be compared. For all methods, estimates were used if yield measurement data was not available. Filtering was carried out on pitched roof orientations, so 0 to 60° and 300 to 360° were left out. The minimum segment area was set to 8.4 square meters. Two sources of height data were used in order to prevent obstacle view errors, as mentioned in section 4.3.2.

As mentioned in section 2.4.3, a constant loss of 7% is taken for the system losses of the Solar Monkey method and SVF&SCF method. In order to compare the different yield prediction methods, each performance prediction was set to a zero mean deviation. By dividing the full performance data of a quick-scan method by its amount of over-prediction or under-prediction, the average prediction

could be set to precisely the average measured performance. For the method neglecting obstacles, this would essentially mean subtracting the average obstacle losses from all roof performances.

In figures 6.8 and 6.9 the three yield prediction methods are compared for roof segment set 1 and 2 respectively. Three variables were measured per yield prediction method. Scatter plots of the predicted performance for each method and each data set can be found in appendix D.1.

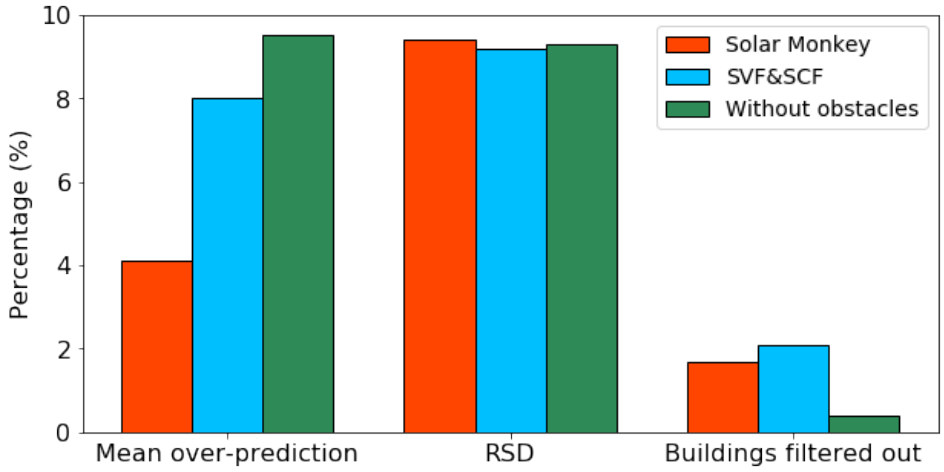

Figure 6.8: Yield prediction method comparison for data set 1.

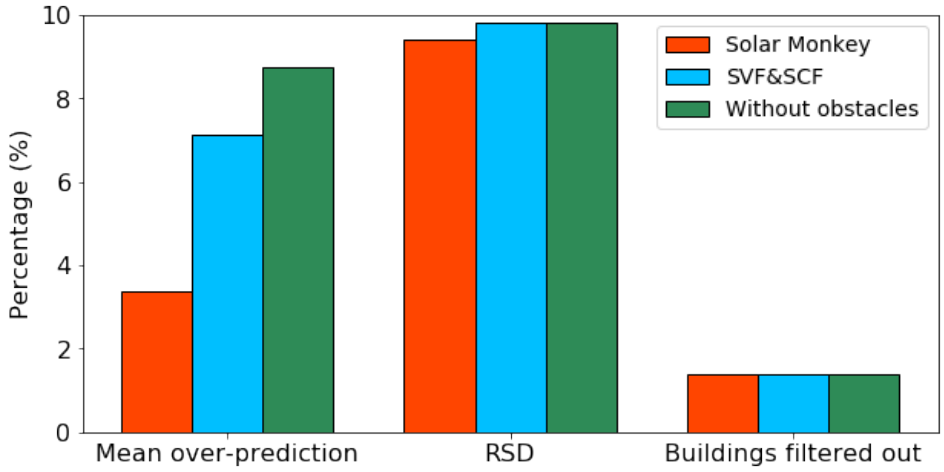

Figure 6.9: Yield prediction method comparison for data set 2.

The average over-prediction was recorded for each yield prediction method. Although the Solar Monkey method had an average over-prediction of about 4 percent, this was less than the over-prediction of the other two methods. It was to be expected that the prediction would be closer to reality, since the 7% system loss was set empirically by Solar Monkey. As expected, the method without obstacles had the highest over-prediction, since the obstacle view was not taken into account. However, it might have turned out close to the SVF&SCF method, because of conservative assumptions in the spectral losses, temperature-dependent module losses and irradiance dependent losses of PVGIS. Also, the applied 3% loss expected on cables and the inverter might have caused this method this method to be less over-predicting. Throughout both sets, the relative standard deviation of the different methods was found to be highly similar. Values found were all between 9.2 and 9.8%. A linear regression was carried out for the individual scatter plots in appendix D.1. The slope of fitted lines is shown in table 6.1.

Table 6.1: Slope of linear regression for performance plots carried out by three methods.

Fitted line slope	Solar Monkey	SVF & SCF	Without obstacles
Roof segment set 1	0.59	0.61	0.39
Roof segment set 2	0.58	0.58	0.42

The methods using obstacle views generally follow a more diagonal trend than the method that doesn't use obstacle views. This is expected, since it neglects the effects of the skyline profile. If the real yield would be lower due to obstacles, the prediction would not decrease for this yield prediction method. Therefore the spread in the scatter plot would be more horizontal than other yield prediction methods. The main reason that the predicted performance is still not horizontal (one value), is the fact that the azimuth and tilt angle of the modules are taken into account. Nonetheless, all methods have a lower slope than the perfect prediction line, having a slope of exactly 1. Since the method without obstacles has a lower amount of outliers, points that are far away from the line, it RSD value is still comparable, while the trend is more horizontal.

Lastly, also the amounts of buildings filtered out have been compared. This variable denotes the combined amount of roofs that have been filtered out by three filtering steps: 1. minimum segment area 2. orientation filtering on pitched segments 3. segment performance. The first filtering step decreases the amount of roof segments examined per roof, but it did not exclude full roofs, since there was always at least one larger-area segment left. The second filtering step did exclude some roofs. This could be the case because customers choose segments for aesthetic reasons and not always for performance reasons. A north-directed pitched roof could be preferred over a south-directed roof at the street side of a house, if the house owner doesn't like the look of PV panels above his/her front door. The third filtering step excluded the most buildings, especially in set 1. All segments with a calculated performance below 650 kWh/kW$_p$ were filtered out, and this resulted in some roofs with no segments left. This effect is only seen for the methods that take obstacles into account, since they will only have such low expected performance values.

6.5.1. Effects of orientation filtering for pitched roofs

For data set 1, further research was done into the effect of orientation filtering of pitched roofs on the relative standard deviation and the percentage of buildings filtered out. Figures 6.10 and 6.11 show the effect on both variables respectively.

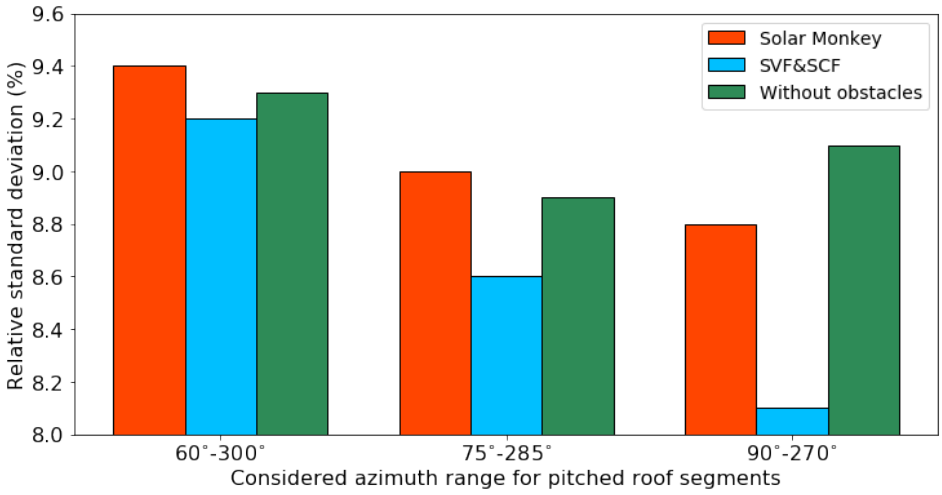

Figure 6.10: Relative standard deviation as a function of azimuth filtering for pitched roofs.

The relative standard deviation decreases as more segments are filtered out. This can be expected, as often the roof segments directed towards the northern half of the hemisphere are not used for PV. By filtering them out, there will be no panels fitted on them, and these segment performances do not contribute to the roof performance in kWh/kW$_p$ per year. It is however interesting to see that the

optimal filtering range for the yield prediction method without obstacles was found to be 75° to 285°, whereas the methods with obstacles had lower RSD values for the 90° to 270° range. It is expected that highly shaded pitched roof segments with an orientation between 75° and 90° or 270° and 285° would be filtered out by the methods taking into account obstacles, since their performance would be below 650 kWh/W_p. The method without obstacles would expect those segments to perform above 650 kWh/kW_p, thereby selecting roof segments that were actually not selected for the installation of panels.

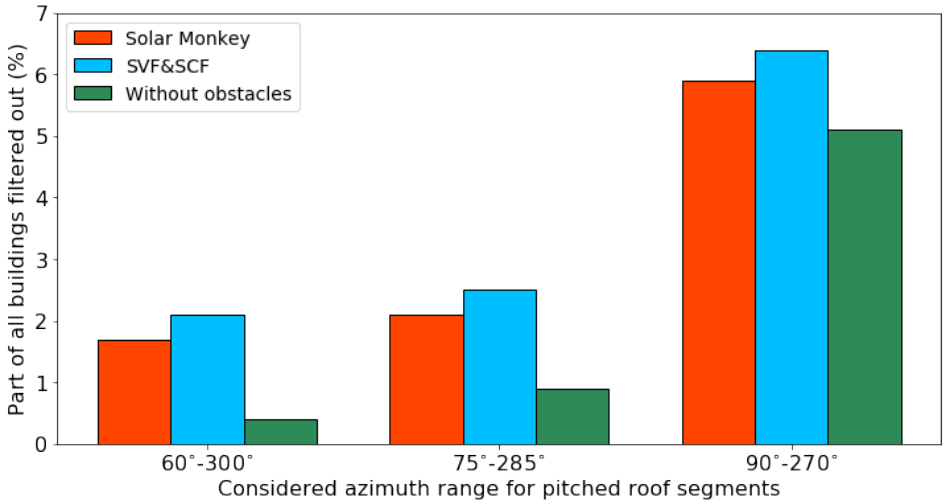

Figure 6.11: Buildings filtered out since pitched roof segments were outside of azimuth filtering range.

Regarding the buildings filtered out, it can be seen that more buildings are filtered out if a wider range of pitched segment orientations is discarded. What must be noted, is that the percentage of roof segments filtered out is far higher, as discussed in section 4.1.1. Figure 6.11 only addresses the roofs of which not a single segment is left after the filtering. Naturally, this is an undesirable side effect of the filtering, since all roofs in the data set actually have PV systems installed, and should therefore be considered suitable for some costumers or PV installers. Looking at the part of all buildings that is filtered out, the most notable difference is between the 75° to 285° and 90° to 270° filtering range. Therefore it is concluded that the 90° to 270° is an undesirable setting for the quick-scan algorithm.

6.5.2. Performance per number of roof segments

For data set 2, the performance of the quick-scan algorithm was investigated per amount of roof segments that were left after filtering on minimum segment area, pitched segment orientation and minimum performance of 650 kWh/kW_p. The results are shown for the Solar Monkey prediction method in figure 6.12, which used one obstacle view for the most central point on each roof segment. The mean over-prediction is in this case the over or under-prediction with respect to the optimised prediction for the full set of roofs, where the over-prediction was set to 0%. The individual scatter plots of performance can be found in appendix D.2.

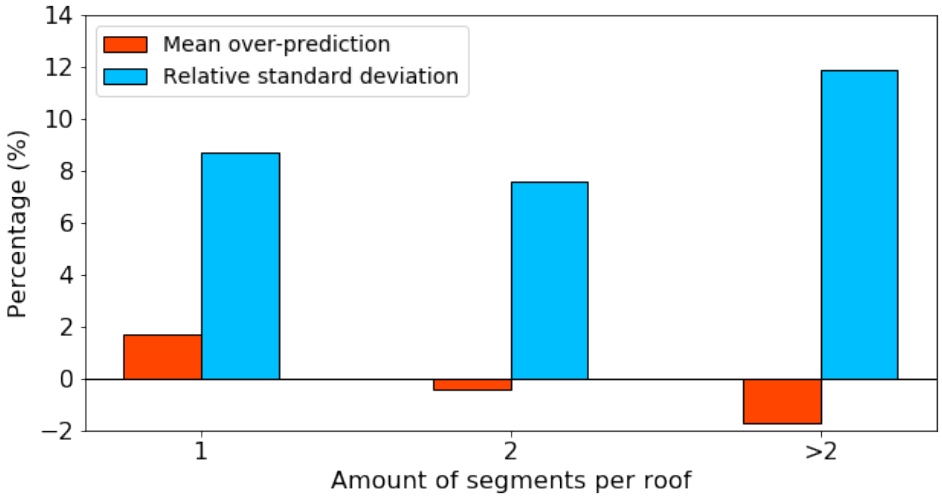

Figure 6.12: Mean over-prediction and relative standard deviation of the quick-scan calculated with Solar Monkey method for roofs composed of different amounts of segments, after filtering on pitched segment orientation and minimum segment area according to table A.1.

The amounts of roofs with 1, 2 or more than 2 segments left were 64, 71 and 72 respectively. Interestingly, the quick-scan performed best for roofs on which two segments were left after the three filtering steps. It is expected that the RSD is larger for 1 segment roofs, because there is a higher chance that the actual roof segment used for PV has been filtered out. Even though the quick-scan might consider another roof segment better, this does not always mean that this is the choice of the customer. This choice can be made due to aesthetic preferences or restrictions of ballast for the roof construction. It does however explain why the quick-scan predicts the performances of these roofs to be high, compared to roofs with more segments.

Roofs with over 2 segments yield the worst results for the quick-scan. The reason behind this might be that over-segmentation has found place in the process of stereo-matching. Over-segmentation results in less panels being placed on promising roof segments, therefore having a lower contribution to the roof performance. If segments with a lower performance have less over-segmentation, this explains why the performance prediction is relatively low for these segments. Alternatively, roofs with many segments are often not used to their full potential. Only the best segments would be selected by the customer to install PV. The roof performance calculated by the quick-scan it is an aggregate of all segment performances above 650 kWh/kW$_p$ on which panels were fitted. Therefore the performance prediction will be low if the customer decides to place less panels, only on the segments performing best.

6.5.3. Pitched segments with large orientation errors

As mentioned before in section 3.4.2 there are pitched segments with a high difference between the orientations found by both implemented methods. Table 3.1 stated that differences of over 16° will be likely to result in problems for panel fitting.

In set 1, 20 segments out of 527 segments (3.8%) have an orientation error above 16°. This creates an increased uncertainty in the final results for 20 out of 237 roofs (8.4%)]. Deleting these roofs from the data set, the relative standard deviation of the Solar Monkey prediction method decreases from 9.42% to 9.32%, while taking the standard settings for the quick-scan as shown in appendix A.

In set 2, 41 segments out of 502 segments (8.2%) have orientation error above 16 °. This creates an increased uncertainty in the final results for 37 out of 210 roofs (17.6%). Deleting these roofs from the data set, the relative standard deviation of the Solar Monkey prediction method decreases from 9.41% to 8.70%, while taking the standard settings for the quick-scan.

6.6. Yield prediction on manual selection of roof segments

Initially the yield prediction methods that take skyline profiles into account were expected to outperform the method that neglected obstacles. However, this expectation was not confirmed by the results found

for data set 1 and 2. The main cause was expected to be that PV systems would not always be placed on the roof segments that were considered best by the quick-scan. If an actual system would be installed on another segment than the one taken into account by the algorithm, the added value of incorporating an obstacle view would be gone. The only way to properly test this assumption was by manually selecting the roof segments on which PV was actually placed, and then using the quick-scan on these segments without filtering on their segment area or orientation.

The selection of roof segments introduced in section 5.4 was used again. According to the visual inspection, 104 segments were fully used for panel fitting, whereas the amount of panels fitted on 66 roof segments were multiplied by 2/3 and the panels fitted on 45 roofs were multiplied by 1/3 to compensate for not all the roof surface being used. Divided over the 3 categories 161 buildings and 215 segments were left from the eventual data set 2. The performance prediction results are shown for all three yield prediction methods in figure 6.13.

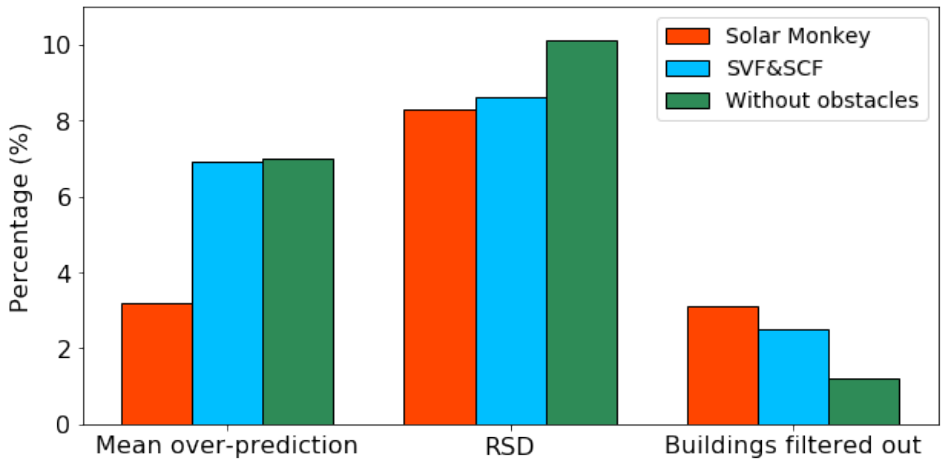

Figure 6.13: Yield prediction method comparison for manual selection of roof segments.

With RSD values of 8.3% and 8.6% respectively, the obstacle-including methods now outperform the simple yield calculation, which has a RSD value of 10.1%. The RSD for the method without obstacles stayed close to unchanged with respect to the full data set 2 results, whereas the yield prediction for the first two methods greatly improved now the exact roof segments were known.

Regarding performance prediction, the Solar Monkey method over-predicts by 3.2%, whereas, the SVF&SCF methods and prediction without obstacles over-predict by 6.9% and 7.0% respectively. Compared to the full data set 2, the over-prediction had decreased for all three methods. This confirms the idea that sometimes not the highest performance segments but lower performance segments are chosen to install PV panels.

Although no segment area filtering or orientation filtering of pitched segments was carried out on the manual selection of roofs, still some roofs were filtered out in the step of requiring a minimum segment performance of 650 kWh/kW$_p$. This shows that the orientation of some segments was such that the expected performance was below this boundary value. The methods that take into consideration the skyline profile also encountered several segments with high obstacle losses, resulting in more roofs being filtered out.

6.6.1. Performance for shaded segments

After making the manual selection of roof segments from set 2, it was investigated how well different yield prediction methods performed for different levels of shading. In order to do this, the SCF was used. The SCF would give an indication of the ratio of direct irradiance and circumsolar diffuse irradiance that would be lost throughout the year by obstacles in the direction of the sun rays. The set of manually selected roof segments was divided in three subgroups of 53 roofs, 56 roofs and 49 roofs, with low shading conditions, average shading conditions, and high shading conditions respectively.

There was however a complication in defining levels of shading for each roof: the performance validation could only be done on a roof level, whereas shading was taking place per roof segment.

Luckily, in the manually selected data set it was already known on which roof segments panels were placed. The SCF value per roof was thus defined as an average of the SCF values of roof segments, weighted by the amount of panels that were fitted on each segment.

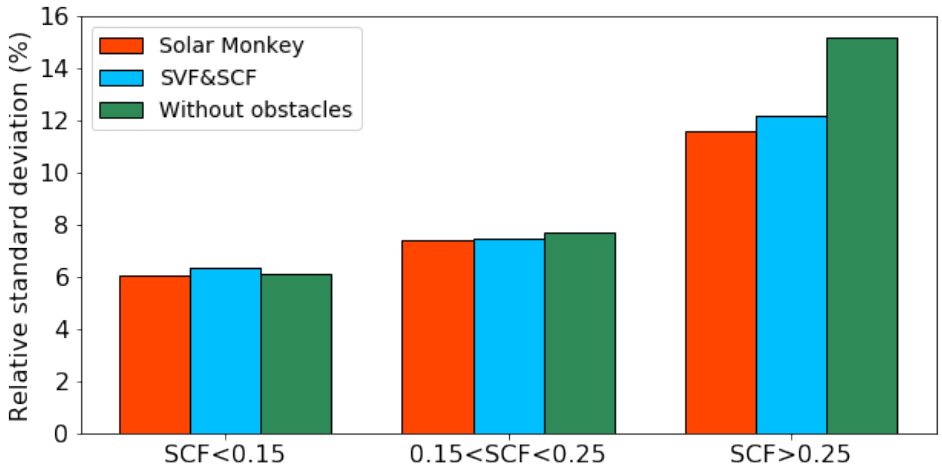

Figure 6.14: Relative standard deviation as a function of average SCF value per roof, weighted by the amount of panels fitted on it.

Figure 6.14 shows the RSD for different levels of shading per roof. For all yield prediction methods, the RSD increased for roofs with higher levels of shading. This increase in spread will partially be caused by the choice to only take one obstacle view per roof segment. Additionally, shaded segments have fewer data points that can be matched on the basis of colour recognition, such that the inaccuracy in segment orientation and pitch angle becomes larger. Lastly, the mean predictions for the three categories are 994, 946 and 849 kWh/kW$_p$ respectively. This means that even the same deviations from the mean would result in a higher RSD for more shaded segments. However, if we look at the standard deviation in the same units, the increasing trend can still be seen with values of 60, 70 and 98 kWh/kW$_p$ respectively for the Solar Monkey method.

It can be seen that the three yield prediction methods perform very similarly for roofs with an SCF below 0.25, however for the highest shading category the first two methods greatly outperform the obstacle-neglecting one. This was to be expected, since for those roofs it is the least valid assumption to neglect the obstacle view.

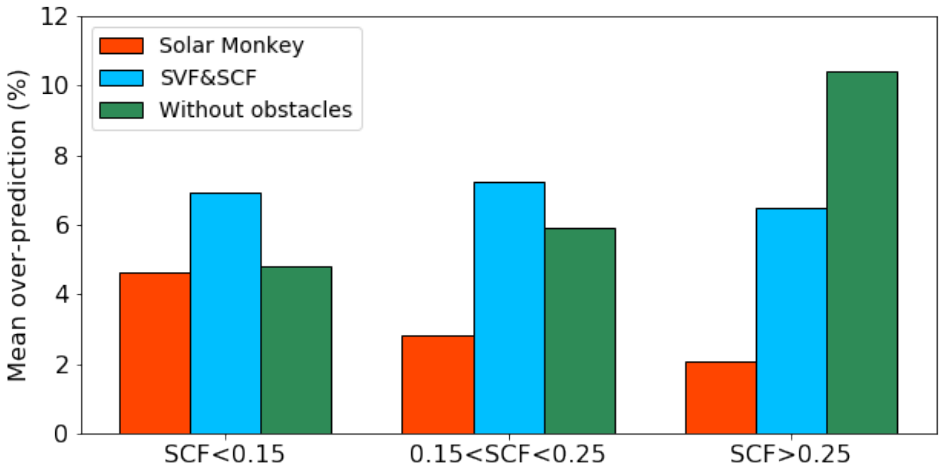

Figure 6.15: Mean over-prediction of roof performance as a function of average SCF value per roof, weighted by the amount of panels fitted on it.

Figure 6.15 shows the average over-estimation of performance for the same subsets of roofs. The

Solar Monkey method decreasingly over-estimates with higher levels of shading. The method using SVF&SCF over-estimates by similar amounts for all levels of shading. Lastly, the method neglecting obstacles increasingly over-estimates with higher levels of shading. For this method, the over-estimation of performance increases from 4.8% for slightly shaded segments to 10.4% for highly shaded segments.

6.6.2. Performance per average roof segment size

A similar exploration has been carried out for the average segment area. For the Solar Monkey yield prediction method, the yield prediction accuracy has been analysed for different sizes of roof segment. In this effort, the same complication occurred as in the previous section, namely that the performance could only be validated on roof level, while the yield prediction was carried out per roof segment. In order to overcome this, an average segment area was defined for each roof within the manual selection on which panels were actually placed. The average segment area per roof was a weighed average of the segment areas, by the amount of fitted panels, to make it reflect their contribution to the performance of the whole roof. For the full set of manually selected roof segments, the average roof segment area was 36.5 m^2.

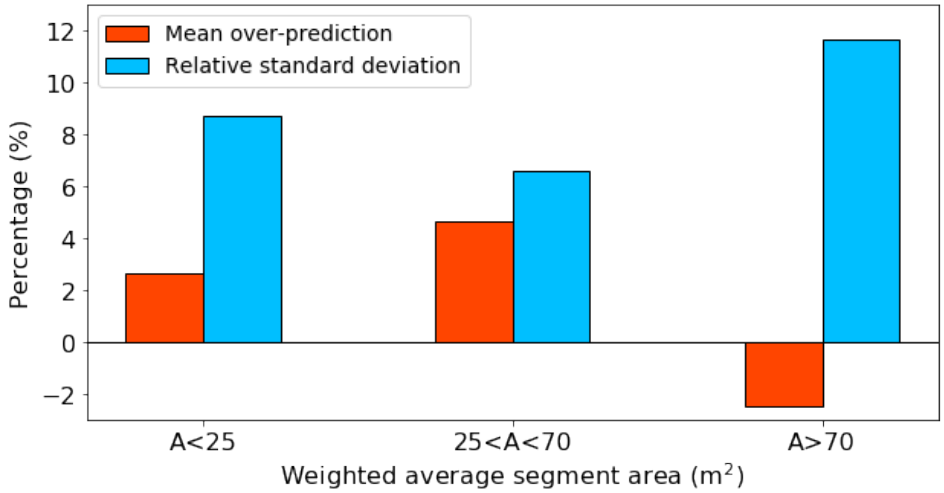

Figure 6.16: Mean over-prediction and relative standard deviation of roof performance by Solar Monkey method as a function of average segment area per roof, weighted by the amount of panels fitted on it, carried out far data set 2.

Figure 6.16 shows the results for three categories of roofs, containing small segments, medium-sized segments, or large segments. The subgroups represent 54, 122 and 45 roofs respectively. The results are described below:

- Medium-sized roof segments resulted in the highest accuracy prediction, but also in the highest percentage of performance over-prediction. This over-prediction could be caused by unidentified obstacles within the roof segments, but also by the customer choosing to not use the best-performing segment, but place panels on a slightly lower-performance one.
- The high RSD that is obtained for roofs with a smaller weighted average segment area could be explained by the over-segmentation of several roof segments in the stereo-matching process. An over-segmentation of a suitable roof can lead to a smaller amount of panels fitted on it, and therefore bias the yield prediction importance of a less suitable roof segment. Additionally, smaller segments contain fewer pixels in the point-cloud described in section 3.2, and therefore given values for roof pitch angle and orientation are less accurate.
- The most different result is found for the largest category of roof segments. Their performance is generally under-predicted, while the RSD is highest with 11.7%. There could be multiple reasons for this. It might be that using one obstacle view is too inaccurate for large roof segments. A large roof segment could be divided in highly shaded parts and parts that are virtually free of

any shade, so one reference point in the centre might not be enough. Apart from that, large roof segments are seldom filled with panels. More often, it was encountered they were only used partially. In this case, the installer would obviously select the less shaded parts for installing PV panels. These decisions could make it hard to test the improvement of performance prediction per roof. It would require selection of the part of a roof segment where PV was actually installed, either by manual inspection of aerial images or by pattern recognition of the PV panels and machine learning.

Proposed approach for large roof segments

The average roof segment area was found to be 29.3 m^2 for pitched segments, whereas it was 64.9 m^2 for flat segments. However, there are far more pitched segments than flat segments within the manually selected segments. In total there were 16 pitched and 29 flat segment with over 70 m^2, so the roofs with a high weighted average segment area did not solely concern flat roof segments.

Two methods are proposed to deal with large roof segments in a more accurate manner:

1. The first method would be to carry out panel fitting in the original way. However, when more than a specific amount is panels is fitted, the panel array is divided into multiple smaller parts. This boundary could be set at 10 panels or about 3 kW_p, since this can be considered a boundary for small residential systems. For each part of the panel grid, a central point could be defined and in this way the yield prediction could be done more accurately. An advantage of this approach would be that the actual positions of panels are taken into account. A disadvantage is that still a new method needs to be developed to erase panels from the system design.

2. Another method could be to divide large roof segments in smaller segments. For example a roof size of 33.4 m^2 could be chosen, since this is the mean surface area which fits 10 panels. In this way, sub-segments with low performance could be discarded, and selection on high performance segments would be possible. Parts of the roof could be considered independently. A large disadvantage of this approach is that the sum of smaller segments cannot fit the same amount of panels as the full larger segment.

6.6.3. Over-segmentation due to PV in aerial image

As introduced in section 5.4.1, several segments were over-segmented by PV panels present in the aerial images used by Readaar. All 16 roofs with over-segmentation that could be the result of underlying panels were filtered out of the manually selected data set. This left 145 roofs for the final validation of the quick-scan.

Due to the orientation errors discussed in section 6.5.3, another 9 roofs were discarded because of their increased chances of having an inaccurate segment slope or orientation. These 9 roofs will be included into the percentage of buildings filtered out. Table 6.2 shows the final results of the quick-scan for this set of manually selected roof segments on which PV was placed, free from over-segmentation issues.

Table 6.2: Results of the quick-scan per yield prediction method, using manual selection of roof segments from set 2, minus over-segmented parts. All roofs with pitched segments with orientation errors above 16° were filtered out.

Yield prediction method	Solar Monkey	SVF & SCF	Without obstacles
Mean over-prediction	3.5%	7.4%	7.2%
Relative standard deviation	7.2%	7.6%	9.5%
Buildings filtered out	9.0%	8.3%	6.9%
Fitted line slope	0.68	0.69	0.47

The average over-prediction of performance per method was found to be comparable to its value for the entire set 2, however the method without obstacles slightly decreased from 8.7 to 7.2%. The RSD values again show that the first two methods perform at a similar accuracy, whereas the method without obstacles has a larger RSD. Lastly, the method without obstacles filters out significantly less buildings, since roof segments seldom have a performance below 650 kWh/kW_p if obstacle losses are not taken into account. Comparing the slope of linear fits with the ones in table 6.1, we can see

that all methods got closer to the perfect prediction slope of 1. The slope could be lower by the underestimation of shading losses for highly shaded segments, or the division by the average over-prediction. For example, panels directed to the South on a pitched segments will generally have higher efficiency losses due to temperature than ones directed at the East or West.

In order to compare the three methods for exactly the same roofs, they were compared again, for only the roofs that were left after filtering for all three methods. For these 132 roofs divided into 156 segments, the results are shown in table 6.3.

Table 6.3: Final results of the quick-scan per yield prediction method, for the same 132 roofs and 156 roof segments.

Yield prediction method	Solar Monkey	SVF & SCF	Without obstacles
Mean over-prediction	3.5%	7.6%	7.8%
Relative standard deviation	7.2%	7.5%	9.1%

The most notable differences between table 6.2 and 6.3, are that the method without obstacles increases in over-prediction, but decreases in RSD. This is because some of the low-performance roofs are not considered anymore.

The RSD of the actual Solar Monkey performance prediction was 6.2% for the same subset of roofs, using one obstacle view at the place where panels were actually placed. If Solar Monkey's under-prediction of 8.4% was compensated for, the RSD would have been 5.7%, as shown in appendix D.3. This can be seen as the absolute minimum RSD value of the quick-scan, since it is intuitive that a method with more obstacle views from the actual locations of panels is more precise.

Sensitivity to minimum segment area

Since the roof segments of the final subset were selected manually, no segment area filtering had been applied to it. However, it would be interesting to see the effect that segment area filtering would have had on the result. For data set 1, a minimum segment area of 8.4 m^2 had been set. Due to improvements of the roof segment edges in data set 2, roof segments had become more rectangular and less of the roof area remained undetected. As such, segment on which 2 or more panels were fitted might have been filtered out. The analysis was carried out for the Solar Monkey method, from which 132 buildings and 156 roof segments were left after all steps described above. Table 6.4 shows the results for this sensitivity analysis.

Table 6.4: Results of Solar Monkey method for roof segment filtering on minimum segment area.

Minimum segment area	Roofs	Roof segments	Relative standard deviation
0 m^2	132	156	7.19%
4.2 m^2	132	155	7.19%
8.4 m^2	132	154	7.26%
12.6 m^2	130	149	7.30%
16.8 m^2	128	144	7.36%

The spacing of minimum segment area values was chosen such that equal steps were taken. As visible, the impact of a minimum segment area of 8.4 m^2 would have been minimal for the manually selected roof segments. A minimum area of 8.4 m^2 would have filtered out two roof segments. Both roof segments fitted only one panel. Even if 2 panels would be filtered out by filtering on minimum segment area, this would still have little significance. During the visual inspection it was found that panels were placed in sections of at least 3. It can however be concluded that the minimum segment area should not be increased, since this would result in filtering out additional roofs, on which PV was actually placed.

6.6.4. Reasons for deviations from measured performance

Deviations between the performance calculations and measurements can be caused by various reasons. In this section, these limiting phenomena will be discussed.

- The actual yield values are measured for the first operational year of the PV system. The systems monitored by Solar Monkey and examined in this research have all been installed between October 2015 and February 2017. However, the quick-scan does yield predictions based on an average climatological year. The standard deviation of annual global irradiance in Europe is ±4% [65]. However, one of the findings of a Swiss research on year-to-year irradiance variability was that "even if the standard deviations don't exceed some percents, specific years can be more than 10% away from the average" [66]. The climatological average irradiance in the province of Brabant, the Netherlands, was found to be 1033.7 kWh/m^2 per year [67]. For 2015, 2016 and 2017 values of 1090.3, 1064.7 and 1054.9 kWh/m^2 were found respectively, by using weather station data from Eindhoven [68]. This would results in deviations of 5.5%, 3.0% and 2.0%. Therefore, the yield and performance prediction can always be off by several percentage points.

- For the method using SVF & SCF, the coordinates of Eindhoven were used for constructing irradiance coefficients. However, the actual PV systems were spread out over the province of Brabant, some up to 30 km away from Eindhoven. Therefore up to 2% added deviation can be expected for these systems [69].

- Different settings can be chosen by the installer or customer. This could be concerning not only a different setup, thus another setting for module tilt, row distance or distance form edge, but also the dimensions or rated power of modules. As mentioned earlier, sometimes the most suitable roof segments are not used for PV, caused by aesthetic considerations or structural restrictions of the roof segment.

- The current method of constructing obstacle views also adds some inaccuracy. In comparison with the fisheye photographic method to determine the SVF, both GPS and the ray-tracing/LiDAR methods slightly overestimate the SVF when the level of obstruction is low [70]. Additionally, semi-transparent obstacles are assumed to be fully blocking, and the room under shading obstacles is also considered blocked. This causes that shading obstacles such as trees are interpreted as cylinders fully blocking all radiation, while in reality it might be more realistic to model them as a fully blocking trunk and a partially transparent surface of branches and leaves. Lastly, the obstacle view could be inaccurate due to recent shading obstacles like planted trees, or neighbours installing a dormer.

- Part of the errors in yield prediction will come from flaws in the roof segment files that were used during this study. The inaccuracy of roof segment borders can greatly impact the amounts of panels fitted. Data set 1 contained very uneven edges, which complicated panel fitting. Data set 2 had more even edges, since they were improved to geometric shapes by intersecting roof segments with each other, and using the straight building contours of cadastre data. However, where in-roof obstacles were often detected in set 1, they mostly remained unidentified in set 2. Apart from that, in a few single cases within set 2, two segments had been merged into one, making their estimates of segment slope and orientation highly inaccurate. This resulted in more buildings being filtered out in section 6.5.3.

6.6.5. Average shading and system losses

Throughout this research, the average over-prediction has been measured for different yield prediction methods. For the final selection of roof segments, the values found for the Solar Monkey, SVF&SCF and obstacle-less method were found to be 3.5%, 7.4% and 7.2%.

- For the Solar Monkey method, 7% of losses were already estimated, however this was too low. The 3.5% over-prediction would result in a combined system loss of 10.0% ($= (1 - 0.93/1.035) \cdot 100\%$).

- For the SVF & SCF method, also 7% of losses were already estimated. The 7.4% over-prediction would result in a combined system loss of 13.4% ($= (1 - 0.93/1.074) \cdot 100\%$).

- The PVGIS API already takes into account the spectral losses/gains, temperature-dependent module losses and low irradiance losses for a crystalline silicon PV module. An additional 3% was already estimated for other system losses. The 7.2% over-prediction would result in a combined

loss of 9.5% ($= (1 - 0.97/1.072) \cdot 100\%$) expected for cable losses, inverter efficiency, soiling and obstacle losses.

Since the same process from irradiance to AC yield was applied to the first two methods, and they both take into account obstacle losses, it was unexpected that the total system losses would be very different. The 3.6% deviation could be caused by a difference in the irradiance predictions in general or a difference in how obstacles were taken into account. No method was found to determine which irradiance predictions would be the right ones. However, judging from figure 6.15, obstacle losses might be over-predicted by the method of Solar Monkey. This is concluded since the mean over-prediction of the Solar Monkey method becomes significantly lower for more shaded roof segments, whereas over-prediction of the SVF& SCF method is nearly constant. However, this would not fully explain the difference is average over-prediction, since even for the lowest category of shading, the average over-prediction of the SVF&SCF method is higher than for the Solar Monkey method. Nonetheless, from these two values it can be concluded that the combined system loss is between 10.0% and 13.4%, referring to all losses attributed to cables, the inverter, soiling, and the effects that temperature and irradiance have on module efficiency.

The method without obstacles gives additional information. The combined loss of cable losses, actual inverter efficiency and obstacle losses was found to be 9.5%. Assuming 2% Ohmic losses from cables, an actual inverter efficiency of 97%, and 1% panel soiling losses, the average shading losses would be in the order of 3.8% ($= (1 - 0.905/(0.98 \cdot 0.97 \cdot 0.99)) \cdot 100\%$) [42, 44, 71].

Losses due to panel degradation were neglected in these approximate losses, since degradation is minimal in the first year after installation.

6.7. Roof categorising approach

In order to categorise roofs, two approaches are discussed. The first approach would be to use the performance in kWh/kW$_p$ as the only metric for roof suitability to PV, whereas the second method would take into account multiple metrics.

6.7.1. Roof suitability measured by PV performance only

Figure 6.17 shows the measured annual performance distribution for 236 PV systems monitored by Solar Monkey. In order to determine the suitability of roofs for PV, the systems could be divided by their performance.

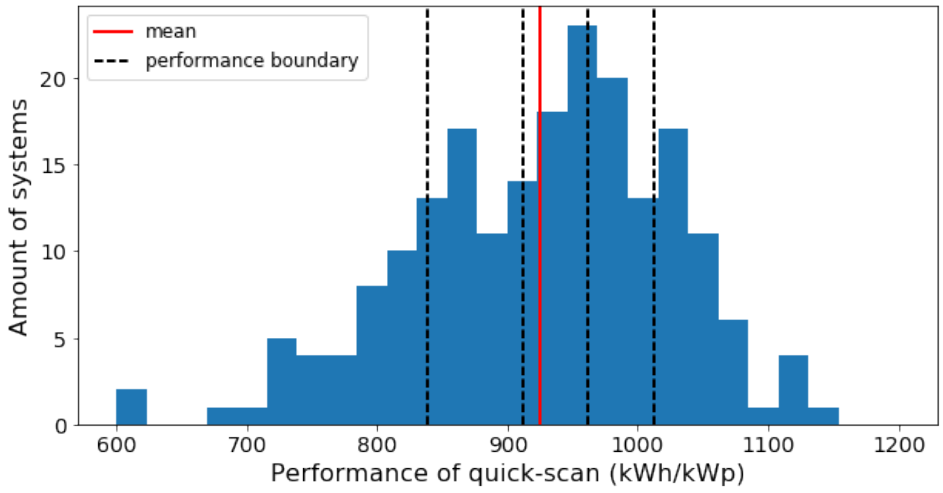

Figure 6.17: Performance distribution for 236 PV systems monitored by Solar Monkey.

For example, five categories could be created with equal amounts of systems. If the list of performance values is sorted, four boundary performance values can be chosen at equal distances. Setting the four boundaries at 839.1, 911.7, 961.5 and 1012.9 kWh/kW$_p$ respectively, five performance categories would be defined. Of course another option would be to create one category below 650

kWh/kW$_p$. This would mean the roof is unsuitable for PV, having a payback time of over 10 years as discussed in section 4.1.1.

This method is easy to implement, however the performance of a system is not the only variable that influences the decision of a PV installer or customer. One way to extend this method would be by first applying a minimum amount of fitted panels to the results found by a quick-scan. If only one or two panels were fitted, it might still not be feasible to install them, since installation costs will be relatively high.

6.7.2. Defining roof suitability by assessing multiple metrics

The decision for a certain PV system design and choosing for rooftop PV in general is a process affected by many factors. In his research, Bronkhorst identified performance, installation and aesthetic aspects as factors in the decision-making process [5].

Performance has been discussed in the previous section, however in large systems also larger cable losses should be taken into account. The installation aspects can be divided in the number of separate panel sections S, the panel orientation (portrait or landscape), the compactness of a section H and the amount of mounting material L required. Compact layouts with a low number of different panel sections would be preferred for the aesthetics of PV.

Bronkhorst proposed a grading system based on a fast elitist non-dominated sorting genetic algorithm for multi-objective optimisation, first published by [72]. This algorithm could be implemented to categorise the systems that were designed on roofs by the quick-scan algorithm. The customer could determine the weight of different metrics taken into account: the performance, total number of fitted panels, S, H and L. Further details about the grading system are mentioned in [5].

6.8. Calculation time per yield prediction method

In this section, the calculation time per yield prediction method is assessed for each yield prediction method. All results include the full algorithm, so including all polygon operations and panel fitting, of which the speed was examined in section 5.5. Next to the three yield prediction methods, also the time measurements were carried out for the loading of obstacle views. This is referred to the time it takes to load surrounding AHN height data, construct a skyline profile and save this in an efficient way. All time measurements are shows in appendix C.

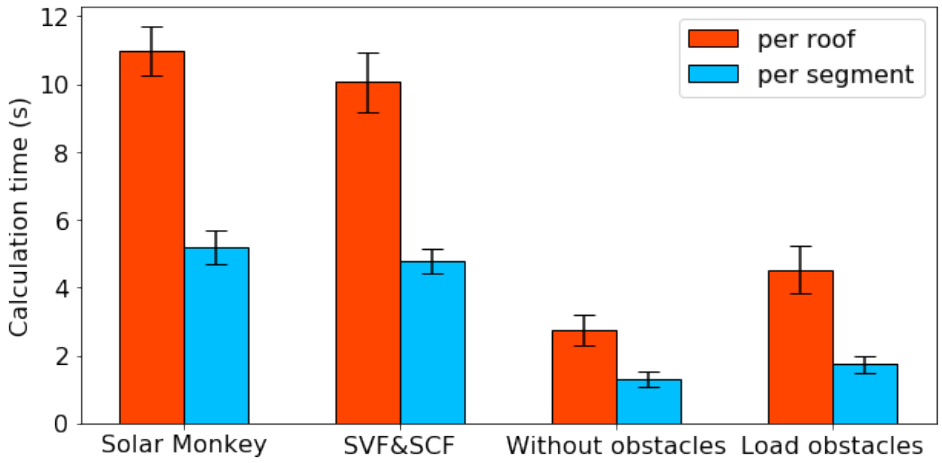

Figure 6.18: Calculation time for three yield prediction methods and loading obstacle views from AHN data. All time measurements are shows in appendix C.

It can be seen that the quick-scan method neglecting obstacles is by far the fastest method with 2.75 $\pm$ 0.44 seconds per roof. After panel fitting, the method uses only a call to the API of PVGIS, and therefore the main time spent in this version of the quick-scan is panel fitting of the more or less 2 segments per roof.

The the Solar Monkey method and SVF&SCF respectively took 15.50 $\pm$ 1.01 and 14.58 $\pm$ 1.13 seconds per roof, including the loading and saving of skyline profiles. It can again be mentioned that

the filtering steps save a lot of time here, since the calculation time per roof is determined by the amount of segments per roof.

The loading time for obstacles needs to be considered as added calculation time to the Solar Monkey and SVF&SCF method. It was however mentioned separately, for two reasons:

- If the quick-scan will be used multiple times for the same set, but with different settings, it is only necessary to load the obstacle views once. Therefore it is interesting to see how much time could be saved.
- If the quick-scan would ever be offered in an API form, it could be considered to already load and save the obstacle views for every roof segment, such that the calculation time of methods using that is decreased.

Chapter summary

In this chapter the results of different yield prediction algorithms were presented and discussed. It can be concluded that the methods taking into account the skyline profile outperformed the method neglecting obstacles, especially for highly shaded segments. Apart from that, the average losses were assessed for PV system components and shading. Lastly, it was found that the method neglecting obstacles was more than 5 times faster than the methods taking into account obstacles.

7

Conclusions

A quick-scan algorithm has been developed in order to evaluate rooftop PV potential. Both its panel fitting and yield prediction functions have been validated with existing systems monitored by Solar Monkey. First, the added value of this specific quick-scan algorithm will be highlighted, after which this chapter will discuss the conclusions that were found per research question. Finally, recommendation will be done regarding a final quick-scan algorithm, its commercial potential and further research.

Added value of the quick-scan algorithm

Regarding the envisioned quick-scan algorithm, there are four main competitors: Zonatlas, Novasole, Sunmapper and Google Project Sunroof. In order to have added value over Zonatlas and Novasole, the assumptions for calculation of any given results and the uncertainty in yield prediction should be accessible to the user. Moreover, the module lay-out and thus panel fitting on roof segments is an essential component of the quick-scan. This would give it added value over its four competitors and make its outcome more visually appealing to customers.

7.1. Research question 1

Question: How realistic is the amount of modules fitted on a roof by the panel fitting algorithm?
Approach: A validation of the algorithm should be carried out, which compares the panel fitting on Readaar's roof segments with the PV systems that were actually built.

7.1.1. New method for calculation of roof segment orientation

For successful panel fitting the exact orientation of roof segments needed to be known. The orientation of roof segments that was given by Readaar was not useful for flat roof segments and inaccurate for pitched ones. A new approach to determine the roof segment orientation was used, using the longest side of the roof segment polygon. For flat roofs, panels would be directed to the South, however aligned with the roof edge orientation as found by longest polygon side. For pitched segments, the longest polygon side was used to increase the accuracy of the segment orientation that was initially given. The new method resulted in accurate orientation prediction for 98.7% of the roof segments it was tested for.

7.1.2. Maximum panel fitting on full data sets

The maximum panel fitting algorithm fitted substantially more panels on the improved roof segments of data set 2. On average the amount of panels was over-predicted by 38.4%. Nevertheless, the spread in results was still very high, with an RSD value of 65.1%.

The maximum panel fitting algorithm is generally hard to validate in any automatic manner. The desired amount of panels to be placed does not have to be the maximum amount that fit on a roof. For example, consumers might not have sufficient energy demand to install the full potential of PV. Moreover, consumers could choose low-performing segments, since they can be preferred for aesthetic reasons. Apart from that, east-west layouts can be placed on flat roofs, instead of panels directed to the South. A better way to validate panel fitting, would be manual selection of the right segments.

7.1.3. Manual selection of roof segments

A visual inspection was carried out for 208 roofs. For this set of roofs, recent aerial images were compared with the set 2 roof segments that were provided by Readaar. 104 segments were fully used for PV, whereas 66 segments were used for about two-thirds and 45 segments for about one-third of their surface. The last two categories were caused by different situations: most commonly, in-roof obstacles were not detected. Sometimes, the customer had no desire to use the full potential of the roof, or chose for a rectangular (aesthetic) panel layout instead of fitting the maximum amount of panels.

Another finding was that the distance kept from the roof segment edge was much smaller than expected. For pitched roofs, there was virtually no distance between the roof edge and installed panels, or at most 10 centimetres. For flat roofs a range of 0 to 20 centimetres was encountered for these domestic rooftop systems. At the end of the manual selection, 145 roofs were left for the final validation of the quick-scan.

7.1.4. Maximum panel fitting on manual selection

Using zero distance from the roof edge, the panel placement was still underestimated by 17.5% on average, however the RSD decreased to 46.3%. For 70.3% of the roofs the amount of fitted panels was too low, however mostly by a small fraction. Only 13.1% of the roofs had more than double the amount of installed panels with respect to what was fitted by maximum panel fitting.

Multiple reasons were identified for fewer panels being fitted than actually installed. Most cases could be traced back to flaws in the shape of the roof segments, such as over-segmentation. Occasionally, parts of roof segments were not detected by the stereo-matching method.

Apart from that, the settings for module layouts could be different. Smaller panels could be used, and on flat roofs less module tilt and therefore smaller row distances could be chosen. These options were not investigated in further detail.

Lastly, it was found that some panels were placed on a garden house or garage instead of the building for which the land register data was available. Also, several systems were spread over multiple buildings, which made it impossible to achieve the same amount of panels by the current quick-scan.

7.2. Research question 2

Question: How accurate is yield prediction carried out by the quick-scan?
Approach: Comparison of predicted values to the real-time generation of monitored PV systems for three different yield prediction methods.

7.2.1. Yield prediction on manual selection of roof segments

After carrying out yield prediction for large data sets filtered by minimum segment area and the orientation of pitched segments, yield prediction was carried out on a manual selection of roof segments on which PV panels were actually installed. Figure 7.1 shows the final results of all three yield prediction methods, after deleting roofs where over-segmentation had taken place.

Table 7.1: Results of the quick-scan per yield prediction method, carried out for 145 roofs.

Yield prediction method	Solar Monkey	SVF & SCF	Without obstacles
Mean over-prediction	3.5%	7.4%	7.2%
Relative standard deviation	7.2%	7.6%	9.5%
Buildings filtered out	9.0%	8.3%	6.9%

In terms of RSD, the obstacle-including methods outperformed the simple yield calculation. The yield prediction accuracy of the first two methods was greatly improved now the exact roof segments on which PV was placed were known. These RSD values for yield prediction are seen as acceptable, since the absolute minimum would be 5.7%, using the Solar Monkey prediction with an obstacle view per panel. Moreover, the prediction is affected by fluctuations in annual irradiance, inaccuracy in determining the obstacle view from LiDar and flaws in roof segments. Regarding performance prediction, the Solar Monkey method over-predicted by 3.5%, whereas, the SVF&SCF methods and prediction

without obstacles over-predicted by 7.4% and 7.2% respectively.

Performance for different levels of shading

The performance of different yield prediction methods was analysed for roofs with different levels of shading. For roofs with SCF values below 0.25 the three yield calculation methods performed similarly in terms of RSD. For highly shaded roofs with SCF values above 0.25 the method neglecting obstacles performed significantly worse. Additionally, it was found that the average over-prediction of the SVF&SCF method was near-constant over varying levels of shading, whereas the Solar Monkey method was decreasing and the method without obstacles was increasing with higher levels of shading.

Performance for different roof segment sizes

The Solar Monkey yield prediction method was tested on its performance for three categories of roof segment area: A<25, 25<A<70 and A>70. It was found that the RSD was highest for large roof segments, while it was lowest for medium-sized segments. The higher RSD that is obtained for roofs with a smaller segments could be explained by the over-segmentation of several roof segments in the stereo-matching process. An over-segmentation of a suitable roof segment can lead to a smaller amount of panels fitted on it, and therefore bias the yield prediction importance of a less suitable roof segment. The performance of large roofs was generally under-predicted, while the RSD was highest with 11.7%. It is expected that using one obstacle view is not accurate enough for large roof segments. Especially if only the least shaded part of a large roof is used, this can lead to under-prediction of the performance by the quick-scan.

7.2.2. Land register data versus roof segments

To demonstrate the added benefit of roof segment data over land register data only, the panel fitting and yield prediction was also carried out with the assumption that all roofs were one-segment and flat, in section 6.4. The performance predictions with obstacles were widely spread with an RSD of 20.4%, while those without obstacles were near-constant at 1070 kWh/kW$_p$ per year. The added value of 3D roof segments was thus shown.

7.3. Research question 3

Question: How fast are different parts of the quick-scan and how can this be optimised?
Approach: Measurement of the calculation speed for different parts of the quick-scan algorithm and an inventory of methods to increase the calculation speed while keeping the preferred accuracy.

7.3.1. Panel fitting time

The panel fitting time was found to be 1.01 seconds per segment, with a standard deviation of 1.08 seconds. The large standard deviation in panel fitting time per segment comes from the wide variety in segment area within the data set, and the difference between flat and pitched segments. For flat segments, only landscape setups are chosen by the quick-scan algorithm, while for pitched segments both landscape and portrait setups are possible. The panel fitting speed was found to be 30.4 ± 18.2 m^{2}s^{-1}. The panel fitting speed for pitched roofs without internal obstacle segments was found to be 20.1 ± 5.0 m^{2}s^{-1}, whereas the panel fitting speed for flat roofs was found to be 56.9 ± 12.0 m^{2}s^{-1}.

7.3.2. Filtering out roof segments with low potential

In order to optimise the quick-scan algorithm in both speed and accuracy, two filtering steps were carried out. The payback time of a PV system is very important to customers. The payback time is directly related to the system performance, expressed in kWh/kW$_p$ per year. Since roof segments pitched towards the North have much lower performance values in the Northern hemisphere, segments with a pitch angle over 10° and an orientation between 0° to 60° and 300° to 360°, were filtered out by the quick-scan algorithm. Since roof segments which fit zero or one panels are generally not interesting for PV systems, another filtering step was carried out on the minimum segment area. All segments with an area less than 8.4m^2 were filtered out, since they could fit a maximum of 1 PV panel. These steps could decrease the amount of roof segments by up to 63%, while decreasing the relative standard deviation for panel fitting and yield prediction.

7.3.3. Calculation time per yield prediction method

The quick-scan calculation times for different yield prediction methods were found to be 15.50 ± 1.01, 14.58 ± 1.13 and 2.75 ± 0.44 seconds per roof, respectively. These times were given for data sets that had around 2 segments per roof after filtering on segment area and pitched segment orientation.

7.4. Final quick-scan algorithm

Taking into account the results found in all previous sections, the following recommendations are made for the use of the quick-scan. The final quick-scan algorithm is advised to be used with panel alignment to the roof edge on flat roofs, and without east-west setups. The distance taken from the roof should be set to 0 cm for pitched roofs and no more than 20 cm for flat roofs.

If the number of roofs is very large or the calculation time should be limited, the yield prediction method neglecting the skyline profile is preferred. In that case, it should always be mentioned that the method assumes average shading losses, and thus over-predicts performance for roofs with SCF>0.25. First determining the SCF value per roof segment and then choosing a yield prediction method is not an option. This would already increase the calculation time significantly, since the AHN height data needs to be retrieved. For any application where time is not the limiting factor, one of the two methods taking into account skyline profiles should be used. Since their accuracy and calculation time do not differ significantly, the Solar Monkey method would be preferred since it is easier to implement within the work-flow of Solar Monkey.

7.5. Commercial potential of the quick-scan

In this section, the commercial potential of the quick-scan will be estimated for three applications: batches, API and integration with the Solar Monkey software. This will be done by assessing the total addressable market, the serviceable addressable market, the serviceable obtainable market and the price per quick-scan for each application.

7.5.1. Quick-scan for large batches

During the last two weeks of September 2018, a commercial quick-scan pilot was carried out with a housing corporation. For 300 addresses, the quick-scan calculated the amount of fitted panels and the expected yield with the Solar Monkey yield calculation method and all settings as mentioned in appendix A. The results of the quick-scan were offered at approximately €3 per roof.

In October 2018 there are prospects of multiple quick-scan pilots, with sizes up to 36,000 addresses. In this case the price per quick-scan would be lower, about €1 per roof. However, there is a large range of institutions that might be interested in the quick-scan: municipalities, housings corporations, utility companies and PV installers.

For the customers such as utility companies or PV installers, the main goal of a batch-form quick-scan would be to make the sales process more efficient. They could contact customers and mention the amount of panels that would fit on their roof, the amount of energy they could generate, and the potential amount of savings on their electricity bill. The sales process would become much more effective than without this information.

The commercial potential of the batch quick-scan will be estimated for all housing corporations in the Netherlands. There are 363 housing corporations owning a total of 2.4 million residential units [73]. A research into the largest 135 housing corporations, owning about 77% of these residential units, showed that 37% of these are one-family units, 45% is within multiple-family buildings up to 4 floors, and 12% are situated in taller buildings, above 4 floors [74]. For the second and third category average amounts of 2.5 and 8 floors are assumed respectively. Then, these three categories would result in a total addressable market of about 1.35 million roofs.

In 2016, 43% of all residential units had an energy label C or lower, while the Dutch energy agreement SER mentions the ambition to have an average energy label B in 2021 [75]. Therefore the serviceable addressable market would be around 550,000 addresses with roofs.

Considering there are only few parties in the Netherlands that offer services like the quick-scan, the market share that Solar Monkey could obtain is significant. Next to Zonatlas and Novasole, Solar Monkey could serve up to 30% of the serviceable addressable market, being 165,000 addresses with roofs.

7.5.2. Quick-scan in API form

In the near future, Solar Monkey plans to offer the quick-scan in an API form. PV installers could select their preferred settings and should get their results in 10 seconds. The value of this would be €0.4 to €1 per roof. A promising application is however that customers could use the quick-scan, being redirected to PV installers in their neighbourhood for the actual system design. Instead of asking the customer to pay for the quick-scan, Solar Monkey could get a fee for each customer referred to a PV installer. This fee could be between 3 and 5 euros per actually installed system.

In the Netherlands, around 150,000 residential rooftop PV systems are installed per year [76]. Customers request around 4 quotations before they make a decision for their final PV system [76]. This means that around 600,000 quotations are made each year. If the quick-scan API is placed on the websites of large PV installers and utility companies, up to 10% of these quotations could be done via the API. If we assume that the quick-scan quotation has an equal chance of being chosen, this could result in 15,000 references towards actually installed systems.

7.5.3. Quick-scan integrated with Solar Monkey software

Apart from this, the quick-scan could be fully integrated with the Solar Monkey software. This means that the quick-scan would generate actual system designs in the Solar Monkey application, and yield prediction could be carried out for the exact locations where panels are placed. These fully automated system designs would be worth between €3 and €5 per design, depending on the average quality of a design. This assumption is based on the current tariffs for prepaid users of the Solar Monkey software, paying €9.50 per manual design and an additional €4.75 for a customised report with yield calculation.

If many of the current customers were to use this functionality in the software, it could save them a lot of time. The average PV installer spends around 15 minutes to design a system and generate a report. If half of the PV systems currently designed by Solar Monkey software would be done automatically, this would be 650 quick-scan projects a week. On an annual basis, 34,000 quick-scan projects would save 8,500 hours of work. This way, the quick-scan could save 4 out of about 9,000 FTE in the Dutch solar market, making it 0.04% more efficient [77].

7.5.4. Conclusions on commercial potential

Table 7.2 shows the commercial potential per quick-scan application, as discussed in the previous sections. One important thing to mention is that the API and software applications would still require significant investments on their development. The batch application is closer to actual application.

Table 7.2: Potential commercialisation of the quick-scan.

Quick-scan application	Batch	API	Integrated in software
Total addressable market	1.35 M	600 k/year	600k /year
Serviceable addressable market	550 k	60k/year	68k /year
Serviceable obtainable market	165 k	15k/year	34k /year
Price per quick-scan	€1-3	€3-5	€3-5
Potential revenue	165-495 k€	45-75 k€/year	102-170 k€/year

The short-term potential of the batch quick-scan is largest, especially since municipalities, utility companies and PV installers were not even taken into account as potential customers yet. However, in a couple of years, most residential units of housing corporations will have higher energy labels, and the potential revenue will not be as high.

Therefore, the other quick-scan applications are more promising for the long-term. The quick-scan would also require fewer internal hours once it is operational in the API or software. After the quick-scan would be properly tested, it would not need continuous time investment in quality assurance. Additionally, the API and software applications would not need customised results for each single customer.

Naturally, all three applications would have a larger potential if international markets were also taken into account. However, this was considered outside the scope of this research.

7.6. Recommendations for further research

The maximum panel fitting algorithm could be further validated by manually selecting exact segments where panels were placed. For each PV system the panel dimensions, tilt angle, row distance and distance kept from the edge should be specified. In this way the panel fitting algorithm can be validated accurately.

Throughout this research, comparisons were made between the roof segments provided by Readaar and real roofs. A further investigation could be done into the systematic errors within the current segments. For example, the uncertainty in the given pitch angle is unknown, and it is unclear how often over-segmentation or under-segmentation of roof segments takes place. Another common issue was that obstacle segments within larger roof segments were not defined as gap in those segments. This is an improvement that Readaar could add to their current segmentation method.

For large roof segments, multiple obstacle views could be taken. Two methods for this were proposed in section 6.6.2. Apart from that, advanced geometrical methods could be used to take calculate the parallax for nearby and far obstacles. Parallax refers to the geometrical translation of shading objects over the horizon for different points on the roof. Thereby multiple obstacle views could be created from skyline profile retrieved for the centre of the roof. Especially if the horizontal distance from obstacles to the roof would be defined, this could be done more easily.

The quick-scan calculation speed could be increased in various ways. First of all, the maximum panel fitting method is not very fast. For rectangular roofs, more analytic method could be implemented, as mentioned by Bronkhorst [5]. Moreover, it could be investigated if a larger step size for shifting the panel grid would still result in satisfactory panel layouts. Apart from that, the loading of AHN height data and the calculation of obstacle views could be made faster through recommendations done by De Koning [39]. Lastly, the current quick-scan code was written in a way to have many optional settings. Choosing one preferred yield prediction method or a fixed set of panel settings would increase the speed, since many *if* statements can be avoided. Moreover, the calculation speed could be improved by making the coding more efficient, avoiding for-loops and a multitude of Python packages, converting data back and forth. Additionally, the Random Access Memory usage could be decreased by preallocating arrays, filling them with zeros, and over-writing existing variables instead of creating new ones where possible [78].

The mean over-prediction of different yield prediction methods could be validated by carrying out yield predictions for different sets of roofs with monitored PV systems. By this, the uncertainty in the mean over-prediction could be found, and the system losses and obstacle losses could be determined more accurately.

It could be investigated if the quick-scan is more accurate for flat or pitched roofs of the same size. This question remained out of the scope of the current research. It is however expected that the quick-scan would be less accurate for flat roof segments, since a larger variability was observed in the settings for panel layouts. For example, panels could have tilt angles of 0° to 20°, and therefore the row distance could also be chosen very differently.

The boundary between flat and pitched roofs could be investigated in further detail. For this research, the boundary was set at 10°, however there might be a standard for installers about when to install panels flatly on a roof and when to incline panels with respect to the roof surface. If there is no such standard, the boundary could be set by inspecting many PV systems on roofs with a pitch angle between 5° and 15° and then noting down how panels had been placed.

The east-west option for panel layouts was only implemented at a very basic level. In future works, it could be made possible to use a different module tilt angle and row distance for these setups. Moreover, east-west performance predictions could be improved significantly, by counting the actual amount of panels directed to the East and West, instead of assuming 50% of the panels are directed towards the East and 50% towards the West.

The boundaries chosen for orientation filtering using data set 1, could turn out to be different for data set 2. Therefore it would be advisable to repeat the analysis for this set of improved roof segments. Alternatively, the boundaries for orientation filtering could be based on a theoretical minimum, by calculating the performance of a panel with a set tilt towards all Southern directions. Similarly, the minimum segment area could be assessed in further detail. For example, if roof segments of 2 panels or less are seldom encountered, it could be increased from 8.4 m^2, but if distances from the roof segment edge are chosen smaller, the minimum segment area should be decreased. Also, the minimum segment area could be based on a theoretical minimum, instead of taking the minimum area fitting

2 panels in a data set. For perfectly rectangular roof segments, at least 5.85 m^2 is needed to fit two panels with dimensions of 1.65x1 m and a distance of 30 cm from the roof segment edge.

Lastly, a manual check could be carried out with aerial images to verify that the number of panels in the Solar Monkey database is correct. As introduced in section 3.5, two examples have already been found where this number was different from the actual number of panels placed on the roof. It is thus not unthinkable there will be more differences with the actual number of panels.

Bibliography

[1] Low Carbon Living, *My Solar PV Array,* article on website (June 1, 2012).

[2] SolarPower Europe, *Global Market Outlook for Solar Power 2017 - 2021*, Tech. Rep. (SolarPower Europe, 2018).

[3] Photovoltaic Power System Programme, *2017 Trends in Photovoltaic Applications*, Tech. Rep. (International Energy Agency, 2017).

[4] E. Karakaya and P. Sriwannawit, *Barriers to the adoption of photovoltaic systems: The state of the art,* Renewable and Sustainable Energy Reviews **49**, 60 (2015).

[5] J. Bronkhorst, *Automatic PV system design using LiDAR data shadow analysis*, Tech. Rep. (Delft University of Technology, 2017).

[6] Photovoltaic-software.com, *Photovoltaic & solar electricity design tools,* comparison on website (2018).

[7] Clean Tech Delta, *Interview with new member: Enshared,* Clean Tech Delta (2017).

[8] Team Zonatlas, personal communication (2018).

[9] Solar Magazine, *Novasole ontvangt ISSO-kwaliteitscertificaat+ voor PV-ontwerp- en calculatiesoftware,* comparison on website (2015).

[10] Novasole B.V., *Identify as a Service (IaaS),* article on website (2018).

[11] W. Rucklidge, Google Project Sunroof, personal communication (January 4, 2018).

[12] C. Schwingshackl, M. Petitta, J. Wagner, G. Belluardo, D. Moser, M. Castelli, M. Zebisch, and A. Tetzlaff, *Wind effect on PV module temperature: Analysis of different techniques for an accurate estimation,* Energy Procedia **40**, 77 (2013), european Geosciences Union General Assembly 2013, EGUDivision Energy, Resources & the Environment, ERE.

[13] E.ON, *E.ON and Google deepen solar partnership around Project Sunroof,* E.ON Press Release (2018).

[14] M. Šúri, T. A. Huld, and E. D. Dunlop, *PV-GIS: a web-based solar radiation database for the calculation of PV potential in Europe,* International Journal of Sustainable Energy **24**, 55 (2005), https://doi.org/10.1080/14786450512331329556 .

[15] T. Huld, *Performance of grid-connected PV - data uncertainty,* JRC ISPRA (2018).

[16] T. Huld and A. M. G. Amillo, *Estimating PV module performance over large geographical regions: The role of irradiance, air temperature, wind speed and solar spectrum,* Energies **8**, 5159 (2015).

[17] T. Huld, PV GIS, personal communication (January 4, 2018).

[18] M. M. A. Khan, M. Asif, and E. Stach, *Rooftop PV potential in the residential sector of the kingdom of saudi arabia,* Buildings **7**, 46 (2017).

[19] J. Ordóñez, E. Jadraque, J. Alegre, and G. Martínez, *Analysis of the photovoltaic solar energy capacity of residential rooftops in andalusia (spain),* Renewable and Sustainable Energy Reviews **14**, 2122 (2010).

[20] K. Mainzer, S. Killinger, R. McKenna, and W. Fichtner, *Assessment of rooftop photovoltaic potentials at the urban level using publicly available geodata and image recognition techniques,* Solar Energy **155**, 561 (2017).

[21] A. Calcabrini, *Integration of PV systems in urban environments - a location-dependent performance study*, Tech. Rep. (Delft University of Technology, 2017).

[22] A. Smets, K. Jäger, O. Isabella, M. Zeman, and R. van Swaaij, *Solar Energy: The Physics and Engineering of Photovoltaic Conversion, Technologies and Systems* (UIT Cambridge, 2016).

[23] H. Ziar, *realtime measurements done at Kipp & Zonen,* (2018).

[24] B. Liu and R. Jordan, *Daily insolation on surfaces tilted towards equator,* ASHRAE J. (United States) **10** (1961).

[25] B. LeBaron and I. Dirmhirn, *Strengths and limitations of the Liu and Jordan model to determine diffuse from global irradiance,* Solar Energy **31**, 167 (1983).

[26] J. E. Hay and J. A. Davies, *Calculation of the solar radiation incident on an inclined surface,* First Canadian Solar Radiation Data Workshop (1980).

[27] F. Sönmez, *An albedo irradiance model usable for bifacial PV modules based on LiDAR data and ray casting*, Tech. Rep. (Delft University of Technology, 2017).

[28] D. T. Reindl, W. A. Beckman, and J. A. Duffie, *Diffuse fraction correlations,* Solar energy **45**, 1 (1990).

[29] R. Perez, P. Ineichen, R. Seals, J. Michalsky, and R. Stewart, *Modeling daylight availability and irradiance components from direct and global irradiance,* Solar energy **44**, 271 (1990).

[30] A. M. Noorian, I. Moradi, and G. A. Kamali, *Evaluation of 12 models to estimate hourly diffuse irradiation on inclined surfaces,* Renewable energy **33**, 1406 (2008).

[31] A. Skartveit and J. A. Olseth, *Modelling slope irradiance at high latitudes,* Solar Energy **36**, 333 (1986).

[32] B. Ridley, J. Boland, and P. Lauret, *Modelling of diffuse solar fraction with multiple predictors,* Renewable Energy **35**, 478 (2010).

[33] J. Coakley, *Reflectance and albedo, surface,* Encyclopedia of the Atmosphere , 1914 (2003).

[34] N. van Zon, *Quality Document AHN2*, Tech. Rep. (Actueel Hoogtebestand Nederland, 2013).

[35] T. de Bruijn, Solar Monkey, personal communication (September 18, 2018).

[36] S. S. Amer Al-Sudani, Hussein Hussein, *Sky view factor calculation - a computational-geometrical approach,* Space Syntax And Ontologies **2**, 673 (2017).

[37] D. Steyn, *The calculation of view factors from fisheye-lens photographs: Research note,* Atmosphere-Ocean **18**, 254 (1980), https://doi.org/10.1080/07055900.1980.9649091 .

[38] R. Santbergen, V. Muthukumar, R. Valckenborg, W. van de Wall, A. Smets, and M. Zeman, *Calculation of irradiance distribution on PV modules by combining sky and sensitivity maps,* Solar Energy **150**, 49 (2017).

[39] G. de Koning, *Correlations and improvements of the Solar Monkey algorithm*, Tech. Rep. (Solar Monkey Data Analysis internship, 2017).

[40] D. A. Chwieduk, *Recommendation on modelling of solar energy incident on a building envelope,* Renewable Energy **34**, 736 (2009).

[41] T. Schoehuijs and T. de Vries, *PV Modules - Photovoltaic Lab Course,* Delft University of Technology, Group 24 Assignment 3 - ET4379 Photovoltaic Lab Course (2017).

[42] PV Perfomance Modeling Collaborative Sandia, *CEC inverter test protocol,* article on website (2018).

[43] F. Baumgartner, H. Schmidt, B. Burger, R. Bründlinger, H. Häberlin, and M. Zehner, *Status and relevance of the DC voltage dependency of the inverter efficiency,* in *22nd European photovoltaic solar energy conference, Milano* (2007).

[44] ABB, *Technical Application Papers QT10 Photovoltaic plants,* (2010).

[45] T. Huld, *Interface for accessing PVGIS data and calculations,* (2017).

[46] R. J. Hyndman and A. B. Koehler, *Another look at measures of forecast accuracy,* International journal of forecasting **22**, 679 (2006).

[47] C. Tofallis, *A better measure of relative prediction accuracy for model selection and model estimation,* Journal of the Operational Research Society **66**, 1352 (2015).

[48] S. Makridakis, *Accuracy measures: theoretical and practical concerns,* International Journal of Forecasting **9**, 527 (1993).

[49] M. Vermeer, *3D roof-models from aerial images,* READAAR website article (February 28, 2018).

[50] M. Vermeer, *Large-scale efficient extraction of 3D roof segments from aerial stereo imagery*, Tech. Rep. (Delft University of Technology, 2018).

[51] S. Briels, Readaar, personal communication (October 1, 2018).

[52] N. Cook, *Designers' Guide to EN 1991-1-4 Eurocode 1: Actions on structures, general actions part 1–4. Wind actions* (Thomas Telford Publishing, 2007).

[53] Marjolein Leenstra, *Alles wat je altijd al wilde weten over een plat dak,* article on website (2017).

[54] Dylan Chalk, *Pitched Roof vs. Flat Roof: What's the Difference?* article on website (2016).

[55] Roofpedia, *Roof types,* article on website (2018).

[56] Spirit Energy, *Flat Roof Solar,* article on website (2017).

[57] J. P. Versluijs, Solar Monkey, personal communication (May 28, 2018).

[58] U. Jahn, D. Mayer, M. Heidenreich, R. Dahl, S. Castello, L. Clavadetscher, A. Frölich, B. Grimmig, W. Nasse, K. Sakuta, *et al.*, *International Energy Agency PVPS Task 2: Analysis of the operational performance of the IEA Database PV systems,* in *16th European Photovoltaic Solar Energy Conference and Exhibition, Glasgow, United Kingdom* (2000) p. 5.

[59] S. J. Ransome and J. H. Wohlgemuth, *kWh/kW$_p$ dependency on PV technology and balance of systems performance,* in *Conference Record of the Twenty-Ninth IEEE Photovoltaic Specialists Conference, 2002.* (2002) pp. 1420–1423.

[60] Solar Solutions Int., *Nationaal Solar Trendrapport 2018,* report composed by Dutch solar branch (2018).

[61] H. T. Nguyen and J. M. Pearce, *Incorporating shading losses in solar photovoltaic potential assessment at the municipal scale,* Solar Energy **86**, 1245 (2012).

[62] A. van Borselen, LENS energie, personal communication (2018).

[63] Renusol, *The ease of PV flat roof installation,* article on website (2018).

[64] SolarCare, *Gemiddelde zon PV opbrengst in nederland,* article on website (2018).

[65] Green Rhino Energy, *Annual Solar Irradiance, Intermittency and Annual Variations,* article on website (2016).

[66] P. Ineichen, *Global irradiation: average and typical year, and year to year annual variability*, Tech. Rep. (University of Geneva, 2011).

[67] V. Schepel, *Dutch PV portal v2.0,* Meteorological climate data download for province of Brabant (2018).

[68] KNMI, *Daily measurements of weather station in Eindhoven,* Meteorological weather data download (2018).

[69] W. van Sark and T. Schoen, *Inventarisatie PV markt Nederland*, Tech. Rep. (Rijksdienst voor Ondernemend Nederland, 2016).

[70] S. Freitas, A. Cristóvão, R. Amaro e Silva, and M. Brito, *Obstruction surveying methods for PV application in urban environments,* in *Proceedings of the 32nd European photovoltaic solar energy conference and exhibition* (2016) pp. 2759–2764.

[71] P. Nepal, *Effect of Soiling on the PV Panel kWh Output*, Tech. Rep. (Delft University of Technology, 2018).

[72] K. Deb, S. Agrawal, A. Pratap, and T. Meyarivan, *A fast elitist non-dominated sorting genetic algorithm for multi-objective optimization: NSGA-II,* in *International Conference on Parallel Problem Solving From Nature* (Springer, 2000) pp. 849–858.

[73] Ministry of Foreign Affairs, *Cijfers over Wonen en Bouwen 2016,* report regarding numbers in housing sector (2016).

[74] E.-J. van Latum and B. van Batenburg, *Potentie Zonnestroom - Bij gestapelde bouw van woningcorporaties voor de collectieve voorzieningen,* Bureau Baanbreker, commissioned by Agentschap NL (2012).

[75] Energie Vastgoed, *Verduurzamen huurwoningen naar energielabel B gaat mislukken,* article on website (2016).

[76] M. van Hoolwerff, Solar Monkey, personal communication (October 10, 2018).

[77] Energie Business, *Solar Trendrapport 2016: omzet richting 2 miljard,* article on website (2016).

[78] S. Mcgarrity, *Maximizing code performance by optimizing memory access,* (June, 2007).

A

Standard settings for quick-scan algorithm

Table A.1: Standard settings for quick-scan algorithm.

Variable	Value	Units
Panel width	99	cm
Panel length	165	cm
Rated power per panel	300	W_p
Pitched or flat roof criterion	10	°
Panel tilt for flat roofs	13	°
Row distance between panels on flat roofs	70	cm
Distance from pitched roof edge	30	cm
Distance from flat roof edge	60	cm
Minimum segment area	8.4	m^2
Acceptable error margin for segment orientation	16	°
Minimum azimuth for pitched roofs	60	°
Maximum azimuth for pitched roofs	300	°
Surface albedo	0.2	-
DC-to-AC yield ratio Solar Monkey	0.93	-
System costs	1300	€/kW_p
Electricity price	0.20	€/kWh
Orientation filtering	On	-
Segment area filtering	On	-
Panel alignment with flat roof edge	On	-
East-west setups	Off	-

B

Quick-scan algorithm structure

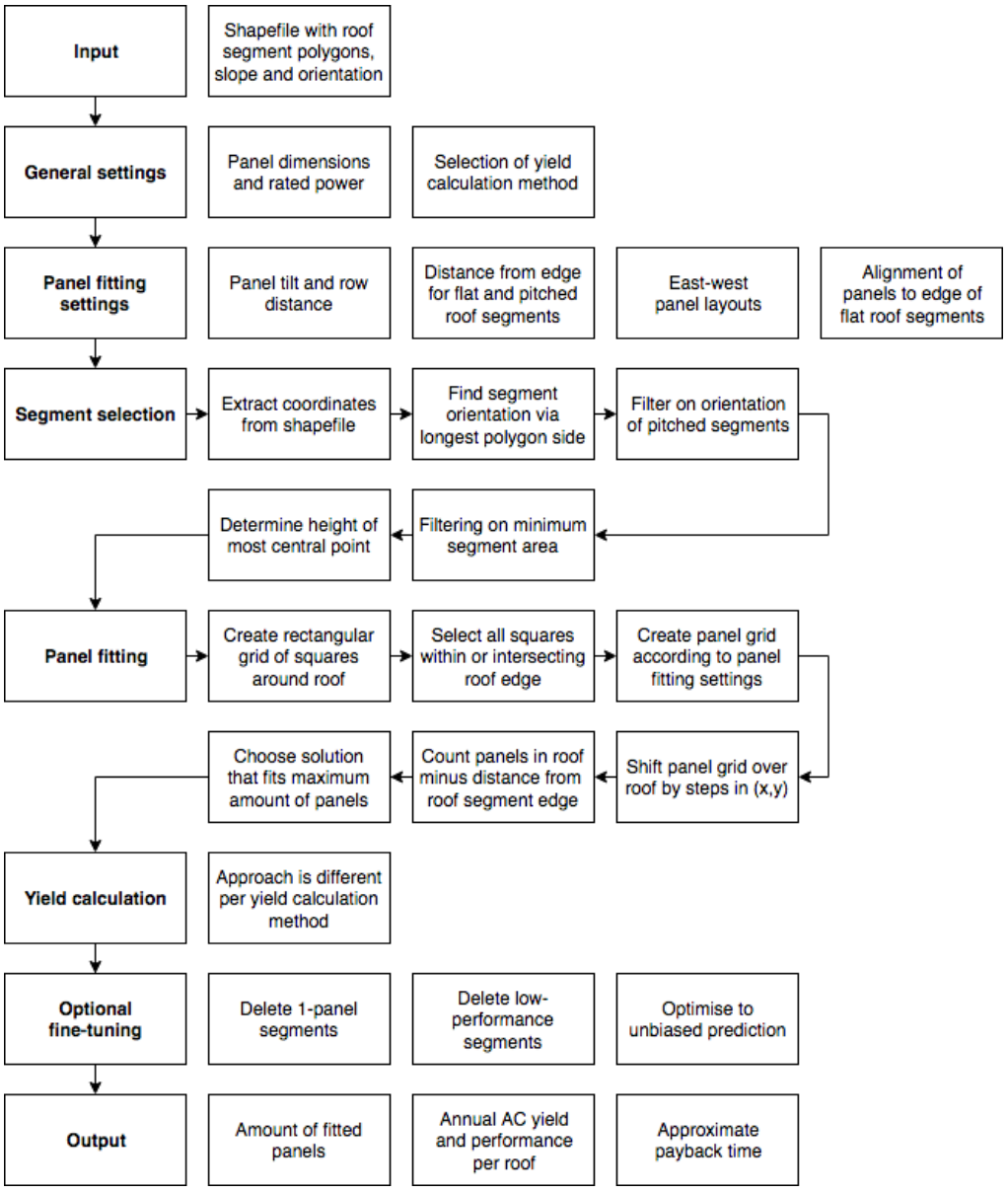

Figure B.1: Detailed structure of the quick-scan algorithm.

C

Calculation time measurements per yield prediction method

The time measurements for different parts of the algorithm will be presented here. Please note that the amount of segments per roof, and thus the time per roof, highly depends on the values chosen for pitched segment orientation filtering and minimum segment area filtering.

Table C.1: Calculation time per yield prediction method for 60° and 300° orientation filtering on pitched roof segments.

Method	Set	Time	Roofs	Segments	Time/roof	Time/segment
Excl. obstacles	1	13.3 min	239	527	3.3 s	1.5 s
Excl. obstacles	2	9.9 min	211	502	2.8 s	1.2 s
Incl. obst. SM	1	45.2 min	239	527	11.3 s	5.1 s
Incl. obst. SM	2	42.0 min	211	502	11.9 s	5.0 s
Incl. obst. SVF&SCF	1	41.4 min	239	527	10.4 s	4.7 s
Inc. obst. SVF&SCF	2	39.4 min	211	502	11.2 s	4.7 s

Table C.2: Calculation time per yield prediction method for 75° and 285° orientation filtering on pitched roof segments.

Method	Set	Time	Roofs	Segments	Time/roof	Time/segment
Excl. obstacles	1	12.5 min	238	491	3.2 s	1.5 s
Excl. obstacles	2	8.8 min	209	468	2.5 s	1.1 s
Incl. obst. SM	1	40.2 min	238	491	10.1 s	4.9 s
Incl. obst. SM	2	34.9 min	209	468	10.0 s	4.5 s
Incl. obst. SVF&SCF	1	34.0 min	238	491	8.6 s	4.2 s
Inc. obst. SVF&SCF	2	35.6 min	209	468	10.2 s	4.6 s

Table C.3: Calculation time per yield prediction method for 90° and 270° orientation filtering on pitched roof segments.

Method	Set	Time	Roofs	Segments	Time/roof	Time/segment
Excl. obstacles	1	10.5 min	232	431	2.7 s	1.5 s
Excl. obstacles	2	7.0 min	207	409	2.0 s	1.0 s
Incl. obst. SM	1	41.8 min	232	431	10.8 s	5.8 s
Incl. obst. SM	2	40.3 min	207	409	11.7 s	5.9 s
Incl. obst. SVF&SCF	1	35.6 min	232	431	9.2 s	5.0 s
Inc. obst. SVF&SCF	2	36.9 min	207	409	10.7 s	5.4 s

Table C.4: Calculation time for loading and saving obstacle views, using Python package "Pickle".

Time	Roofs	Segments	Time/roof	Time/segment
17.7 min	193	576	5.5 s	1.4 s
14.1 min	217	598	3.9 s	1.8 s
56.1 min	801	1693	4.2 s	2.0 s

D

Additional performance plots

D.1. Scatter plots for three yield prediction methods

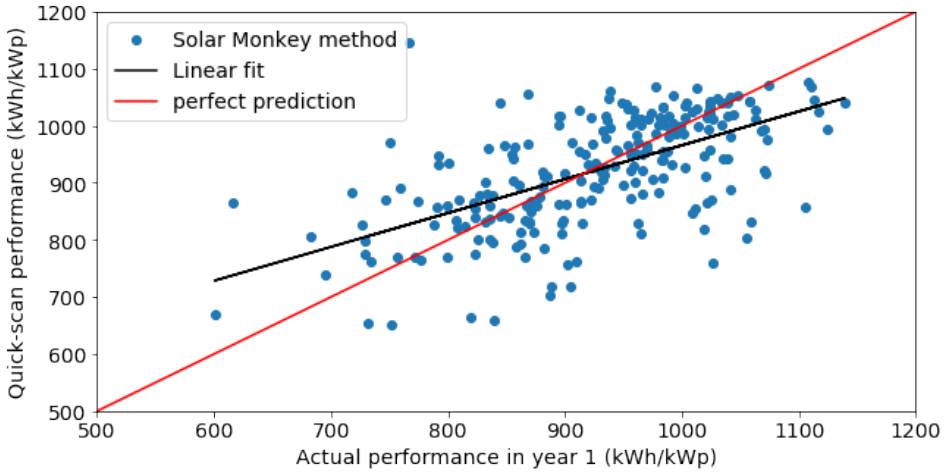

Figure D.1: Zero-mean over-prediction quick-scan performance estimation with Solar Monkey method on roof segment set 1.

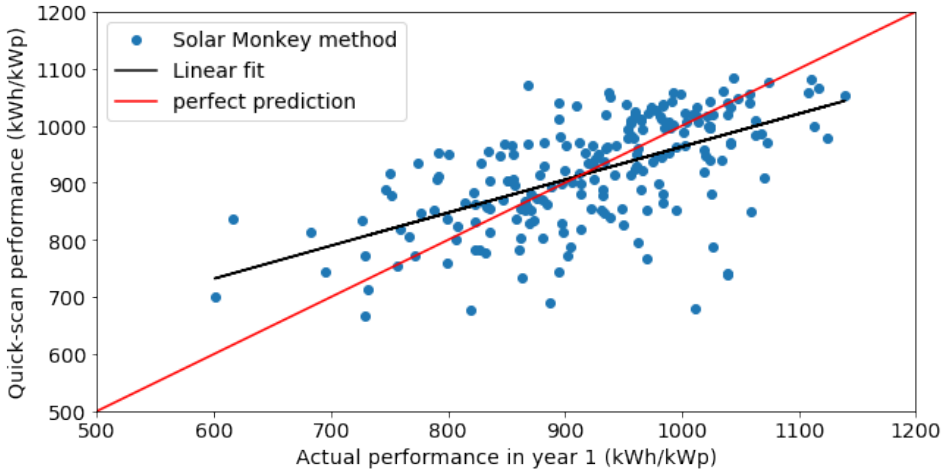

Figure D.2: Zero-mean over-prediction quick-scan performance estimation with Solar Monkey method on roof segment set 2.

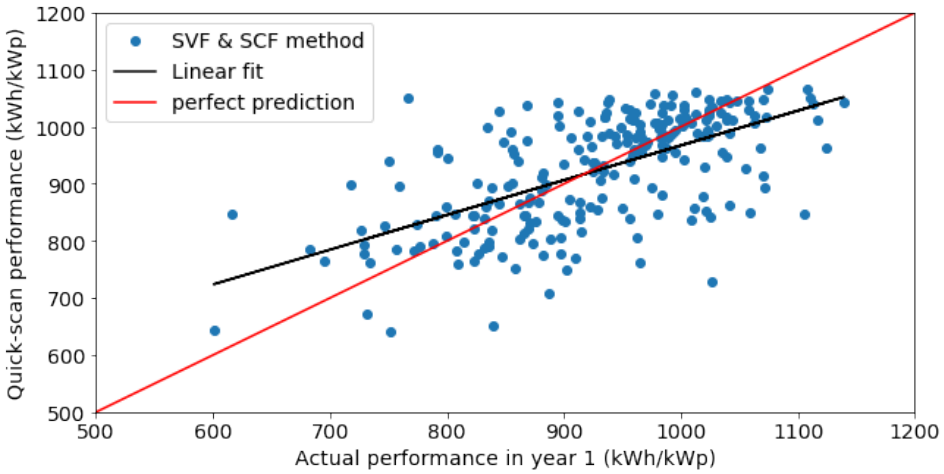

Figure D.3: Zero-mean over-prediction quick-scan performance estimation with SVF & SCF method on roof segment set 1.

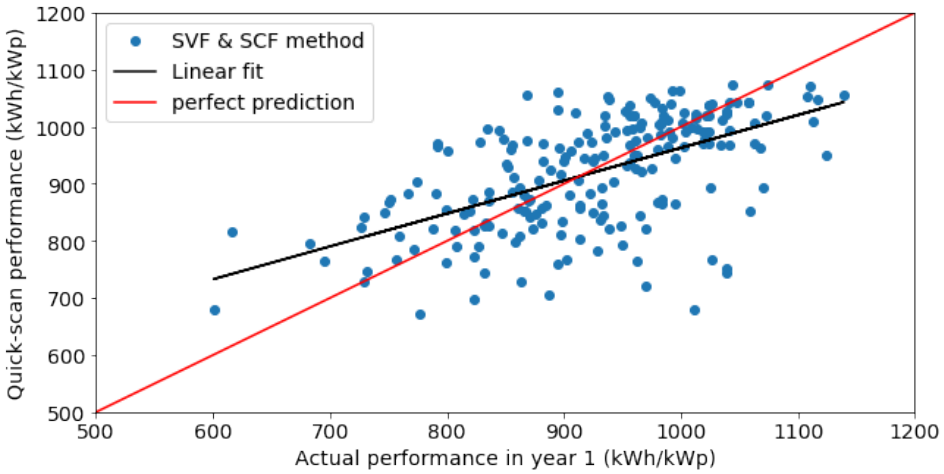

Figure D.4: Zero-mean over-prediction quick-scan performance estimation with SVF & SCF method on roof segment set 2.

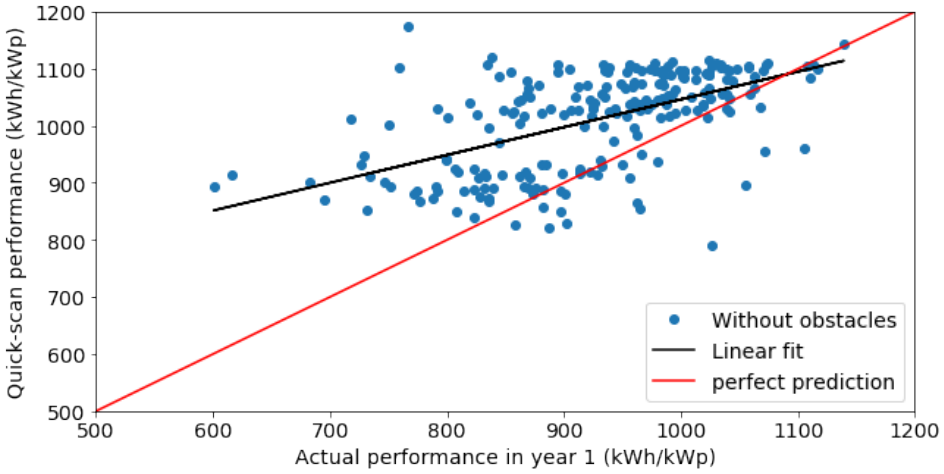

Figure D.5: Zero-mean over-prediction quick-scan performance estimation without obstacles on roof segment set 1.

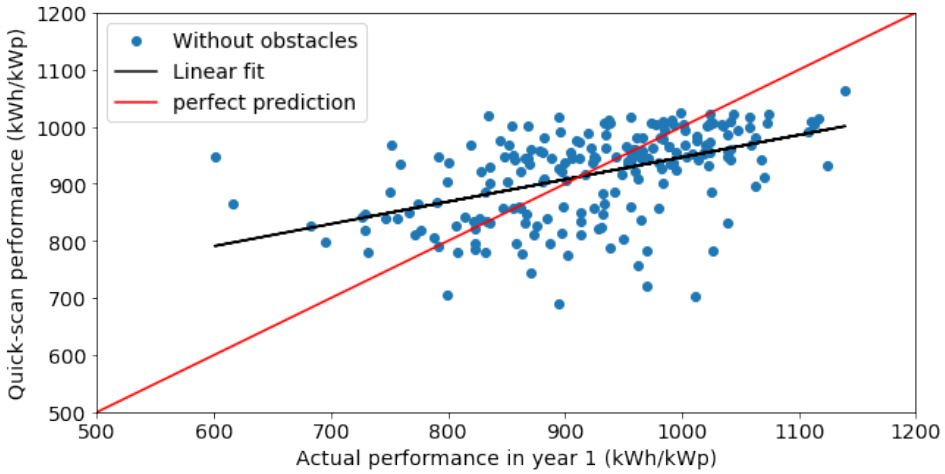

Figure D.6: Zero-mean over-prediction quick-scan performance estimation without obstacles on roof segment set 2.

D.2. Scatter plots for amount of segments per roof

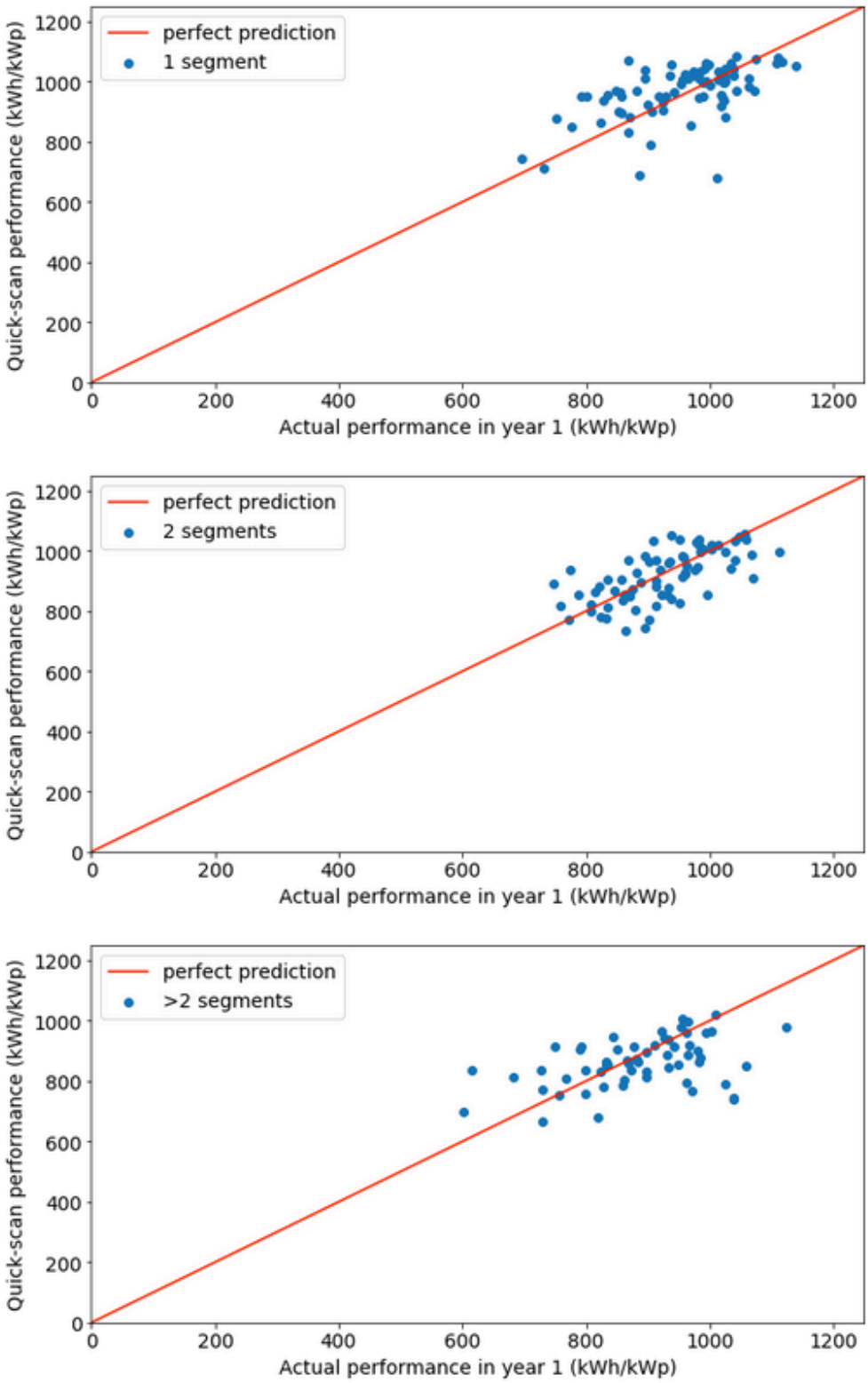

Figure D.7: Performance of the quick-scan calculated with Solar Monkey method for roofs composed of different amounts of segments after filtering on pitched segment orientation and minimum segment area according to table A.1.

D.3. Quick-scan vs. actual Solar Monkey prediction

The quick-scan plot related to performance table 6.2 is compared to the actual Solar Monkey prediction for the same roofs.

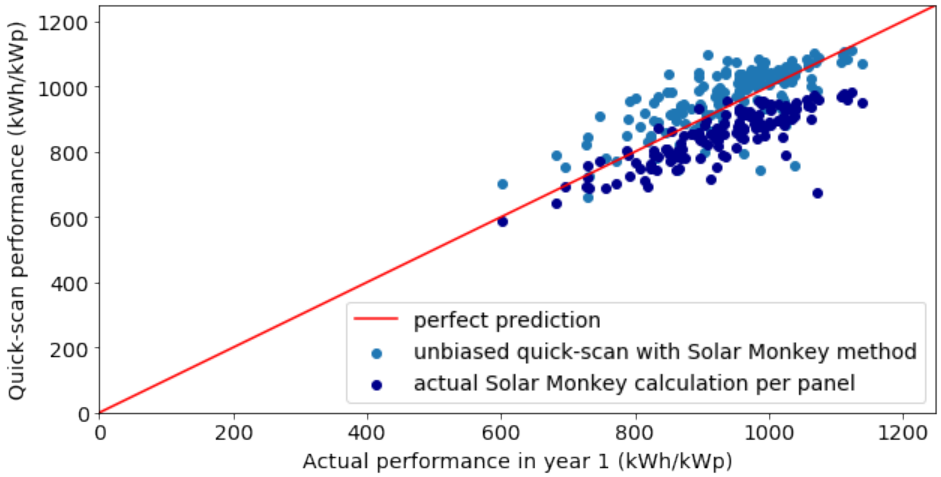

Figure D.8: Final quick-scan with Solar Monkey method compared with initial Solar Monkey predictions for designed system.

In figure D.8, the actual calculations of Solar Monkey under-predict the performance by 8.40% on average. The relative standard deviation is 6.23%.

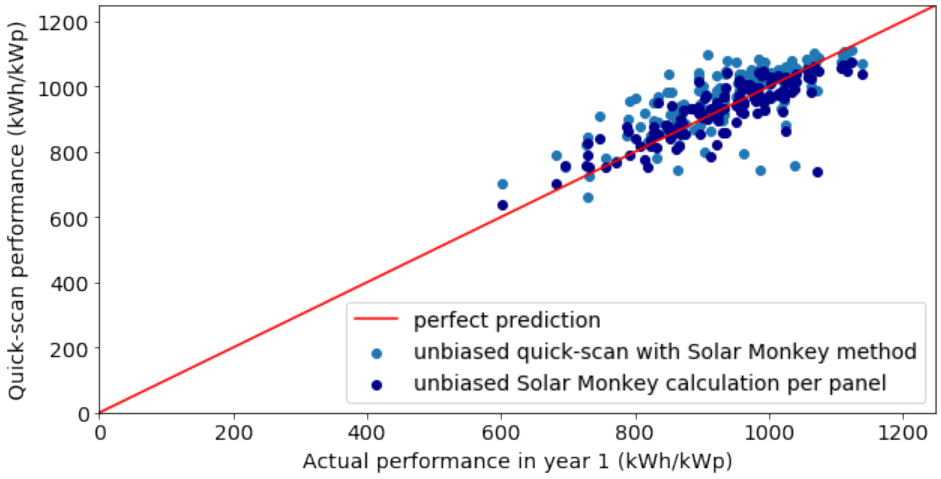

Figure D.9: Final quick-scan with Solar Monkey method compared with unbiased Solar Monkey predictions for designed system.

If the Solar Monkey prediction would be unbiased, the relative standard deviation could be reduced to 5.72%. This can be seen as the absolute minimum RSD value that could be achieved for the quick-scan algorithm when using the Solar Monkey yield prediction method.